GALLIUM NITRIDE-BASED ELECTRONIC DEVICES

By

ANPING ZHANG

A DISSERTATION PRESENTED TO THE GRADUATE SCHOOL
OF THE UNIVERSITY OF FLORIDA IN PARTIAL FULFILLMENT
OF THE REQUIREMENTS FOR THE DEGREE OF
DOCTOR OF PHILOSOPHY

UNIVERSITY OF FLORIDA

2001

To my parents and my wife, for their love and support.

ACKNOWLEDGMENTS

I would like to express my deepest thanks to Dr. Fan Ren for introducing me to this exciting field and for his patient guidance as my research advisor. His hard work to provide an extremely well-equipped lab and high standards for research, along with a very professional work environment, gives each of his students a unique opportunity to gain valuable experience.

I must also express my thanks to Dr. Stephen J. Pearton for his invaluable knowledge on III-V material processing and devices which has been very helpful to me; and to Dr. Fred Sharifi for letting me use his facilities and providing a lot of help.

I would also like to thank Drs. Cammy R. Abernathy, Timothy J. Anderson and Chang-Won Park for being members of my committee and spending time on my behalf. I especially appreciate the lab mates from our group and collaborators from Dr. Pearton's

I am forever indebted to my parents, who always encouraged me to achieve excellence in every aspect of life and supported me throughout my educational endeavors; and to my wife for her selfless support and never-ending understanding.

TABLE OF CONTENTS

Page

ACKNOWLEDGMENTS……..iii

ABSTRACT……...vi

CHAPTERS

1. INTRODUCTION……...……...……1

1.1 Gallium Nitride-Based Materials……..……5
1.2 Gallium Nitride-Based Optoelectronic and Electronic Devices……..……...11
1.2.1 Gallium Nitride-Based Optoelectronic Devices……..……11
1.2.2 Gallium Nitride-Based Electronic Devices……..13

2. GALLIUM NITRIDE-BASED DEVICE PROCESSING……18

2.1 Chlorine/Argon(Cl_2/Ar) High Density Inductively Coupled Plasma Damage in GaN Schottky Diodes…...…….…..……..……19
2.1.1 Introduction……...19
2.1.2 Experimental Methods.……20
2.1.3 Results and Discussion…...……..21
2.1.4 Summary and Conclusion……31
2.2 Effect of N_2 Inductively Coupled Plasma Treatment on n-AlGaN/GaN OhmicContacts……..……31
2.2.1 Introduction……...31
2.2.2 Experimental Methods.……33
2.2.3 Results and Discussion…...……..34
2.2.4 Summary and Conclusion……37

3. GALLIUM NITRIDE AND ALUMINUM GALLIUM NITRIDE HIGH VOLTAGE POWER RECTIFIERS……..……...…….……...……43

3.1 Introduction…….…....43
3.2 Gallium Nitride Schottky Rectifiers with 3.1 kV Reverse Breakdown Voltage……...……....46
3.3 Aluminum Gallium Nitride Schottky Rectifiers with 4.1 kV Reverse Breakdown Voltage……..…..…58
3.3.1 Introduction…….……..58
3.3.2 Experimental Methods.……59
3.3.3 Results and Discussion…...……..60

3.3.4 Summary……...65
3.4 Temperature Dependence and Current Transport Mechanisms in $Al_xGa_{1-x}N$ Schottky Rectifiers……65
3.4.1 Introduction……...65
3.4.2 Results and Discussion…..……..66
3.4.3 Summary……...…71
3.5 Lateral AlxGa1-xN Power Rectifiers with 9.7 kV Reverse Breakdown Voltage…….……..74
3.5.1 Introduction……...74
3.5.2 Experimental Methods.……74
3.5.3 Results and Discussion…..……...…75
3.5.4 Summary and Conclusion……78
3.6 Vertical and Lateral GaN Rectifiers on Free-Standing GaN Substrate…….....83

4. GALLIUM NITRIDE p-i-n POWER RECTIFIERS…….... 93

4.1 Comparison of GaN p-i-n and Schottky Rectifiers Performance……...93
4.1.1 Experimental Methods.……94
4.1.2 Results and Discussion…..……..95
4.1.3 Summary and Conclusion……...……107

5. GALLIUM NITRIDE-BASED BIPOLAR DEVICES……112

5.1 Gallium Nitride pnp Bipolar Junction Transistors Operated to 250 °C……112
5.1.1 Introduction……....112
5.1.2 Experimental Methods.……...112
5.1.3 Results and Discussion…..……....114
5.1.4 Summary and Conclusion……...……118
5.2 Direct-Current Characteristics of pnp AlGaN/GaN Heterostructure Bipolar Transistors……....118
5.2.1 Introduction……..……...118
5.2.2 Experimental Methods.……...…120
5.2.3 Results and Discussion…..……....121
5.2.4 Summary and Conclusion……...…126
5.3 Self-Aligned Small-Area GaN/AlGaN Heterojunction Bipolar Transistors…..……...126
5.3.1 Introduction……126
5.3.2 Experimental Methods.……...…129
5.3.3 Results and Discussion…..……....130
5.3.4 Summary and Conclusion……...…133

REFERENCES 137

BIOGRAPHICAL SKETCH 145

Abstract of Dissertation Presented to the Graduate School
of the University of Florida in Partial Fulfillment of the
Requirements for the Degree of Doctor of Philosophy

GALLIUM NITRIDE-BASED ELECTRONIC DEVICES

By

ANPING ZHANG

August 2001

Chairman: Fan Ren
Major Department: Chemical Engineering

Gallium Nitride (GaN) and related materials (especially AlGaN) have recently attracted a lot of interest for applications in high-power electronics capable of operation at elevated temperatures and high frequencies. The AlGaInN system offers numerous advantages. These include wider bandgaps, good transport properties, the availability of heterostructures (particularly AlGaN/GaN), the experience base gained by the commercialization of GaN-based laser and light-emitting diodes; and the existence of a high-growth-rate epitaxial method (hydride vapor phase epitaxy, HVPE) for producing very thick layers or even quasi-substrates. These attributes have led to rapid progress in the realization of a broad range of GaN electronic devices.

$Al_XGa_{1-X}N$ (X=0~0.25) Schottky rectifiers were fabricated in a lateral geometry using p^+-implanted guard rings and rectifying contact overlap onto an SiO_2 passivation layer. The reverse breakdown voltage (V_B) increased with the spacing between Schottky and ohmic metal contacts, reaching 9700 V for $Al_{0.25}Ga_{0.75}N$ and 6350 V for GaN,

respectively, for 100 μm gap spacing. Assuming lateral depletion, these values correspond to breakdown field strengths of $\leq 9.67\times10^5$ V-cm^{-1}, which is roughly a factor of 5 lower than the theoretical maximum in bulk GaN. The figure of merit $(V_B)^2/R_{ON}$, where R_{ON} is the on-state resistance, was in the range 94–268 MW-cm^{-2} for all the devices. Edge-terminated Schottky rectifiers were also fabricated on quasi-bulk GaN substrates grown by HVPE. For small diameter (75 μm) Schottky contacts, V_B measured in the vertical geometry was ~700 V, with an on-state resistance (R_{ON}) of 3 mΩ·cm^2, producing a figure-of-merit V_B^2/R_{ON} of 162.8 MW-cm^{-2}.

Gallium nitride (GaN) p-i-n diodes were also fabricated. A direct comparison of GaN p-i-n and Schottky rectifiers fabricated on the same GaN wafer showed higher reverse breakdown voltage for the former (490 V versus 347 V for the Schottky diodes), but lower forward turn-on voltages for the latter (~3.5 V versus ~5 V for the p-i-n diodes). The reverse current in both types of rectifiers was dominated by surface perimeter leakage at moderate bias. Finally, all of the devices we fabricated showed negative temperature coefficients for reverse breakdown voltage due to high defect level, which is a clear disadvantage for elevated temperature operation.

Bipolar devices are particularly interesting for high current applications such as microwave power amplifiers for radar, satellite and communication in the 1~5 GHz range, powers >100 W and operating temperatures >425 ºC. We demonstrated pnp Bipolar Junction Transistors (BJT) and pnp Heterojunction Bipolar Transistors (HBT) for the first time. For power microwave applications, small area self-aligned npn GaN/AlGaN HBTs were attempted. The devices showed very promising direct current characteristics.

CHAPTER 1
INTRODUCTION

For the last three decades or so, the III-nitride semiconductor material system has been viewed as highly promising for semiconductor device applications at blue and ultraviolet (UV) wavelengths in much the same manner that its highly successful As-based and P-based counterparts have been exploited for infrared, red and yellow wavelengths. As members of the III-V nitrides family, AlN, GaN, InN and their alloys are all wide band gap materials, and can crystallize in both wurtzite and zinc-blende polytypes. Wurtizite GaN, AlN and InN have direct room temperature bandgaps of 3.4, 6.2 and 1.9 eV, respectively (Figure 1-1). In cubic form, GaN and InN have direct bandgaps, while AlN is indirect. In view of the available wide range of direct bandgaps, GaN alloyed with AlN and InN may span a continuous range of direct bandgap energies throughout much of the visible spectrum well into the ultraviolet wavelengths. This makes the nitride system attractive for optoelectronic device applications, such as light emitting diodes (LEDs), laser diodes (LDs) and detectors which are active in the green, blue or UV wavelengths [1]. Although similar applications based on InGaAlP heterostructures have been successfully demonstrated, this material system is limited to about 550 nm. The addition of III-V nitrides to the family of device-quality semiconductors is essential for developing full-color displays (Fig. 1-2), coherent sources required by high density optical storage technologies, and very likely devices for signal

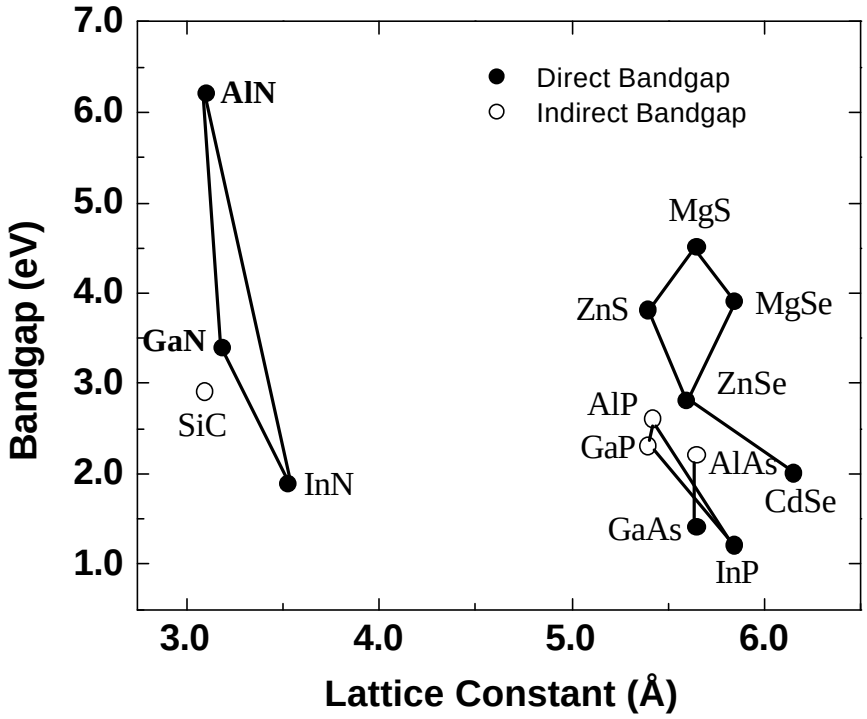

Figure 1-1 Bandgap of hexagonal (α-phase) InN, GaN and AlN and their alloys versus lattice constant.

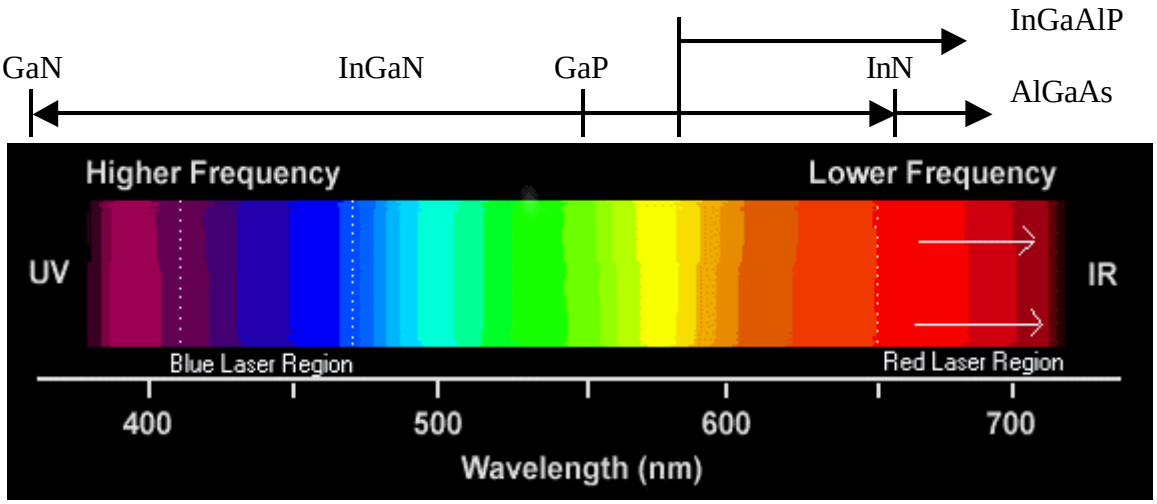

Figure 1-2 The various ternary and quaternary materials used for LEDs with the wavelength ranges indicated.

and illumination application. Particularly, the combination of GaN-based blue and green LEDs with GaAs-based red LEDs forms the basis for large-scale full displays and white light illumination. The solid-state white-light source generated by mixing the primary colors in a light scrambling configuration would provide not only compactness and high lifetime, but also would reduce power consumption by 80~90% compared to incandescent or fluorescent light sources.

Another area gaining a lot of attention for III-V nitrides is high-temperature/high-power electronics [2,3,4,5]. The interest stems from two intrinsic properties of this group of semiconductors. The first is their wide bandgap nature. The wide bandgap materials, such as GaN and SiC, are promising for high-temperature applications because they go intrinsic at much higher temperatures than materials like Ge, Si and GaAs. It means that GaN power devices can operate with less cooling and fewer high-cost processing steps associated with complicated structures designed to maximize heat extraction. The second attractive property of III-V nitrides is that they have high breakdown fields. The critical electric field of the breakdown scales roughly with the square of the energy band gap, and is estimated to be >4 MV/cm for GaN [6], as compared to 0.2 and 0.4 MV/cm for Si and GaAs, respectively.

GaN also has excellent electron transport properties, including good mobility, and high saturated drift velocity [7], thus making this material suitable for general electronics and promising for microwave rectifiers, particularly. The material properties associated with high temperature, high power, and high-frequency application of GaN and several conventional semiconductors are summarized in Table 1-1. It is anticipated that GaN may eventually prove to be superior to SiC in this area.

Table 1-1. Comparison of 300K semiconductor material properties [8].

	Si	GaAs	GaN	AlN	6H-SiC
Bandgap (eV) @300 °C	1.1	1.4	3.4	6.2	2.9
	indirect	direct	direct	direct	indirect
Electron mobility (cm2/V· s), RT	1400	8500	1000 (bulk)	135	600
			2000 (2D-gas)		
Hole Mobility (cm2/V· s), RT	600	400	30	14	40
Saturation velocity (cm/s), 10^7	1	2	2.5	1.4	2
Breakdown field (V/cm), 10^6	0.3	0.4	>5		4
Thermal conductivity (W/cm)	1.5	0.5	1.5	2	5
Melting temperature (K)	1690	1510	>1700	3000	>2100
CFOM*	1	8	489		458

*CFOM=$\chi\varepsilon\mu v_s E_B^2/(\chi\varepsilon\mu v_s E_B^2)_{Si}$, combined Figure of Merit for high temperature/high power/high frequency application.

The strongest feature of the III-V nitrides compared to SiC is the heterostructure technology it can support. Quantum well, modulation-doped heterointerface, and heterojunction structure can all be made in this system, giving access to new spectral regions for optical devices and new operation regimes for electronic devices. From this point of view, III-V nitrides can be considered the wide-bandgap equivalent of the AlGaAs/InGaAs system which has set the modern benchmark for microwave device performance.

Other attractive properties of III-V nitrides include high mechanical and thermal stability, large piezoelectric constants and the possibility of passivation by forming thin layers of Ga_2O_3 or Al_2O_3 with band gaps of 4.3 and 9.2 eV, respectively. In addition, AlN has received considerable attention for its insulating property [9], particularly as a potential isoelectronic insulator for GaAs field effect transistors (FETs).

1.1 Gallium Nitride-Based Materials

Substantial research on III-V nitrides growth was initiated in the early 1960s. However, they have trailed behind the easier-to-grow Si and GaAs semiconductors on the development curve. Nearly 30 years later, Si and GaAs have been pushed to their theoretical limits, while nitrides are just beginning to show their promise. The technological spin-offs came late because ideal substrates could not be found and the consequent growth of GaN thin films contained substantial concentration of defects and had high n-type background. Even in films with relatively small background electron concentration, p-type doping could not be achieved until recently.

One particular difficulty in the growth of GaN thin films is the unavailability of sufficiently large (>1 cm) single crystals for use as substrate for homoepitaxial growth. Thus up to now, heteroepitaxial growth has been a practical necessity and the choice of substrate is critical. Possible substrate materials should have low thermal expansion and lattice mismatch with the grown crystals. Also, they should be unaffected by the growth chemistries (such as NH_3 or H_2) at high growth temperatures (in excess of 1000 °C in some cases). Under these constraints, sapphire (Al_2O_3) and SiC are the most popular substrate materials used currently. When hexagonal GaN is grown on the (0001) basal plane of Al_2O_3, a lattice misfit of ~13% exits at the growth temperatures. A high density of threading dislocations is observed in GaN layers. The residual strain is comparable to the lattice misfit between 6H-SiC and GaN, and the result is comparable with dislocation densities observed [10]. Today, SiC substrates, though more costly, are of increasing interest for high temperature and high-power devices like transistors due to their good thermal conductivity and possibility of n- and p-type doping. The materials with a close

lattice match with GaN, such as $LiAlO_2$ [11] and $LiGaO_2$ [12], were also used for epitaxial substrates. However, the grown GaN lacked the desired electronic properties due to either the rough growth or unintentional contamination from the substrates. The ideal candidate substrate is clearly a GaN wafer. Several research groups are investigating the growth of the bulk GaN crystals and very thick films through various techniques [13-15]. However, commercially available large area GaN wafers appear to be several years away. The nitride community is, therefore, challenged with growing of heteroepitaxial films having large MISFITs.

Many epitaxial thin-film growth processes have been developed, including molecular beam epitaxy (MBE) [16,17], hydride vapor-phase epitaxy (HVPE) [13-15,18], metal organic chemical vapor deposition (MOCVD) [19-24], and derivatives of these methods. In the past few years, MOCVD [19-24] has evolved as a leading technique for production of III-V nitride optoelectronic and microelectronic devices. One remarkable application worth mentioning is the achievement of super-bright blue LEDs [22]. Characteristics of this method include the use of high purity chemical sources, a high degree of composition control and uniformity, high growth rates, large scale manufacturing potential and the ability to grow abrupt junctions.

Initially the growth of GaN was performed directly on sapphire and SiC substrates, with large crystalline defects threading vertically from the substrate interface through the newly deposited thin film. The wafer usually had rough surfaces mainly caused by the 3D-growth mode. In 1986, Amano et al. [20] succeeded in remarkably improving the GaN surface morphology as well as the electrical and optical properties by depositing a thin low-temperature AlN buffer layer before the high-temperature growth

of GaN. The essential role of this buffer is to serve as a template for the nucleation of growth and promote lateral growth of the GaN film due to the decrease in interfacial free energy between the film and the substrate. Although the buffer layer has reduced the effects of the lattice mismatch, the densities of the threading defects in these thin films are still in the range of 10^{9}~10^{10} cm^{2}, and on the order of one million times higher than in other semiconductor systems such as Si and GaAs. These defect-laden materials, to date, have had a surprisingly small effect on the performance of both optical and electronic devices, but they may raise major questions as to the long-term stability of these devices. It is unlikely that the full promise of GaN and related alloys can be realized without a major reduction in the defect densities in the as-grown materials.

In 1994, the lateral epitaxial overgrowth (LEO) technique was used to further improve the quality of the heteroepitaxially grown GaN, resulting in a marked reduction in defect density [23]. In this method, a layer of GaN grown by MOCVD is covered with 100~200 nm of amorphous SiO_2 and Si_3N_4 with ex situ techniques. Small circular or rectangular "windows" are then etched through to the underlying GaN. A GaN film is then regrown under conditions such that growth occurs epitaxially only in the windows and not on the mask. If growth continues, lateral growth over the mask eventually occurs. Since most of the extended dislocations propagate in the growth direction through GaN, very few threading dislocations are visible in the regrown GaN that extends laterally over the mask. Marchand et al. [24] observed that the density of dislocations reaching the surface of LEO GaN was in the 10^{4}~10^{5} cm^{2} range, while the film over the window regions still contained high levels of the threading defects. Figure 1-3 compares the cross-

section transmission electron microscopy (TEM) of a typical MOCVD growth (a) and LEO GaN (b).

A refined approach to a nearly dislocation free GaN substrate for devices can be used by two successive LEO steps with the mask of the second step positioned over the opening defined by the mask of the first step, thus blocking the defects that have grown out of the first windows. This complicated procedure offers the possibility of eliminating the disadvantages of heteroepitaxy, and will be important until GaN substrates become available.

In addition to growing GaN films with low defect densities, another key requirement for fabricating devices is the ability to precisely control the desired electrical properties of the thin film. In general, wide bandgap semiconductors are difficult to dope due to native defects. When the enthalpy for defect formation is lower than the band gap energy, the probability of generating a defect increases with the bandgap, i.e., the energy released by donor-to-acceptor transition. Particularly for GaN, MOCVD grown material is commonly n-type, and N-vacancy was long believed to be the dominant donor. Many attempts have been made to avoid N-vacancy formation by growing GaN at high pressures and high temperatures [25,26]. Efficient n-type doping of GaN through incorporation of Si during the growth proved relatively easy to achieve. High doping can also be achieved by implanting Si or Group VI donors. Recently, Burm et al. [27] have shown a shallow Si implant at high dose to produce a doping density of 4×10^{20} cm^{-3} resulted in an extremely low Ohmic contact resistance of 4×10^{-8} $\Omega\cdot cm^2$ using Ti/Au contacts.

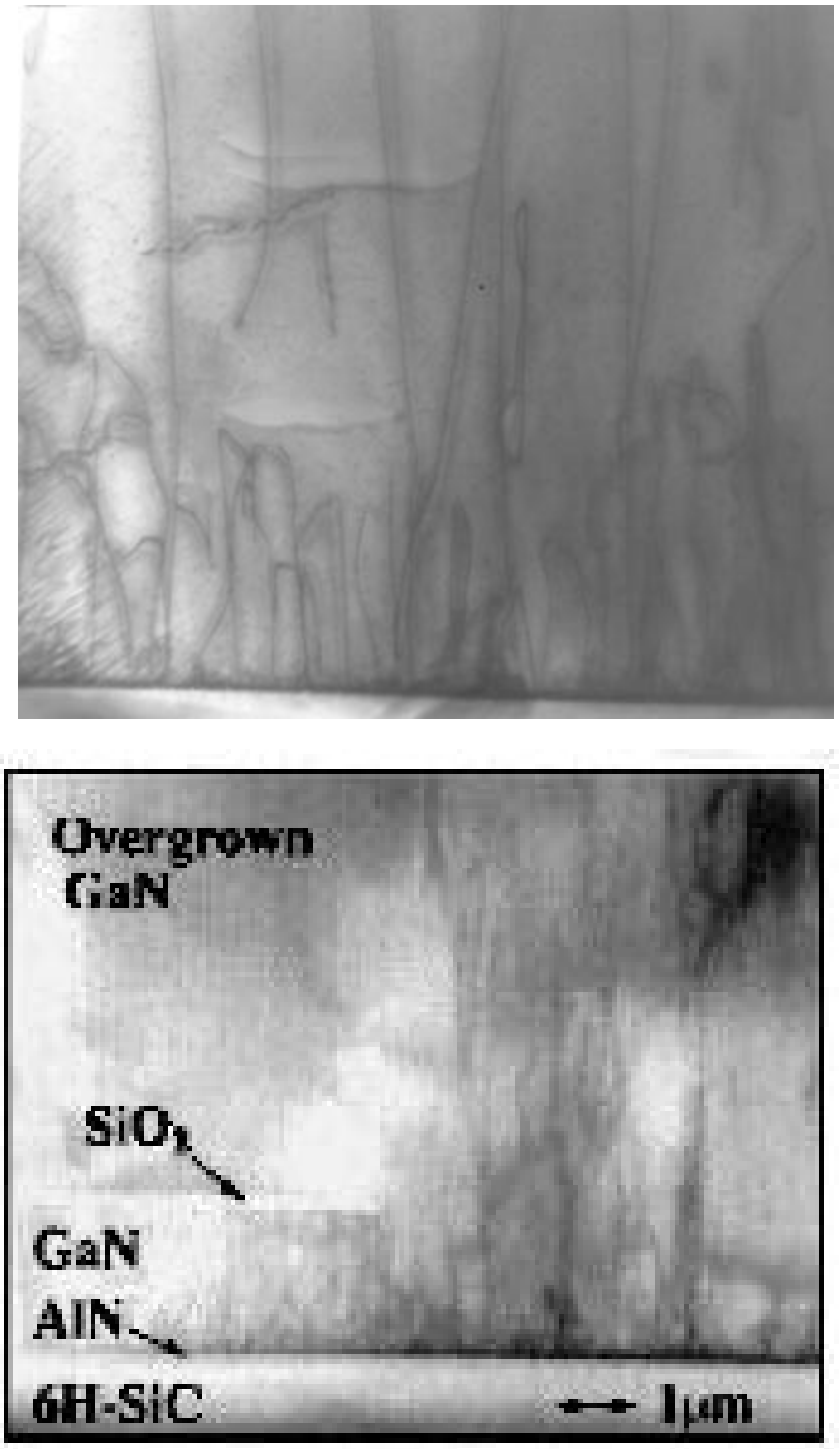

Figure 1-3 Cross-section TEM of typical MOCVD grown GaN using a AlN buffer on Sapphire (left) and typical LEO GaN (right, after [24]).

Since conductivity is proportional to the product of carrier concentration and Hall mobility, another goal for GaN used in device applications is to obtain the highest Hall mobilities possible [28,29]. As can be seen, the experimental data are roughly half of the calculated value, possibly due to significant scattering from impurities and defects in the state-of-the-art materials.

The III-V nitrides are expected to be made p-type by substituting Column II elements such as Zn, Mg Be and Ca on Ga sites to form single acceptors. However, all of these divalent elements form deep acceptors, the shallowest being Mg with an ionization level of 0.17 eV which is still many kTs above the valence bandedge of GaN [30]. At this acceptor level, one should only expect <10% of the Mg atoms to be ionized at room temperature, which means the Mg concentration needs to be approximately two orders of magnitude larger than the desired hole concentration. When MOCVD is used as the growth method, it has been difficult to obtain p-type conductivity. It was later found that hydrogen plays a crucial role in passivating the Mg acceptors, and creates a neutral complex Mg-H that prevents the formation of holes in GaN [31]. It was first shown by Amano et al. [32] that p-type conductivity could be achieved by activating Mg-doped GaN using low-energy electron irradiation. Nakamura then showed that the activation of Mg can also be realized by thermal annealing at ~700ºC [33]. Note that MBE grown GaN doped with Mg may be p-type without a thermal activation process, because of the absence of hydrogen and H-N radicals during growth. In addition, p-type doping was also achieved by implant of Ca or Mg into GaN, followed by high-temperature annealing (~1100 ºC) [34,35]. The highest hole concentration reported so far is ~10^{18} cm^3, and the typical hole mobility is very low, often 10 $cm^2/V{\cdot}s$ or below, but allowing the realization

of p-n junctions. Achieving low-resistance Ohmic contacts to the GaN layers with poor p-type doping concentrations has proven troublesome. Recently, Brandt et al. [36] found that by compensating Be with O, a neutral dipole is formed that does not scatter the holes. Hence a record high hole mobility of 150 $cm^2/V \cdot s$ was obtained. This may be the ideal contact layer for GaN based devices.

1.2 Gallium Nitride-Based Optoelectronic and Electronic Devices

1.2.1 Gallium Nitride-Based Optoelectronic Devices

The current level of the progress in the development of GaN commercially viable devices, namely GaN based-LEDs, LDs and UV detectors, has been the direct result of the realization of high-quality layers of GaN, AlGaN, InGaN, and relatively recent achievement of p-type conduction in GaN. The first p-n junction LED was demonstrated by Amano et al. [32] in 1989. Then, Nichia Chemical Industries announced the commercial availability of blue LEDs with high efficiency and luminous intensities over 1 cd [22]. Since then, high-brightness single quantum-well structure blue, green, and yellow InGaN LEDs with luminous intensities above 10 cd [37,38] have been commercialized. In 1996, Nakamura et al. [39] reported the first current-injection GaN-based LDs with separate confinement heterostructure, and subsequently achieved continuous-wave (CW) lasing at room temperature [40]. Figure 1-4 shows the cross-section of a nitride-based laser diode. The active layer is an InGaN multiquantum well with a large number of well layers. Gallium nitride (GaN) and AlGaN were used as the waveguide and cladding layers, respectively. The mirror facet was formed by numerous methods, including dry etching, polishing or cleaving.

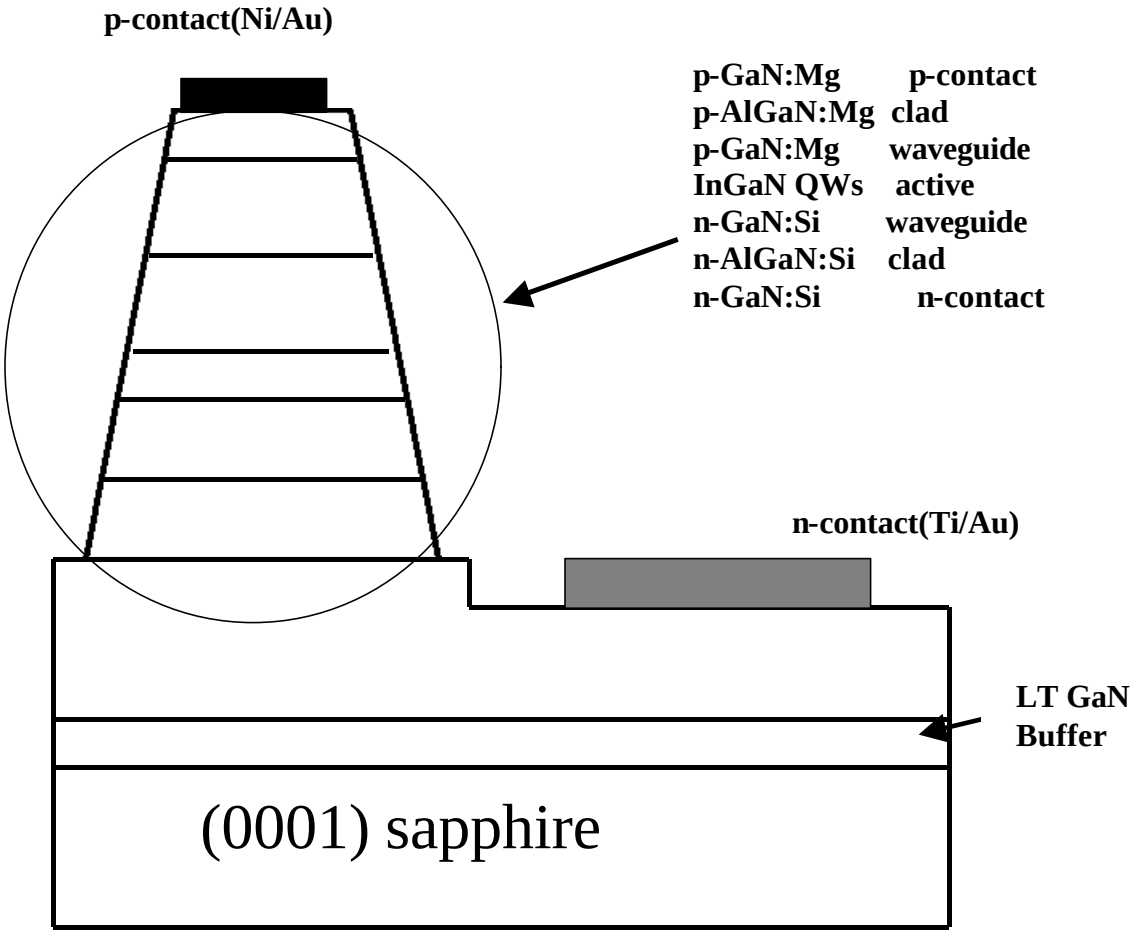

Figure 1-4 Cross-sectional view of a typical structure of GaN-based laser diode.

Surprisingly, the high-density dislocations resulting from the heteroepitaxial growth on sapphire in these optical devices did not appear to be efficient non-radiative centers, as they are in other III-V materials. However, the crystalline defects do affect device reliability. Nichia used the LEO growth technique for their blue LDs and achieved an increase in device lifetime from a few hundred hours to an estimated 10,000 h [41]. Another major problem limiting diode performance is high specific contact resistance of

Ohmic contact on the p-GaN side of the junction. Present lateral GaN lasers suffer significant IR drops due to poor p-type doping and Ohmic metallization.

1.2.2 Gallium Nitride-Based Electronic Devices

The nitride material growth technology that supports the optical device efforts has also proven to be compatible with the development of electronic devices. In the past several years, the electronic device development has emphasized field effect transistor (FET) structures, because this important class of devices places smaller demands on the growth and fabrication technique compared to bipolar transistors. The rapid progress that has been made, especially in modulation-doped FETs (MODFETs), has been sufficient to show that GaN and related alloys will play a significant role in the future development of high temperature, high power and high-frequency electronic devices [42-45].

GaN-based transistors have a unique combination of high current density, high breakdown electric field, and good thermal conductivity, that enable previously unrealizable microwave power performance for solid state transistors. For microwave transistor performance, two figures of merit (FOMs) have been developed for comparing the inherent semiconductor material capabilities. These FOMs are Johnson's FOM $(\nu_{sat}E_C)^2$ and the Baliga's high frequency FOM (μE_C^2), where E_C is the critical breakdown field, ν_{sat} is the electron saturation velocity , and μ is the low field electron mobility. Fig. 1-5 shows these figures of merit normalized to silicon for all the potential microwave semiconductor materials. The FOM comparison clearly shows the advantage of the GaN material system [46].

Figure 1-6 shows a GaN/AlGaN heterostructure. Due to the large conduction band discontinuity, the electrons diffusing from the large bandgap AlGaN into the smaller

bandgap GaN form a two-dimensional electron gas (2DEG) in the triangle quantum well at the interface, which is the hallmark of MODFET. The sheet carrier density of the 2DEG was found to be further enhanced by the strong pizeoelectronic effect in GaN. Pizeoelectronic coefficients in nitrides were measured to be about an order of magnitude higher than in traditional Group III-V semiconductors [47]. Theoretical simulations have predicted a high peak electron velocity of ~3×10^7 cm/s [29] and an electron mobility of ~2000 $cm^2/V{\cdot}s$ in the GaN channel at room temperature at a carrier concentration of 10^{17} cm^{-3} [48]. Gaska et al. [8] found the highest measured Hall mobility at room temperature was 2019 $cm^2/V{\cdot}s$, and increased approximately fivefold to 10,250 $cm^2/V{\cdot}s$ below 10 K for growth on 6H SiC substrate.

In 1993, Khan et al. [42] demonstrated the first AlGaN/GaN MODFET, with a g_m of 23 mS/mm and 2DEG mobility of 563 $cm^2/V{\cdot}s$ at 300 K. They also reported the first microwave results with f_t of 11 GHz and f_{max} of 14 GHz [43]. In the early stages, the MODFETs exhibited very low transconductances and relatively poor frequency response. This is consistent with the defect-laden nature of the early GaN and AlGaN layers. With improvements in the materials quality, the transconductance, current capacity, and drain breakdown voltage are all increased to the point that GaN-based MODFETs are now strong contenders in the arena of high-power devices and amplifiers. To date, the highest power density achieved for a 0.45×125 μm GaN MODFET is 6.8 W/mm at 10 GHz and associated gain of 10.65 dB. The operation temperature has been pushed to 750ºC by employing a thermally stable Pt/Au gate contact [45].

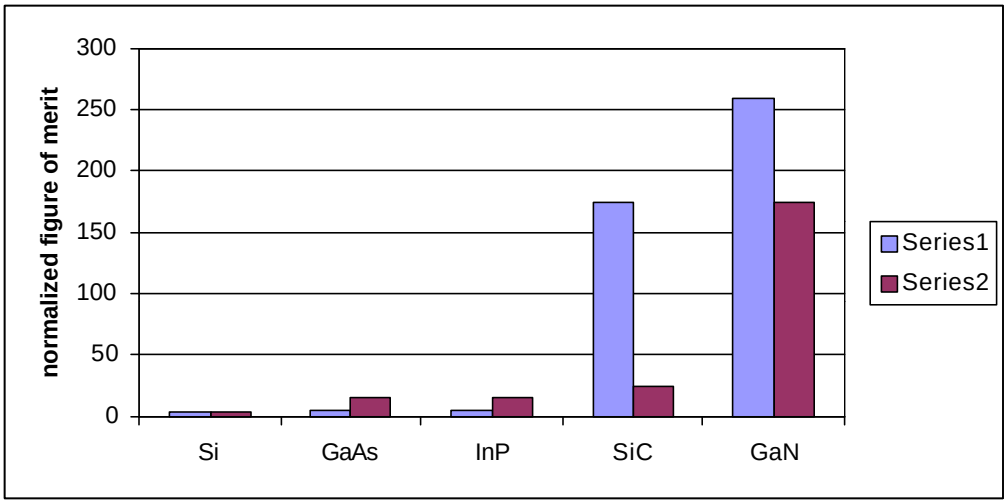

Figure 1-5 Johnson's (series 1) and Baliga's (series 2) high frequency figure-of-merit normalized to silicon.

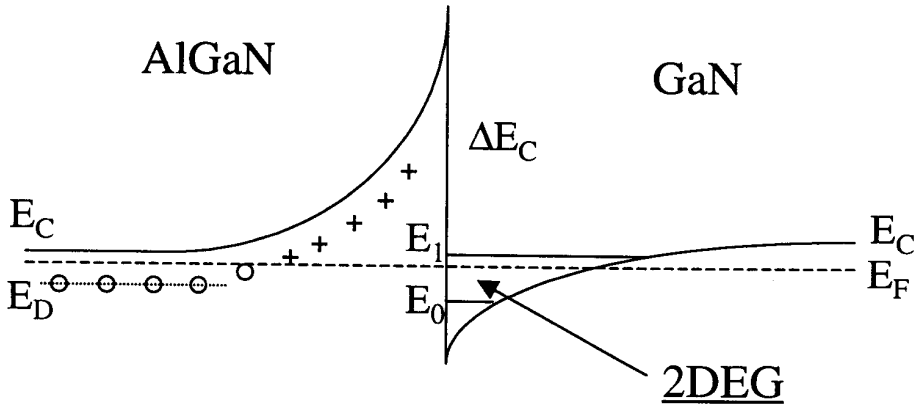

Figure 1-6 Conduction band structure of a modulation-doped structure.

The published performances of epitaxial GaN-based MESFETs show that all the required components for a MESFET-based technology are in place [49, 50]. That is, an appropriate high resistivity buffer and substrate combination has been developed for doped layer epitaxial growth, FET channels can be grown with thin n^+ contact layers on which Ohmic contact with adequate contact resistances have been achieved, gate metallizations that can pinch off the channel and support a high drain bias have been demonstrated, and it has shown that both mesa etch and implant isolation can be used to define the active device area. Recently, an all implanted GaN junction FET, an Si_3N_4 gated GaN MISFET [52], and a Ga_2O_3 (Gd_2O_4) gated GaN MOSFET with reasonable performance were also reported. These types of devices potentially have an advantage over MESFET, especially at high temperatures due to low reverse leakage currents.

So far, few reports exist on development of GaN-based bipolar transistors [54,55]. Basically the device performance is limited by the difficulty in growth and processing related to the buried p-type layer and the small minority carrier lifetime. It is still far from commercialization of these devices, but their developments will follow the material improvements in the new decade, and much impetus comes from defense applications where ultrawide bandwidth and linearity are desired.

Group III-V nitrides offer a valuable combination of electrical, optical and pizeoelectrical behavior, and enable the fabrication of LEDs, LDs, detectors, and transistors. In the past, the poor quality of the materials, the lack of p-type doping, and the absence of reliable processing procedures thwarted engineers and scientists from fabricating these useful devices. However, the 1990s have brought significant advances in the sophistication of growth techniques, the purity of the chemicals used for film

deposition, the controlled introduction and activation of selected impurities, and progress in processing techniques. Most of the aforementioned obstacles have been sufficiently overcome, and the electronic and optical devices have been demonstrated and partially commercialized. Market projections show that GaN-based blue and green LEDs will represent most of the estimated US$ 3 billion per year GaN-based device market by 2006. In transistors, GaN can go where no other semiconductors have gone before. The future development in this area will definitely be fueled by the increasing demand for high-temperature, high-power applications. From materials science to device engineering, from laboratory research to commercial products, III-V nitride technologies have shown a late but exciting development.

CHAPTER 2
GALLIUM NITRIDE-BASED DEVICE PROCESSING

While further improvements in the III-V nitride materials quality can be expected to enhance device operation, further device advances will also require improved processing technology. Owing to their wide bandgap nature and chemical stability, GaN and related materials present a host of device processing challenges, including poor p-type doping (by implantation), difficulty in achieving reliable low-resistance p-Ohmic contacts, high temperatures needed for implant activation, lack of efficient wet etch process, generally low dry etch rates and low selectivity over etching masks, and dry etch damage. These problems constitute a major obstacle to successful demonstration and commercialization of some GaN-based devices, such as bipolar transistors and power switches, whose performance are much more affected by the immature fabrication techniques. To fully exploit these device applications, a number of critical advances are necessary in the areas of implantation doping and isolation, high-temperature thermal processing, Ohmic contact to p-type material, dry etching process, and device passivation. The current state-of-the-art results on advanced GaN processing were have been reviewed [8]. In this chapter, the results from Cl_2/Ar high density inductively coupled plasma damage in GaN Schottky diodes and N_2 inductively coupled plasma discharge treatment on n-AlGaN/GaN Ohmic contacts will be presented.

2.1 Chlorine/Argon (Cl_2/Ar) High Density Inductively Coupled Plasma damage in GaN Schottky Diodes

2.1.1 Introduction

Precise pattern transfer during fabrication of GaN-based devices requires use of dry etching methods with relatively high ion energy in order to break the strong Ga-N bonds (8.92 eV/atom) [56]. Under those conditions generally some ion-induced damage remains in the GaN after dry etching, along with the possibility of a non-stoichiometric near-surface region due to preferential loss of atomic nitrogen in the form of N_2 [57-59]. The Ga etch product in Cl_2-based discharges is $GaCl_3$, and this is less volatile than N_2 both from a pure chemical vapor presence and from a preferential sputtering viewpoint.

There has been relatively little work on understanding the effects of plasma processes on the electrical characteristics of GaN. Exposure to pure Ar discharges was found to produce higher reverse-bias leakage currents in p-n junction structures compared to use of Ar/N_2 discharges [60]. Even relatively low power reactive ion etching (RIE) conditions were found to deteriorate the quality of Schottky contacts deposited on plasma-etched n-GaN [61,62]. The preferential loss of nitrogen from the GaN surface does improve the specific contact resistance of n-type ohmic contacts because of the creation of a degenerately doped surface layer [63], but may increase the average sheet resistance of the GaN. Previous results have shown that exposure of GaN to H_2 or N_2 Inductively Coupled Plasmas (ICP) prior to deposition of Schottky contacts creates a damaged region ~500 Å deep that can be essentially restored to its original characteristics by annealing at 750 °C. There are also situations where GaN device structures use a metal contact as a self-aligned etch mask. In this case it is of interest to examine the effects of plasma exposure on samples with existing Schottky contacts.

2.1.2 Experimental Methods

GaN Schottky devices already have the contacts in place. The degradation of reverse breakdown voltage (V_B) and Schottky barrier height (ϕ_B) was strongly dependent on the incident ion energy and flux. Both annealing and UV ozone treatment were employed to try to remove the plasma damage.

Planar diodes were fabricated on nominally undoped ($n \sim 10^{17}\ cm^{-3}$) GaN layers ~3 μm thick grown on an n^+ ($10^{18}\ cm^{-3}$) GaN buffer on a c-plane Al_2O_3 substrate [64]. Ohmic contacts were formed with lift-off Ti/Au subsequently annealed at 600 °C, followed by evaporation of the 250 μm diameter Pt(250 Å)/Au(1500 Å) Schottky contacts through a stencil mask.

The samples were briefly exposed (~10secs controlled by the system software) to $10Cl_2/5Ar$ (total gas load 15 standard cubic centimeters per minute) ICP discharges in a Plasma Therm 790 reactor. During the ignition stage of the discharge, the dc self-bias takes ~2 secs to reach its final value. From limited measurements we found that damage saturates in this time frame. The gases were injected directly into the source through electronic mass flow controllers, and the 2MHz source power was varied from 100-1000 W. The samples were placed on an rf-powered (13.56 MHz, 5-300 W), He backside-cooled chuck. Process pressure was hold constant at 2 m Torr.

The current-voltage (I-V) characteristics of the diodes were recorded on a HP 4145A parameter analyzer. Barrier heights (ϕ_B) and ideality factors (n) accurate to ±5% were obtained from the forward I-V characteristic according to the relationship [1]:

$$J = A^{**}T^2 \exp\left(\frac{e f_B}{kT}\right)\left[\exp\left(\frac{eV}{nkT} - 1\right)\right] \qquad 2\text{-}1$$

Where J is the current density, A** the effective Richardson constant, T the measurement temperature (25 °C), e the electronic charge and k is Boltzmann's constant. The reverse breakdown voltage (V_B) was defined as the voltage at which the current density was 3.06×10^4 mA/cm^2 (i.e. a current of 15 mA).

Some diodes were annealed at temperatures up to 800 °C for 30 secs under N_2 after plasma exposure, while others were treated in UV-ozone at 25 °C for periods up to 20 minutes in a Jelight 200S system, followed by rinsing in HCl solutions. Auger Electron Spectroscopy (AES) was performed in some cases on blanket (unmetallized) samples.

2.1.3 Results and Discussion

Figure 2-1 shows some typical I-V characteristics from GaN diodes after exposure to the ICP Cl_2/Ar discharges at fixed ICP source power and varying rf power. The latter parameter controls the average energy of ions (predominantly Ar^+ and Cl_2^+ in this case) incident on the samples. There is a clear degradation in V_B as this rf chuck power is increased. Control diodes not exposed to the plasma had I-V characteristics that were similar to curves 1 and 2, with V_B of 38 V and ϕ_B of 0.82 eV.

The dependence of V_B and ϕ_B on rf chuck power is shown in the upper part of Figure 2-2. Both of these parameters, at least initially, decrease with increasing power. The ϕ_B values saturate beyond 50 W. The main effect on ϕ_B is from damage created around the contact periphery. This would expected to saturate once a N_2-deficient region

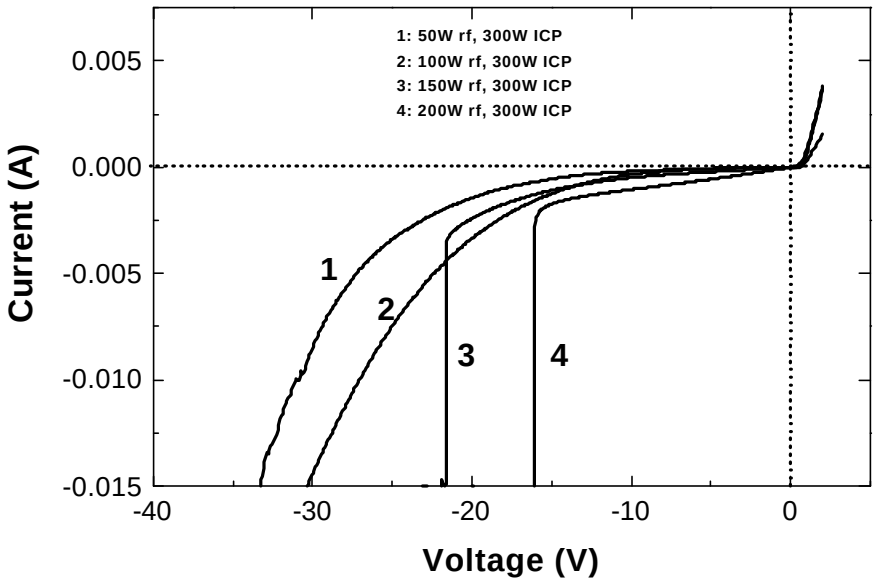

Figure 2-1 I-V characteristics from GaN diodes after Cl_2/Ar plasma exposure (300W source power, 2m Torr) with different rf

is created because much of the resultant ϕ_B is still determined by the unexposed region under the contact metal. Under these conditions, the dc chuck self-bias increases from -105 V at 50 W to -275 V at 200 W. The average ion energy is roughly the sum of this voltage plus the plasma potential which is 20-25 V in this system under these conditions. After plasma exposure, the diode ideality factor was always ≥2, which is a further indication of the degradation in electrical properties of the structures. The results are consistent with creation of an ion damaged, non-stoichiometric GaN surface region. This region exists in the plasma-exposed area outside the metal contacts. Note that the GaN etch rate increases monotonically with rf chuck power (Figure 2.2, bottom), but this more rapid removal of material is not enough to offset the greater amount of damage caused by the higher-energy ion bombardment. We believe the GaN must be non-stoichiometric and

hence more n-type at the surface because of the sharp decreases observed in V_B. In the case of semiconductors such as GaAs where ion bombardment creates more resistive material by introduction of deep compensating levels rather than shallow donor states, the breakdown voltage is generally found to increase with exposure to plasmas [65-67].

The dependence of V_B and ϕ_B on ICP source power is shown in Figure 2-3 (top). While ϕ_B continues to decrease as the ion flux increases, V_B initially degrades but shows less of a decrease at higher source powers (Figure 2-3, bottom). This is most likely a result of the continued decrease in the self-bias at higher source power. This also leads to a decrease in GaN etch rate above 500 W. The results of Figure 2-2 and 2-3 show that both ion energy and ion flux are important in determining not only the GaN etch rate, but also the amount of residual damage in the diodes.

As mentioned previously, past measurements on ICP damaged GaN surfaces have established the damage depth as being of order 500 Å. One method for trying to remove the damaged material between the contacts is by oxidizing it by UV/ozone (O_3) exposure, followed by stripping of the oxide. Figure 2-4 shows the dependence of V_B and ϕ_B on UV ozone treatment time. In each case after the oxidation, a 1:20, HCl: H_2O solution was used for removal of the oxidized material. While there is some improvement in both parameters up to 5 min, there is no further improvement for longer times. We assume the oxidation distance is diffusion-controlled (i.e. dependent on $\sqrt{t}$), and from preliminary measurements we believe that only ~30 Å of GaN is oxidized and removed for 5 minute UV ozone exposure. Therefore the process would have to be repeated approximately 15-20 times to remove the damaged region of the GaN, assuming the oxidation rate remains

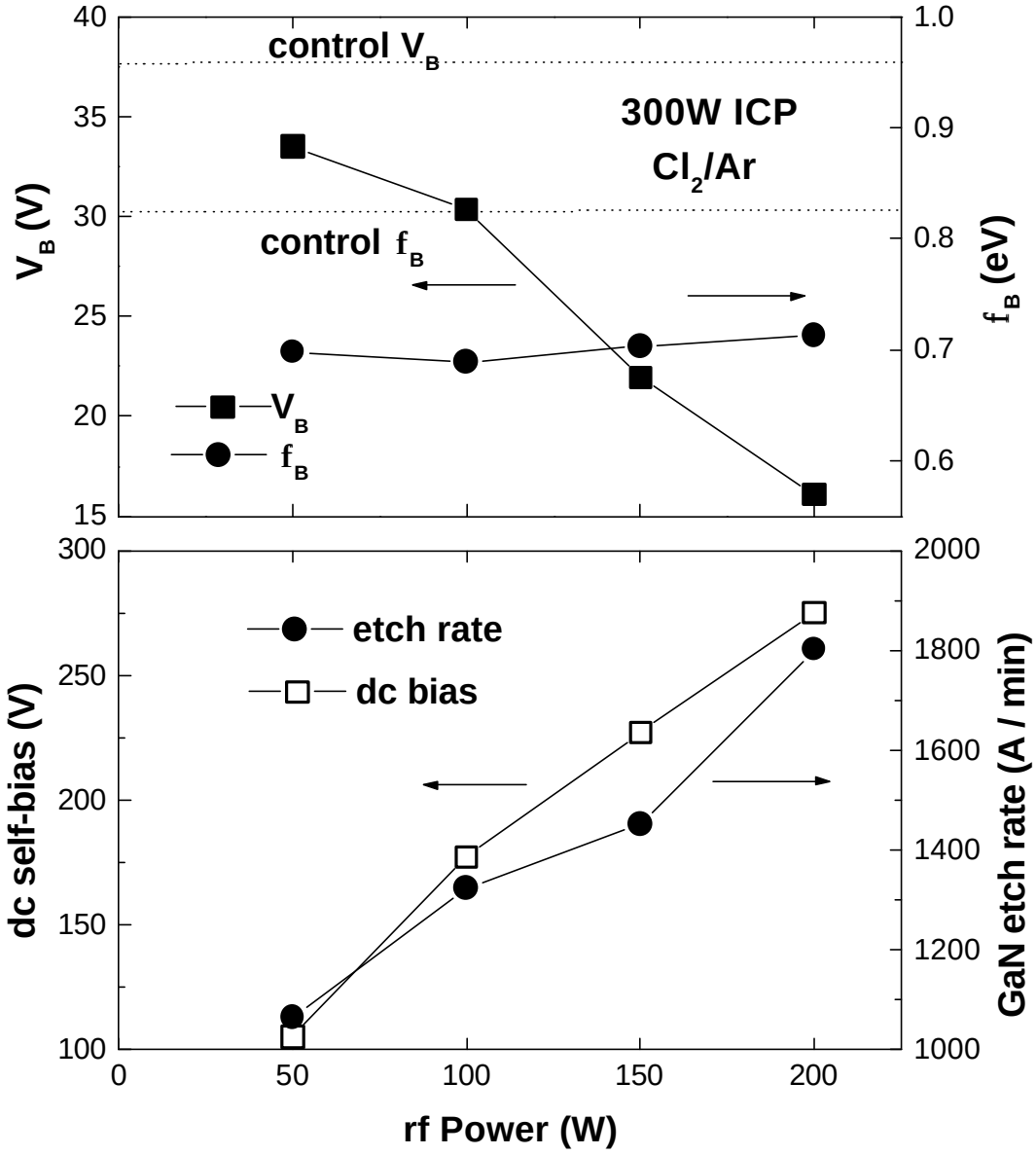

Figure 2-2 rf chuck power dependence of V_B and ϕ_B in Cl_2/Ar plasma exposed GaN diodes (top) and of dc chuck self-bias and GaN etch rate under the same conditions (bottom)

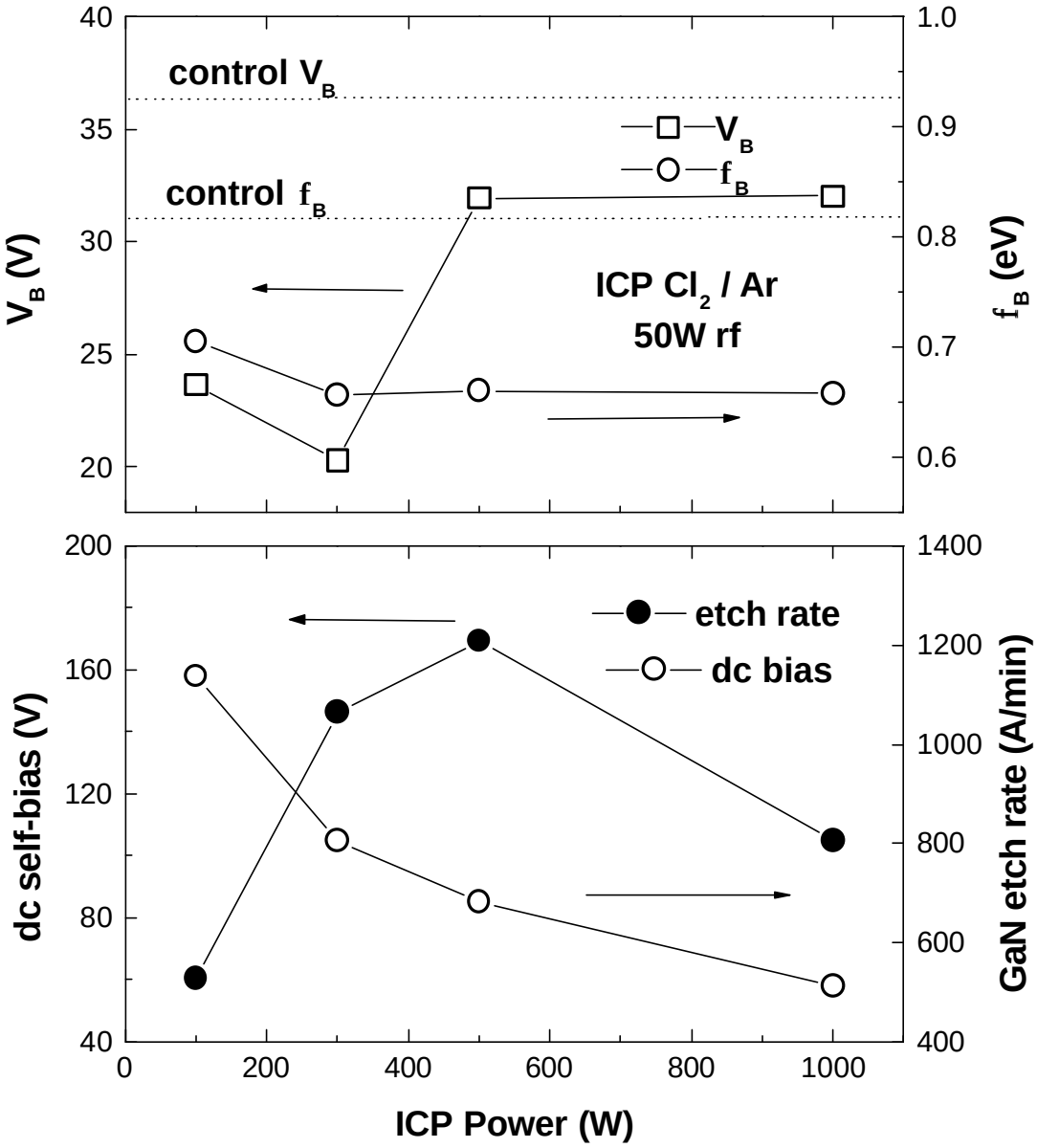

Figure 2-3 ICP power dependence of V_B and ϕ_B in Cl_2/Ar plasma exposed GaN diodes (top) and of dc chuck self-bias and GaN etch rate under the same conditions (bottom)

the same deeper into the material. Use of a stronger HCl solution improves the V_B value compared to use of the 1:20 solution (Figure 2-5), but there is no improvement in ϕ_B. We emphasize that the damaged GaN is the exposed region outside the contact area. This will lead to reductions in V_B by increasing the surface conductivity and degrade ϕ_B by incr easing leakage current at the contact periphery.

Figure 2-6 shows the effect of anneal temperature on the recovery of V_B and ϕ_B. There is a clear improvement in V_B for anneals in the range 500-700 °C, and little change thereafter and it remains lower than the unetched control value. However, ϕ_B changes very little with annealing. These results are somewhat different than in the case where the surface is exposed to the ICP discharge, annealed and then the Schottky contact is deposited. For that sequence, essentially full recovery of the electrical characteristics was obtained for 750 °C annealing. In the present case where the contact is in place we believe the metal begins to react with the GaN at ~600 °C, accounting for the lack of recovery of ϕ_B at higher temperatures.

The effect of annealing time at fixed temperature (700 °C) on V_B and ϕ_B is shown in Figure 2-7. The improvement in both parameters is saturated beyond 60 secs. It would be expected that the recovery mechanism should be most critically dependent on temperature since most defect annealing processes involve dissociation and diffusion of defects and their complexes. In this case, the recovery would be dependent on the square root of annealing time and exponentially on temperature.

To establish the chemical state of the GaN surface at different stages, AES was performed on an unmetallized sample. Figure 2-8 shows surface scans before (top) and

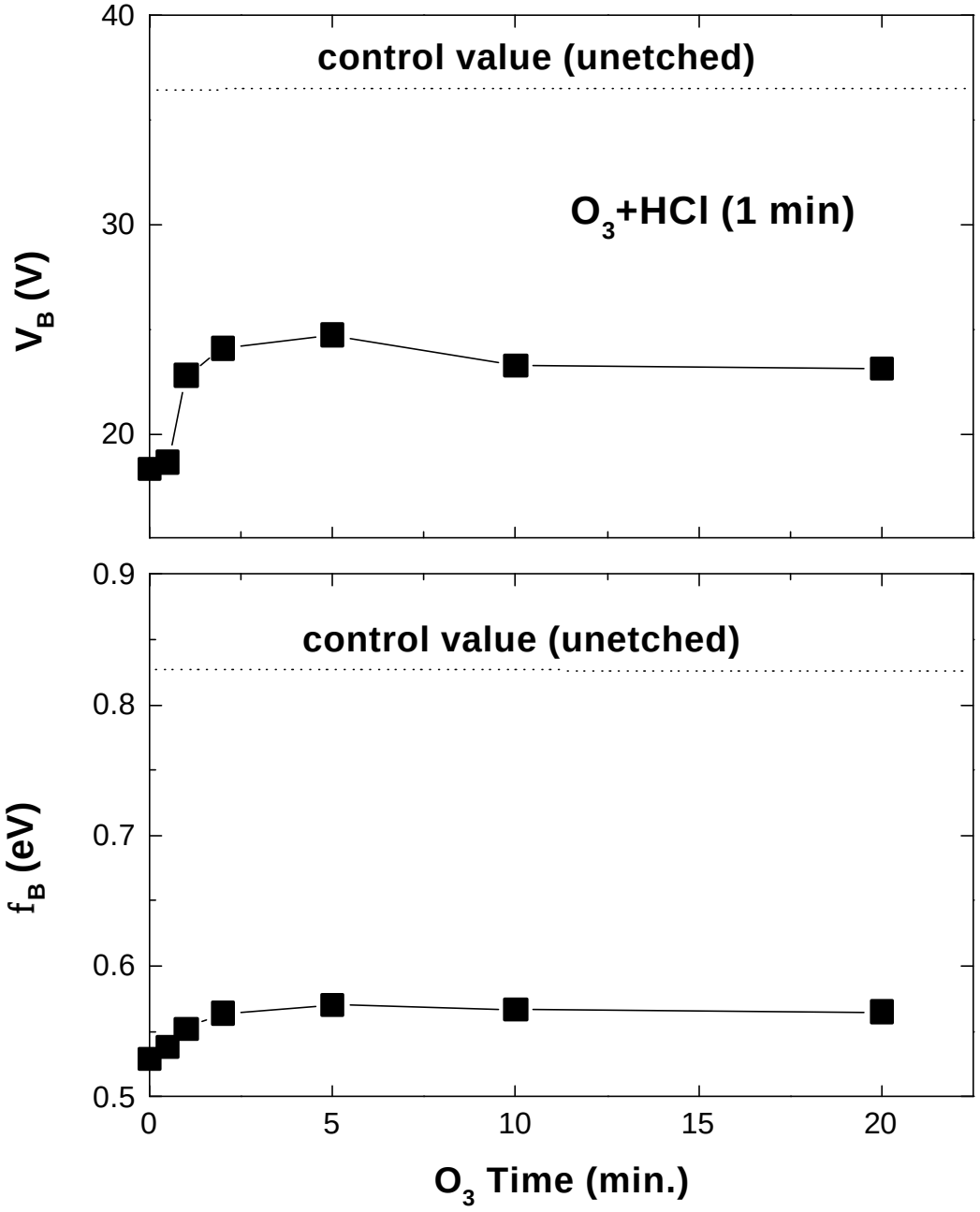

Figure 2-4 UV ozone oxidation time dependence of V_B (top) and ϕ_B (bottom) in Cl_2/Ar plasma exposed GaN diodes. After oxidation, the samples were rinsed in 1HCl: 20H_2O for 1 min.

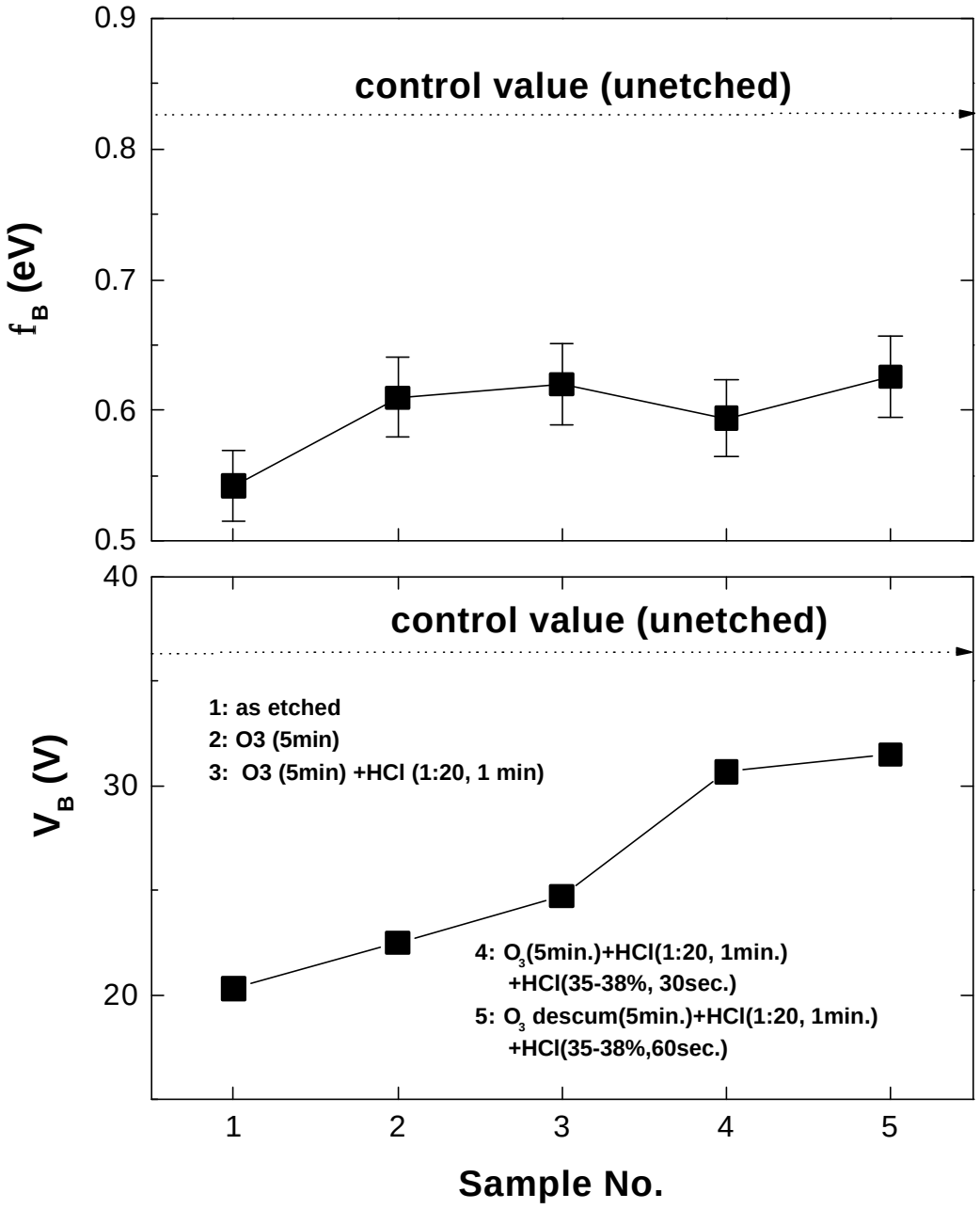

Figure 2-5 Dependence of V_B (top) and ϕ_B (bottom) on process condition in Cl_2/Ar plasma exposed GaN diodes. After UV ozone oxidation, the samples were rinsed in 1HCl: $20H_2O$ for 1 min or aqueous HCl (35-38%) for 30-60 seconds.

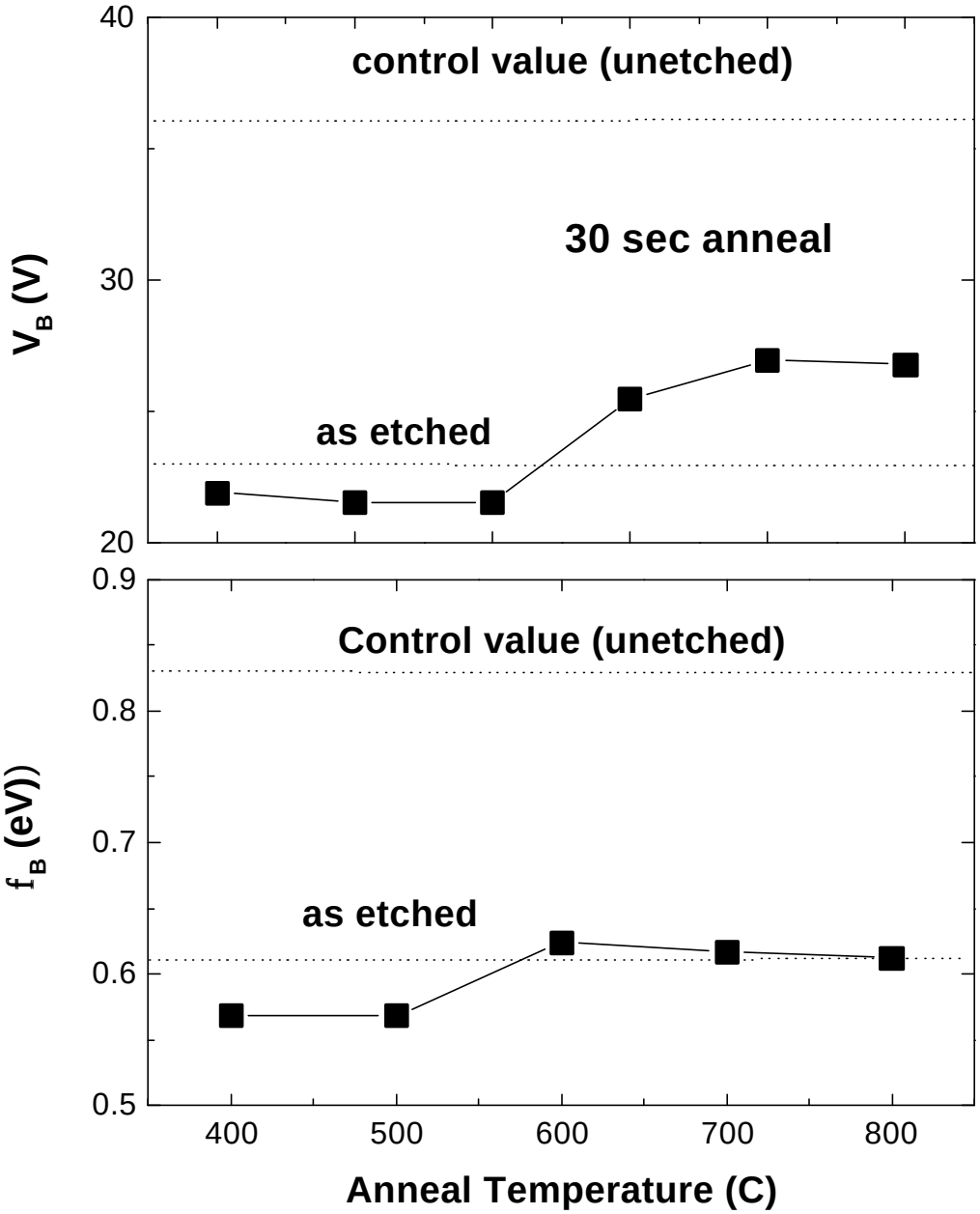

Figure 2-6 Annealing temperature dependence of V_B (top) and ϕ_B (bottom) in Cl_2/Ar plasma exposed GaN diodes. Anneal time was 30 sec at each temperature.

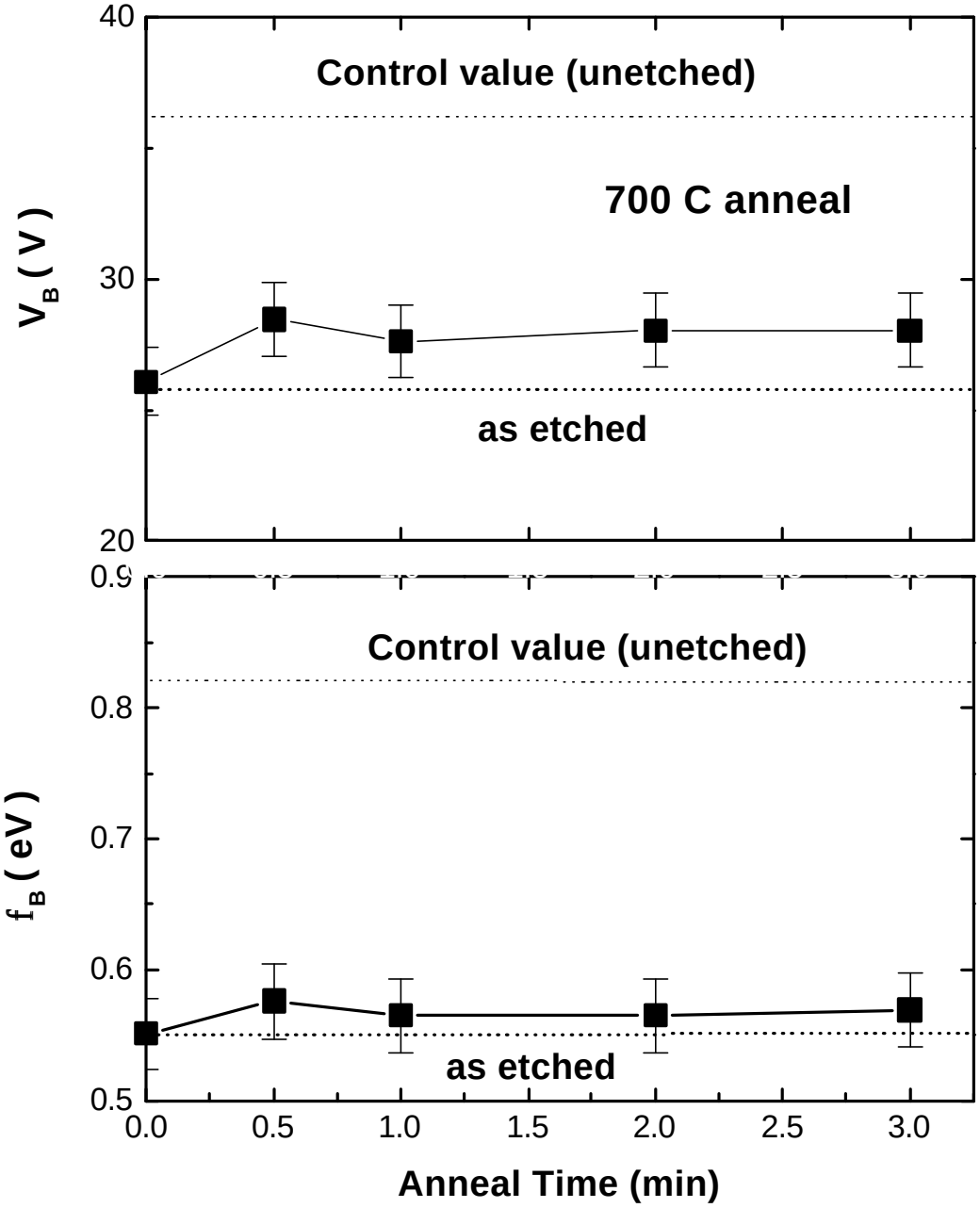

Figure 2-7 Annealing time dependence (at 700 °C) of V_B (top) and ϕ_B (bottom) in Cl_2/Ar plasma exposed GaN diodes.

after (lower) exposure to a 500 W source power, 50 W chuck power Cl_2/Ar discharge. The main change is a reduction in the N_2 signal in the latter sample (by ~20%), confirming the preferential loss of this element during dry etching. Subsequent annealing at 700 °C in N_2 restored some of this deficiency (Figure 2-8, bottom).

2.1.4 Summary and Conclusion

The main points of our study may be summarized as follows:

- ICP Cl_2/Ar discharges degrade the performance of GaN Schottky diodes, with ion energy and ion flux both playing important roles.
- UV ozone oxidation of the surface and subsequent dissolution of the oxidized region in HCl provides some restoration of the electrical properties of the GaN.
- Annealing at 700 to 750 °C also restores some of the initial reverse breakdown voltage characteristics, but little change in ϕ_B for Pt/Au contacts on GaN.
- The degradation mechanism appears to be creation of a conducting, non-stoichiometric (N_2-deficient) near-surface region on the GaN.

2.2 Effect of N_2 Inductively Coupled Plasma Discharge Treatment on n-AlGaN/GaN Ohmic Contacts

2.2.1 Introduction

Both the dc and rf performance of AlGaN/GaN High Electron Mobility Transistors (HEMTs) are strongly dependent on the specific contact resistance of the source/drain contacts [68-77]. There have been four basic classes of metallization employed for n-type ohmic contacts to GaN-based materials, namely Al [78-80], Ti or

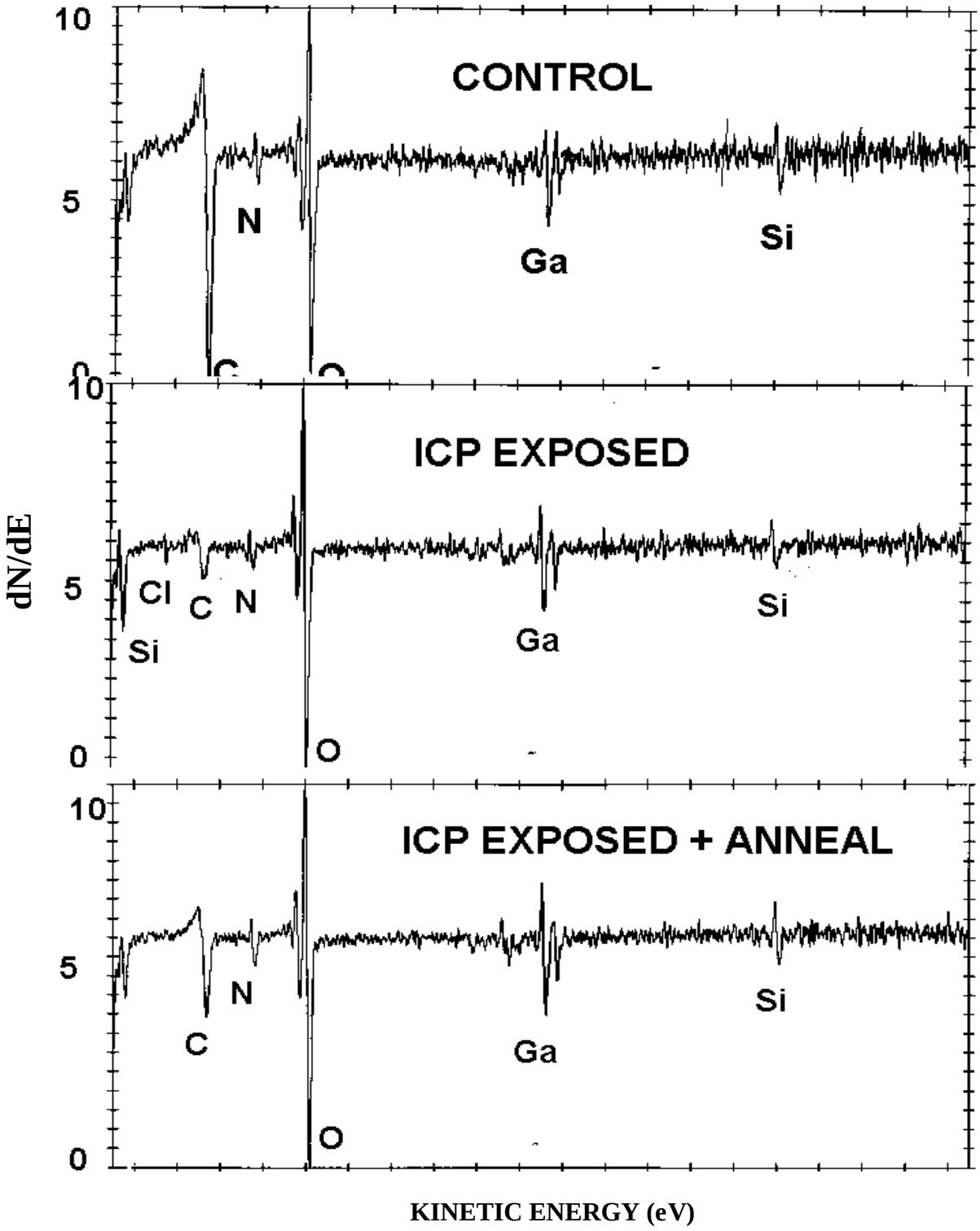

Figure 2-8 AES surface scans from GaN (top) or after (center) Cl_2/Ar plasma exposure, and subsequent annealing at 700 °C for 60 seconds (bottom).

TiN [81-86], W or other refractory metals [87-90] or multilayers such as Ti/Al/Ni/Au [91-93] which appear to give wider process windows by reducing oxidation of the Ti [91-93]. Modifications to the GaN by high temperature annealing [94] or reactive ion etching [91,95] to produce preferential loss of nitrogen can improve n-type ohmic contact resistance by increasing electron concentration in the near-surface region. In all cases, the best specific contact resistitity has been achieved after annealing the metallization at 900-950 °C [91,96,97].

We have previously found that exposure of n- or p- type GaN to high density Inductively Coupled Plasmas (ICP) degrades the rectifying properties of subsequently deposited Schottky contacts [98]. The degradation mechanism is loss of nitrogen, as described above. To this point, there have been no investigation of the effect of ICP exposure on the properties of n-type ohmic contacts, especially on HEMT structures where the contact resistivity can be high due to presence of AlGaN donor and contact layers. In this paper we report the results of a systematic study to understand the effect of ion energy, ion flux and exposure time of N_2 ICP discharges on the contact resistance of Ti/Al/Pt/Au metallization on AlGaN/GaN HEMTs.

2.2.2 Experimental Methods

The AlGaN/GaN structures were grown by rf plasma activated Molecular Beam Epitaxy on (0001) sapphire [99]. After nitridation of the surface, at low temperature, 300 Å thick AlN buffer was grown, followed by a 1 µm undoped GaN layer grown at 750 °C under Ga-rich growth conditions. This was followed with a 30 Å undoped $Al_{0.15}Ga_{0.85}N$ spacer layer, 100Å $Al_{0.15}Ga_{0.85}N$ donor layer (Si-doped, $n=10^{19}$ cm^{-3}) and a 100 Å undoped $Al_{0.15}Ga_{0.85}N$ cap layer. A schematic of the structure is shown in Figure 2-9.

Typical room temperature sheet electron densities were ~3.5×10^{12} cm^{-2}, with Hall mobilities of ~400 $cm^{-2}V^{-1}\cdot sec^{-1}$ [96].

The N_2 plasma exposures were carried out in a Plasma Therm 790 reactor, in which the ion flux is controlled by a 1500 W ICP source operating at 2 MHz, and the ion energy is controlled by rf power (13.56MHz) applied to the sample chuck. The N_2 gas was injected into the source at a total flow rate of 15 standard cubic centimeter per minute and process pressure was held constant at 2 m Torr. After plasma exposure, e-beam deposited Ti(200 Å)/Al(800 Å)/Pt(400 Å)/Au(1500 Å) was patterned by lift-off and annealed under N_2 in an AG associates Heatpulse 610T system. The specific contact resistance was obtained from Transmission Line Method (TLM) measurement using gap spacings of 2, 4, 8, 16 and 32 μm. In some cases the plasma exposed AlGaN/GaN structures were examined by Atomic Force Microscopy (AFM) and Auger Electron Spectroscopy(AES) for measurement of surface morphology and composition, respectively.

2.2.3 Results and Discussion

Figure 2-10 shows the measured contact resistances for the Ti/Al/Pt/Au metallization on unexposed (control) samples, as a function of post-deposition annealing temperature. We will use this data for comparison with the plasma-exposed samples. Note that a value of 7×10^{-3} $\Omega\cdot cm^2$ was obtained for 950°C annealing.

The effect of rf chuck power on contact resistance of the N_2 plasma exposed samples is shown in Figure 2-11. In this case the ICP source power was held constant at 300 W (equivalent to an ion flux of ~4×10^{16} $cm^{-2}\cdot sec^{-1}$). The lowest contact resistances were obtained for samples exposed at 40 W chuck power and subsequent annealed for

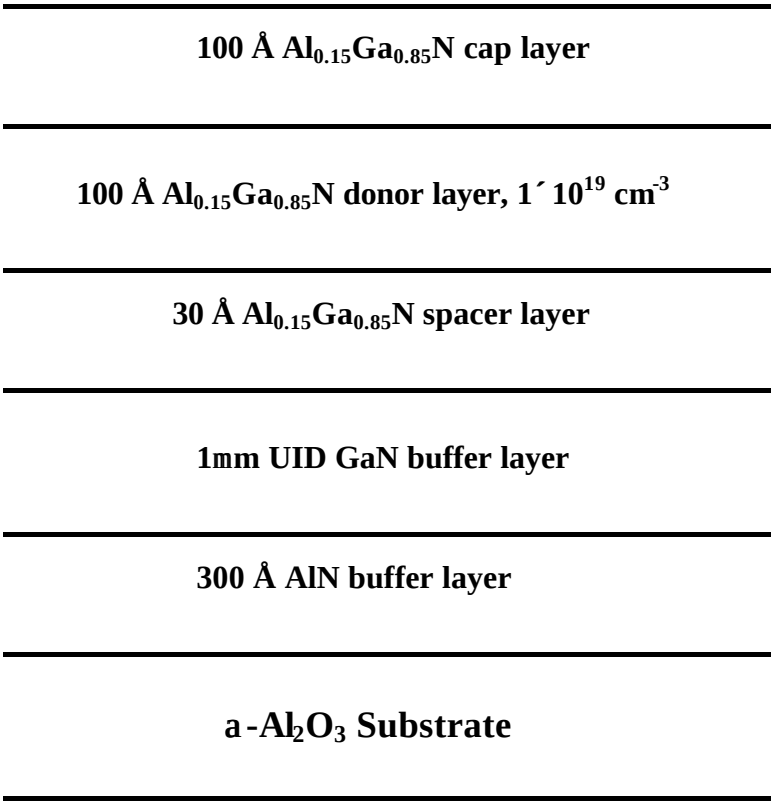

Figure 2-9 Schematic of AlGaN/GaN HEMT structure.

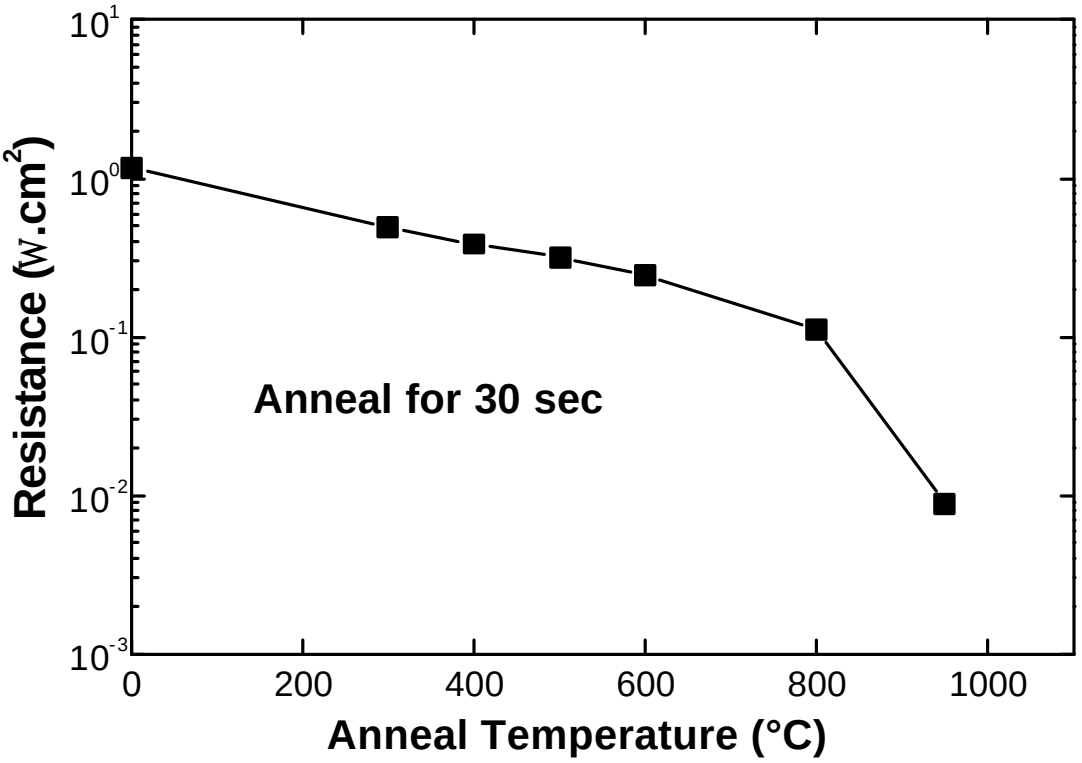

Figure 2-10 Contact resistance for Ti/Al/Pt/Au metallization as a function of annealing temperature for AlGaN/GaN structures not exposed to N_2 discharges prior to metal deposition.

30 sec at 950 °C, producing a value of 2×10^{-4} $\Omega\cdot cm^2$. This is approximately a factor of three improvement over contacts annealed at the same temperature on control samples. The ion energy at this condition is roughly -125 eV, the sum of the dc self-bias(lower part of Figure 3) and plasma potential (about –25 eV under these conditions).

We fixed the rf chuck power at 40 W and examined the effect of varying the ICP source power during the plasma exposure (Figure 2-12). For annealing at 800 or 950 °C, there is a broad minimum in contact resistance centered at 300 W source power. We believe that at lower powers the ion flux is too low to produce efficient preferential loss

of the nitrogen, while at higher fluxes there are large concentrations of defects created that degrade current transport in the AlGaN. Note that while flux increases with source power, the ion energy decreases slightly due to the higher plasma conductivity.

The improvement in contact resistance saturated with exposure time, as shown in Figure 2-13. This result is not unexpected, since part of the surface is removed by sputtering during plasma exposure and the creation of an N_2-deficient surface region will come to an equilibrium condition. The plasma exposure did not roughen the AlGaN surface, as shown by the AFM scans of Figure 2-14. The root-mean-square (RMS) roughness of the controlled sample was 1.3 nm, compared to 1.0 nm for the sample exposed to a 300 W source power, 40 W rf chuck power N_2 discharge for 30 secs. It is likely that at high chuck power, corresponding to high ion energies, surface roughening should be more prevalent.

To confirm that the mechanism for the contact resistance improvement was loss of nitrogen, we performed AES measurements. Surface scans before and after N_2 plasma exposure (300 W source power, 40 W rf chuck power, 30 sec) showed that the average composition of N in the top 100 Å of the surface dropped from 10% in the control sample to 7.1% in the plasma exposed sample (Figure 2-15). Scanning electron microscopy of the contact metallization showed good morphology and edge definition for both the control and plasma exposed samples.

2.2.4.Summary and Conclusion

ICP N_2 discharges were used to improve contact resistances on AlGaN/GaNHEMT structures by inducing preferential loss of nitrogen from the near-

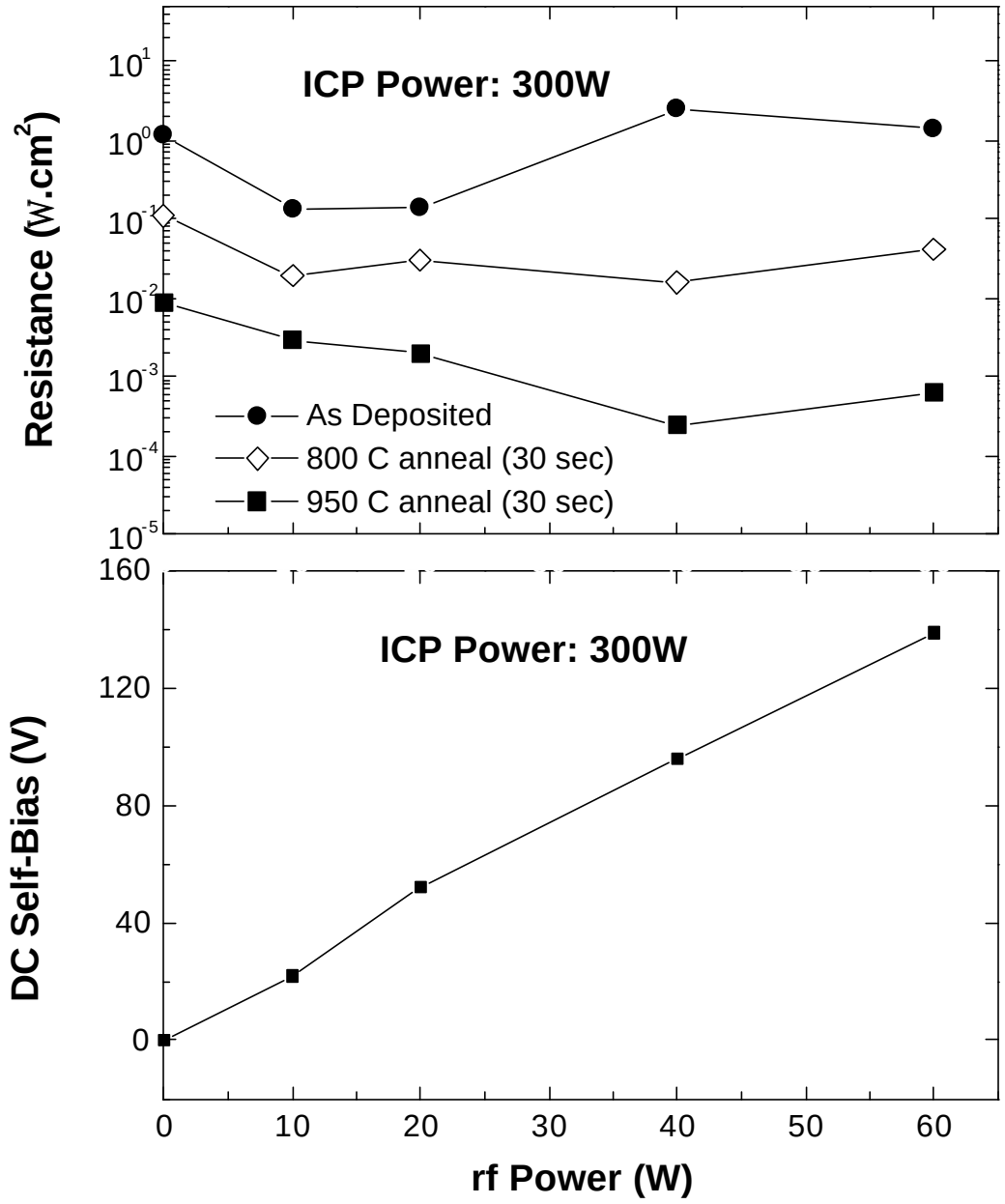

Figure 2-11 Contact resistance for Ti/Al/Pt/Au metallization as a function of rf chuck power for AlGaN/GaN structures exposed to ICP N_2 discharges prior to metal deposition, for several annealing temperatures (top) and dc self-bias as a function of rf power (bottom).

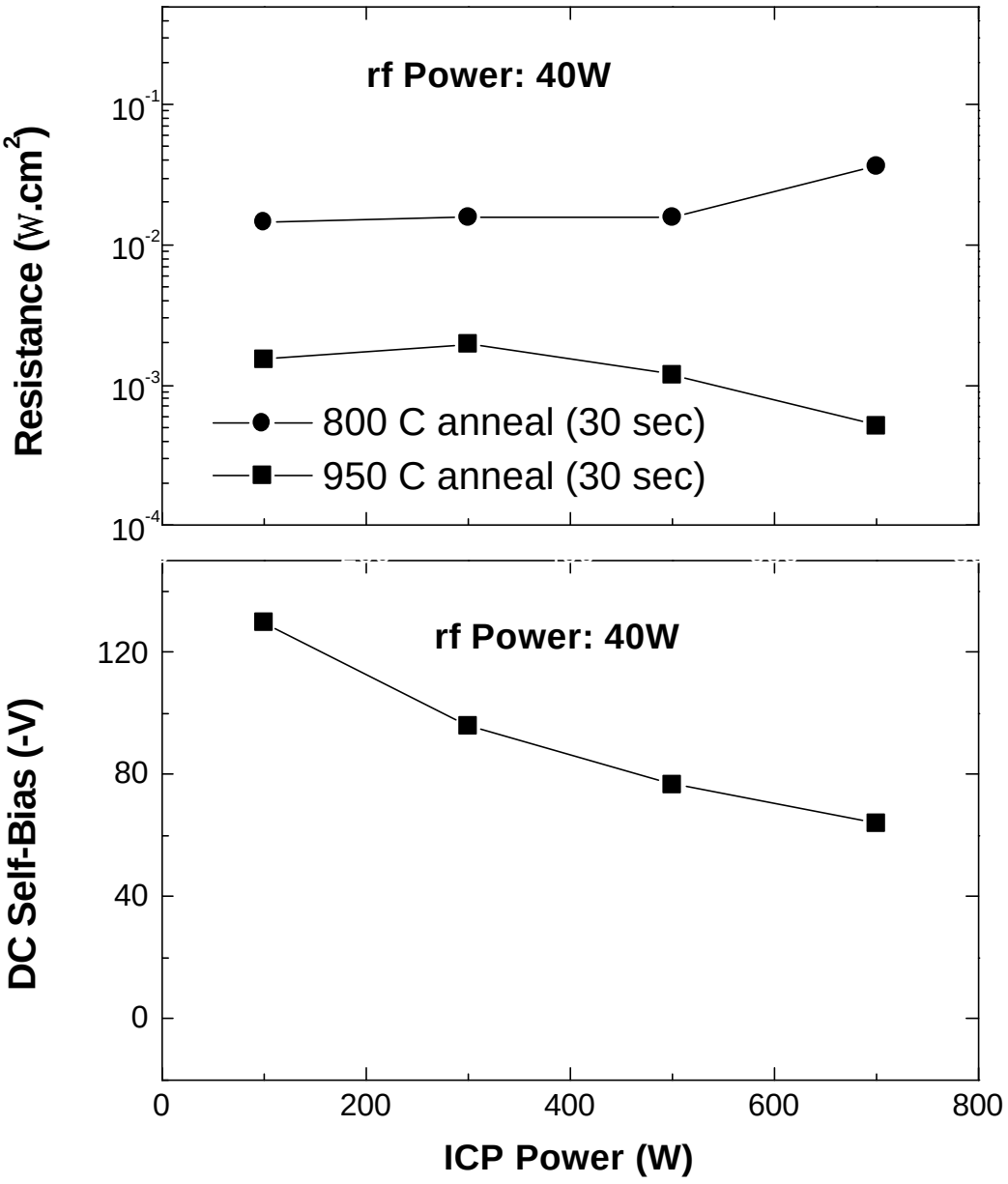

Figure 2-12 Contact resistance for Ti/Al/Pt/Au metallization as a function of ICP power for AlGaN/GaN structures exposed to ICP N_2 discharges prior to metal deposition, for two annealing temperatures (top) and dc self-bias as a function of ICP power (bottom).

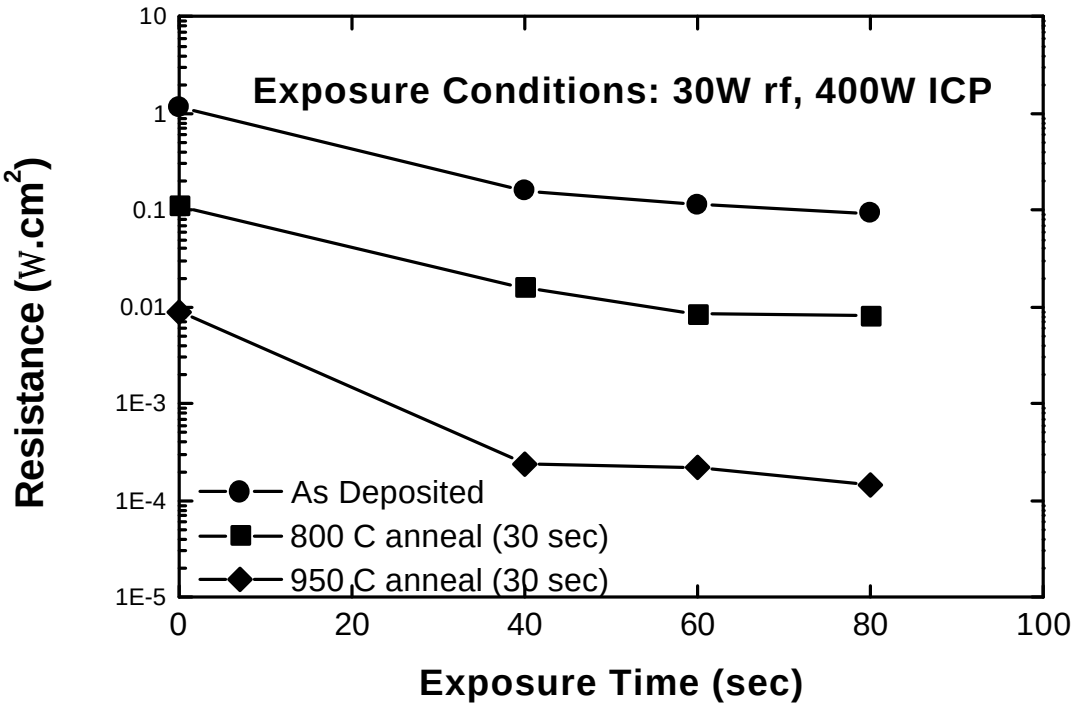

Fig. 2-13 Contact resistance for Ti/Al/Pt/Au metallization as a function of exposure prior to ICP N_2 discharges for AlGaN/GaN structures annealed at several different temperatures.

surface 100 Å) region. The N_2 plasma chemistry is a good choice for this application, since it produces light ions (N_2^+, N^+) for bombardment of the AlGaN surface that do not create heavy lattice disorder and associated trapping states that could degrade current transport in the semiconductor. It also avoids the chemical effects of H_2 or O_2 discharges on the AlGaN surface. Under optimized conditions, the contact resistance of Ti/Al/Pt/Au metallization deposited on the plasma exposed samples and subsequently annealed at 950 °C was lowered by a factor of 3 relative to unexposed contact samples annealed in the same fashion. This is a simple and effective method for reducing ohmic contact resistance on AlGaN/GaN HEMTs.

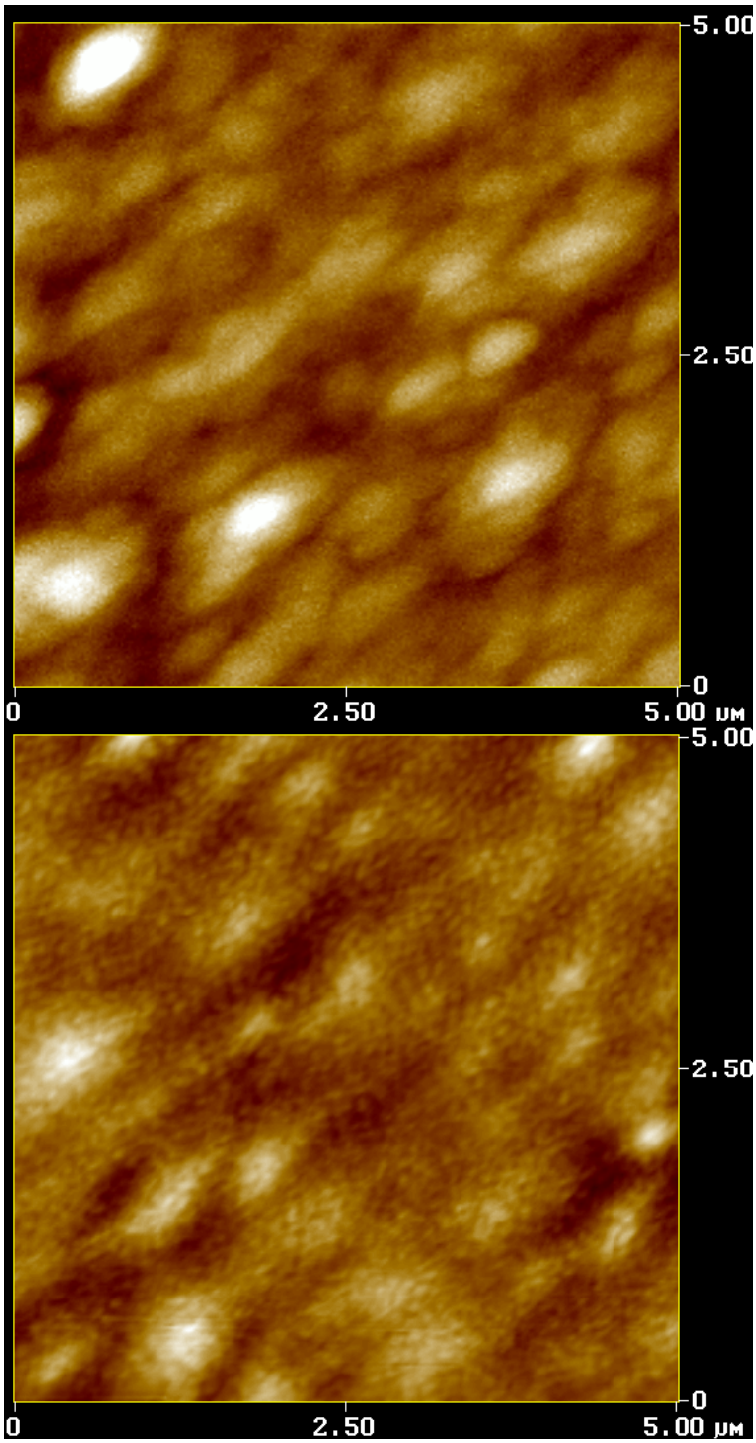

Figure 2-14 Atomic Force Microscopy (AFM) scans of AlGaN/GaN structure before (top) and after (bottom) exposure to an ICP N_2 discharge (300 W source power, 40 W rf chuck power, 30 secs).

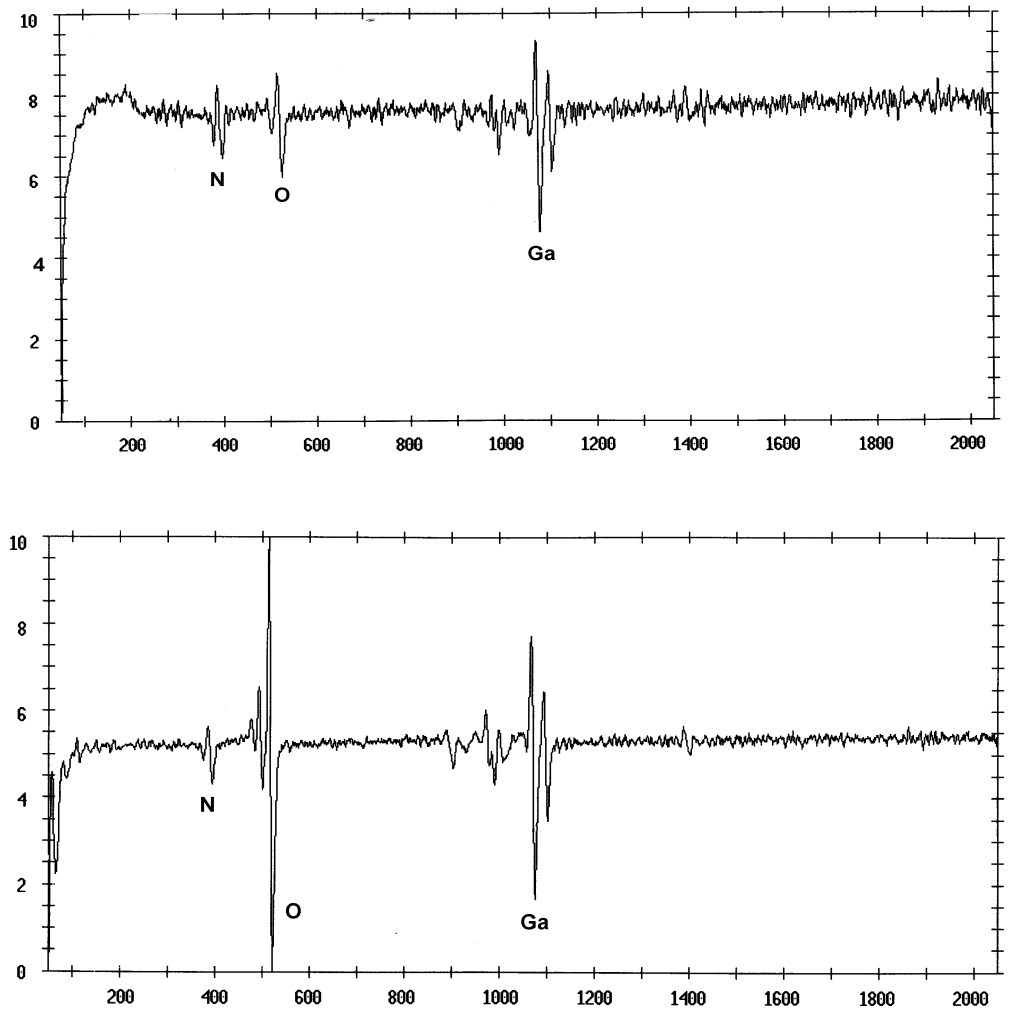

Figure 2-15 Auger Eelectron Spectroscopy (AES) surface scans of AlGaN/GaN structure before (top) and after (bottom) exposure to an ICP N_2 discharge (300 W source power, 40 W rf chuck power, 30 secs).

CHAPTER 3
GALLIUM NITRIDE AND ALUMINUM GALLIUM NITRIDE HIGH VOLTAGE POWER RECTIFIERS

3.1 Introduction

There is a strong interest in developing wide bandgap power devices for use in the electric power utility industry [3, 100-102]. With the onset of deregulation in the industry, there will be increasing numbers of transactions on the power grid in the US, with different companies buying and selling power. The main applications are in the primary distribution system (100~2000 kVA) and in subsidiary transmission systems (1~50 MVA). A major problem in the current grid is commentary voltage sags, which affect motor drives, computers and digital controls. Therefore, a system for eliminating power sags and switching transients would dramatically improve power quality. For example it is estimated that a 2-second outage at a large computer center can cost US$ 600,000 or more, and an outage of less than one cycle, or a voltage sag of 25% for two cycles, can cause a microprocessor to malfunction. In particular, computerized technologies have led to strong consumer demands for less expensive electricity, premium quality power and uninterruptible power.

The basic power electronics hierarchy would include the use of widegap devices such as Gate Turn-Off Thyristors (GTOs), MOS-Controlled Thyristors (MCT) or Insulated Gate Bipolar Transistors (IGBTs) combined with appropriate packaging and thermal management techniques to make subsystems (such as switches, rectifiers or

adjustable speed devices) which then comprise a system such as Flexible AC Transmissions (FACTS). Common power electronics systems, which are inserted between the incoming power and the electrical load include uninterruptible power supplies, advanced motors, adjustable speed drives and motor controls, switching power supplies, solid-state circuit breakers and power conditioning equipment. About 50% of the electricity in the US is consumed by motors. Motor repairs cost ~US$ 5 billion each year and could be dramatically reduced by high power electronic devices that permit smoother switching and control. Moreover, control electronics could dramatically improve motor efficiency. Other end uses include lighting, computers, heating and air-conditioning.

Some desirable attributes of next generation, widegap power electronics include the ability to withstand currents in excess of 5 kA and voltages in excess of 50 kV, provide rapid switching, maintain good thermal stability while operating at temperatures above 250 °C, have small size and light-weight, and be able to function without bulky heat-dissipating systems.

The primary limits of Si-based power electronics are as follows:

- Maximum voltage ratings <7 kV
  - Multiple devices must be placed in series for high-voltage systems.
- Insufficient current-carrying capacity
  - Multiple devices must be placed in parallel for typical power grid applications.
- Conductivity in one direction only

- Identical pairs of devices must be installed in anti-parallel for switchable circuits.

- Inadequate thermal management
  - Heat damage is a primary cause of failure and expense.
- High initial cost
  - Applications are limited to the highest-value settings.
- Large and heavy components
  - Costs are high for installation and servicing, and equipment is unsuitable for many customers.

For these reasons, there is a strong development effort on widegap power devices, predominantly SiC, with lesser efforts in GaN and diamond, which should have benefits that Si-based or electromechanical power electronics cannot attain. The higher standoff voltages should eliminate the need for series stacking of devices and the associated packaging difficulties. In addition these widegap devices should have higher switching frequency in pulse-width-modulated rectifiers and inverters.

The absence of Si devices capable of application to 13.8 kV distribution lines (a common primary distribution mode) opens a major opportunity for widegap electronics. However, cost will be an issue, with values of US$ 200~2000 per kVA necessary to have an impact. It is virtually certain that SiC switches will become commercially available within 3~5 years, and begin to be applied to the 13.8 kV lines. MOS Turn-Off-Thyristors involving a SiC GTO and SiC MOSFETare a promising approach [103]. An inverter module can be constructed from an MOS turn-off thyristor (MTO) and a SiC power diode.

Packaging and thermal management will be a key part of future power devices. For current Si IGBTs, there are two basic package types - the first is a standard attached die, wire bond package utilizing soft-solder and wire-bonds as contacts, while the second is the presspack, which employs dry-pressed contacts for both electrical and thermal paths [104,105]. In the classical package the IGBTs and control diodes are soldered onto ceramic substrates, such as AlN, which provide electrical insulation, and this in turn is mounted to a heat sink (typically Cu). Thick Al wires (500 mm) are used for electrical connections, while silicone gel fills the package [104]. In the newer presspack style, the IGBT and diode are clamped between Cu electrodes, buffered by materials such as molybdenum or composites [105], whose purpose is to account for the thermal expansion coefficient differences between Si and Cu. The package is again filled with gel for electrical insulation and corrosion resistance.

3.2 Gallium Nitride Schottky Rectifiers with 3.1 kV Reverse Breakdown Voltage

The GaN materials system is attractive from the viewpoint of fabricating unipolar power devices because of its large bandgap and relatively high electron mobility [106-109]. An example is the use of Schottky diodes as high-voltage rectifiers in power switching applications [106-108, 8]. These diodes will have lower blocking voltages than p-i-n rectifiers, but have advantages in terms of switching speed and lower forward voltage drop. Edge termination techniques such as, field rings on filed plates, bevels or surface ion implantation are relatively well-developed for Si and SiC and maximize the high voltage blocking capability by avoiding sharp field distributions within the device. However, in the few GaN Schottky diode rectifiers reported to date [106, 107], there has been little effort made on developing edge termination techniques. Proper design of the

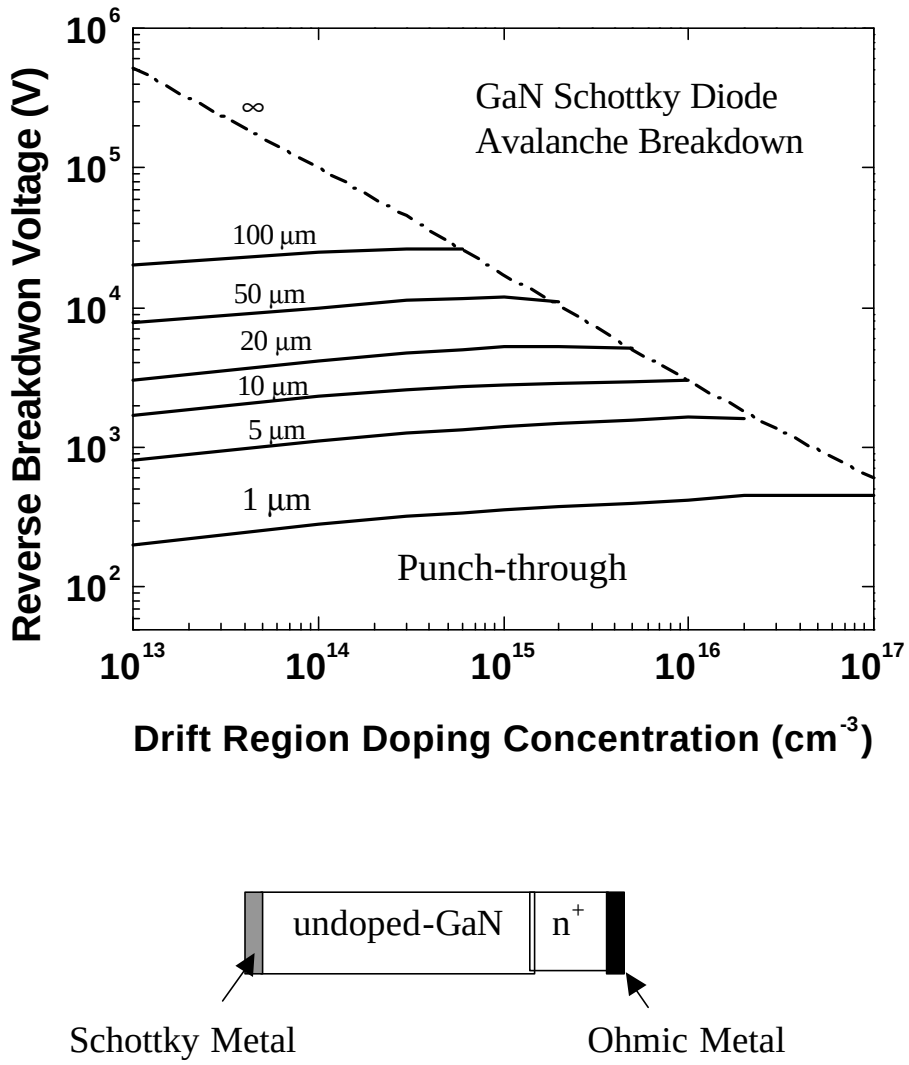

Figure 3-1 The calculation of reverse breakdown volatge as a function of doping concentration and standoff region thickness based on a punch-through model.

edge termination is critical both for obtaining a high breakdown voltage and reducing the on-state voltage drop and switching time.

Based on the punch through model, Figure 3-1 shows a plot of avalanche and punch through breakdown of GaN Schottky diodes calculated as a function of doping concentration and standoff layer thickness. It can be seen that 20 kV device may be obtained with ~100 μm thick GaN layer with doping concentration $<10^{15}$ cm^{-3}.

In this chapter we investigate on the effect of various edge termination techniques on the reverse breakdown voltage, V_B, of planar GaN Schottky diodes which deplete in the lateral direction. A maximum V_B of 3.1 kV at 25ºC was achieved with optimized edge termination, which is a record for GaN devices. We also examined the temperature dependence of V_B in mesa diodes and found a negative temperature coefficient of this parameter in these structures.

The GaN was grown on c-plane Al_2O_3 substrates by MOCVD using trimethylgallium and ammonia as the precursors. To create a Schottky rectifier with high breakdown voltage, one needs a thick, very pure GaN depletion layer. Figure 3-2 shows SIMS profile of H and other background impurities in a 2 μm thick, high resistivity (10^7 Ω·cm) GaN layer grown by MOCVD. The reverse breakdown voltage of simple Schottky rectifiers fabricated on this material was > 2 kV, a record for GaN. Notice that in this material the hydrogen concentration is at the detection sensitivity of the SIMS apparatus. The amount of hydrogen present in GaN after cooldown from the growth temperature will depend on the number of sites to which it can bond, including dopants and point and line defects. In the absence of p-type doping, it is clear that the number of these sites is ≤ 8×10^{17} cm^{-3} under our growth conditions.

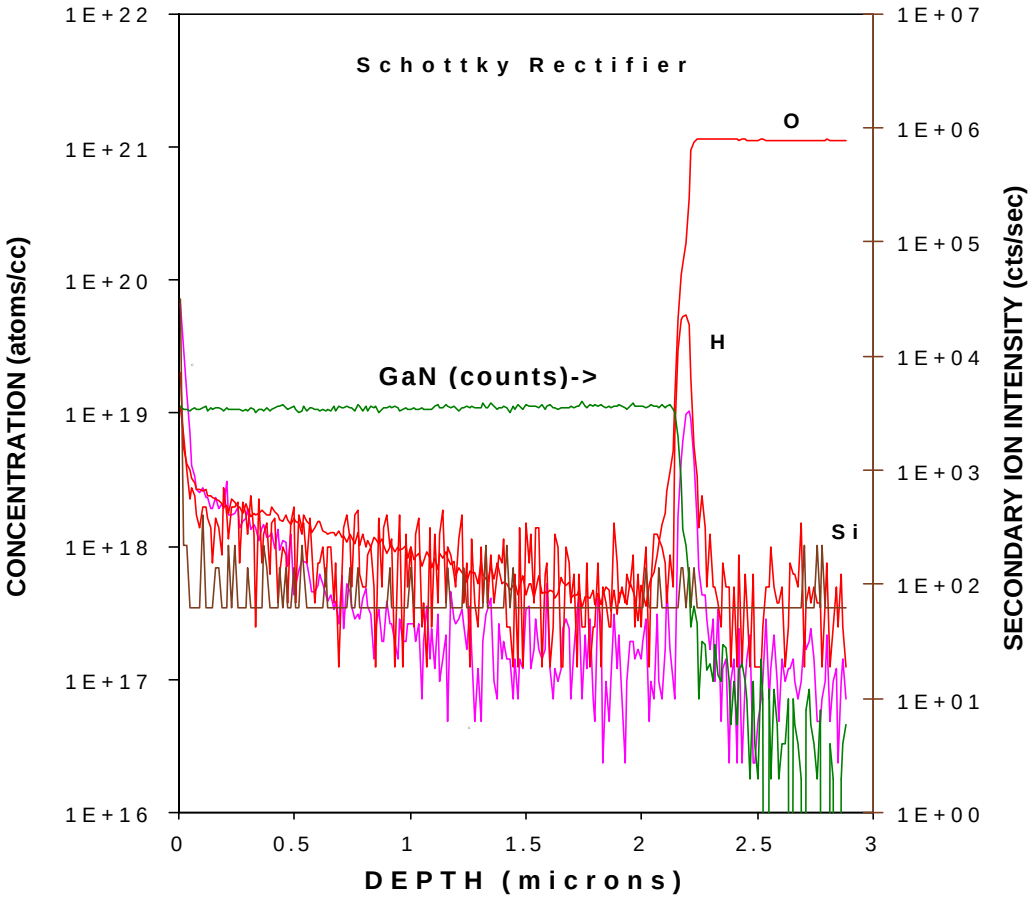

Figure 3-2. SIMS profiles of H and other background impurities in as-grown, MOCVD Schottky rectifier structure.

For vertically-depleting devices, the structure consisted of a 1 μm n^+ (3×10^{18} cm^{-3}, Si-doped) contact layer, followed by undoped ($n\sim2.5\times10^{16}$ cm^{-3}) blocking layers which ranged from 3 to 11 μm thick. These samples were formed into mesa diodes using ICP etching with Cl_2/Ar discharges (300 W source power, 40 W rf chuck power). The dc self-bias during etching was -85 V. To remove residual dry etch damage, the samples were annealed under N_2 at 800 ºC for 30 s. Ohmic contacts were formed by lift-off of e-beam evaporated Ti/Al, annealed at 700 ºC for 30 s under N_2 to minimize the contact

resistance. Finally, the rectifying contacts were formed by lift-off of e-beam evaporated Pt/Au. Contact diameters of 60-1100 μm were examined.

For laterally depleting devices, the structure consisted of ~3 μm of resistive (10^7 Ω/€) GaN. To form Ohmic contacts, Si^+ was implanted at 5×10^{14} cm^{-2}, 50 keV into the contact region and activated by annealing at 150 °C for 10 s under N_2. The Ohmic and rectifying contact metallization was the same as described above.

Three different edge termination techniques were investigated for the planar diode:

1. Use of a p-guard ring formed by Mg^+ implantation at the edge of the Schottky barrier metal. In these diodes the rectifying contact diameter was held constant at 124 μm, while the distance of the edge of this contact from the edge of the Ohmic contact was 30 μm in all cases.
2. Use of p-floating field rings of width 5 mm to extend the depletion boundary along the surface of the SiO_2 dielectric, which reduces the electric field crowding at the edge of this boundary. In these structures a 10 μm wide p-guard ring was used, and one to three floating field rings employed.
3. Use of junction barrier controlled Schottky (JBS) rectifiers, i.e., a Schottky rectifier structure with a p-n junction grid integrated into its drift region.

In all of the edge-terminated devices the Schottky barrier metal was extended over an oxide layer at the edge to further minimize field crowding, and the guard and field rings formed by Mg+ implantation and 1100 ºC annealing.

Figure 3-3 shows a schematic of the planar diodes fabricated with the p-guard rings, while the lower portion of the figure shows the influence of guard ring width on

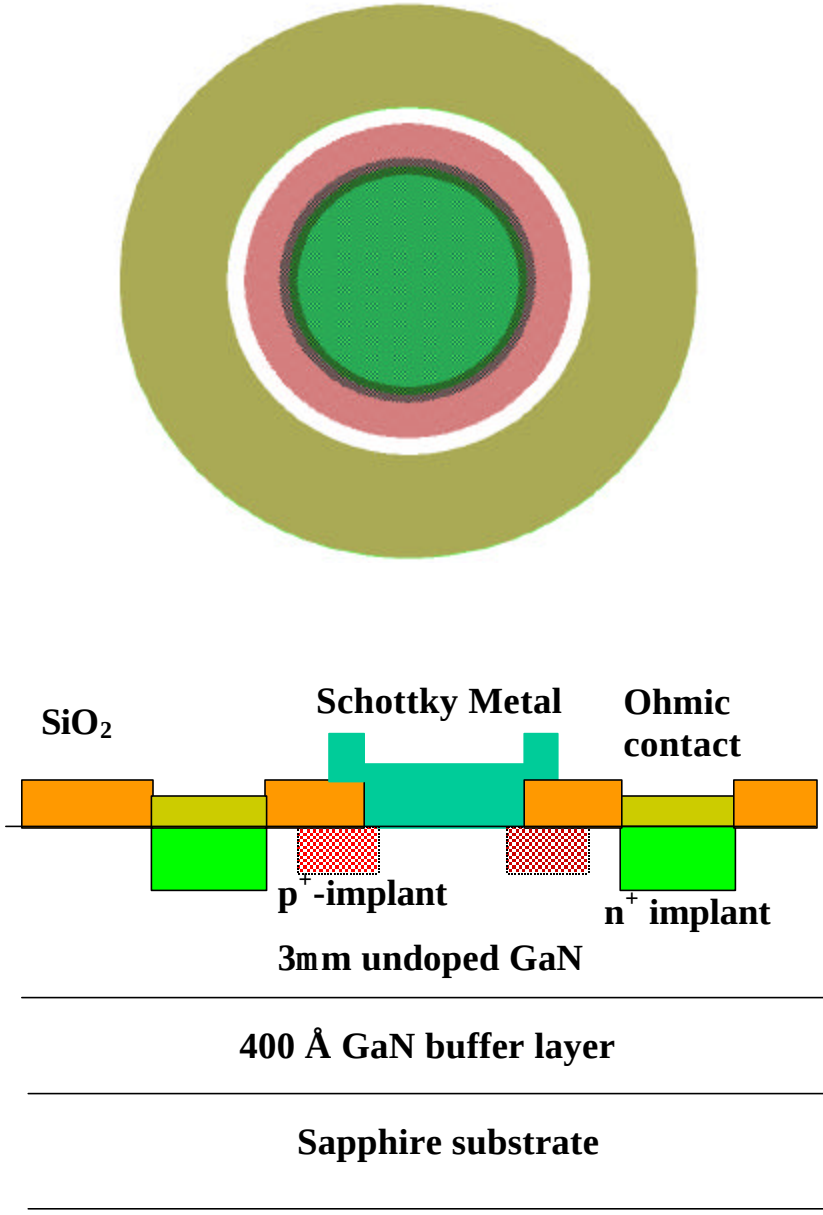

Figure 3-3 GaN power rectifiers with p-guard ring for edge terminations.

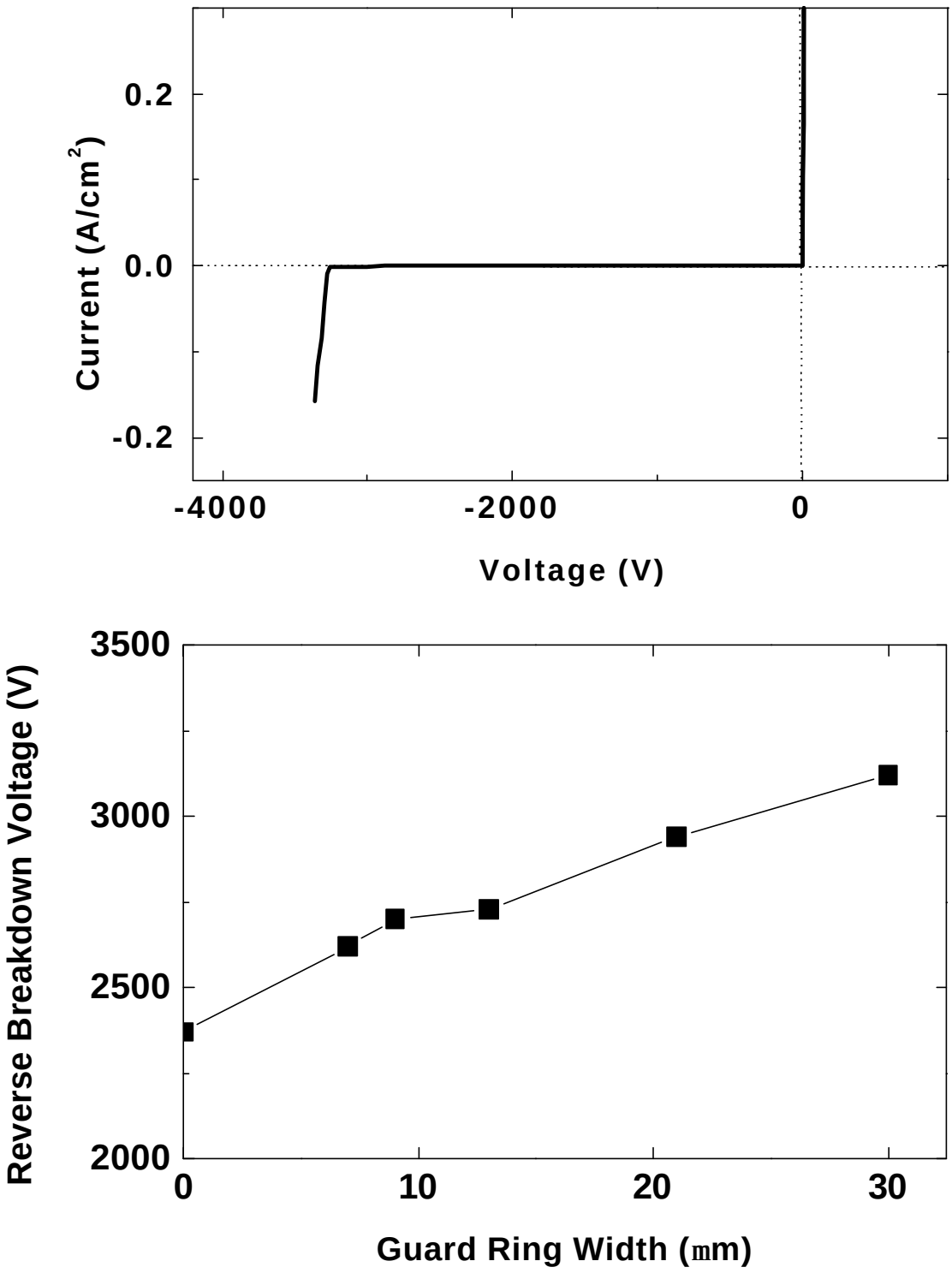

Figure 3-4 Current-Voltage characteristics of GaN power rectifiers with p-guard ring for edge terminations (top), and effect of p-guard ring on the reverse breakdown voltage of GaN power rectifiers (bottom).

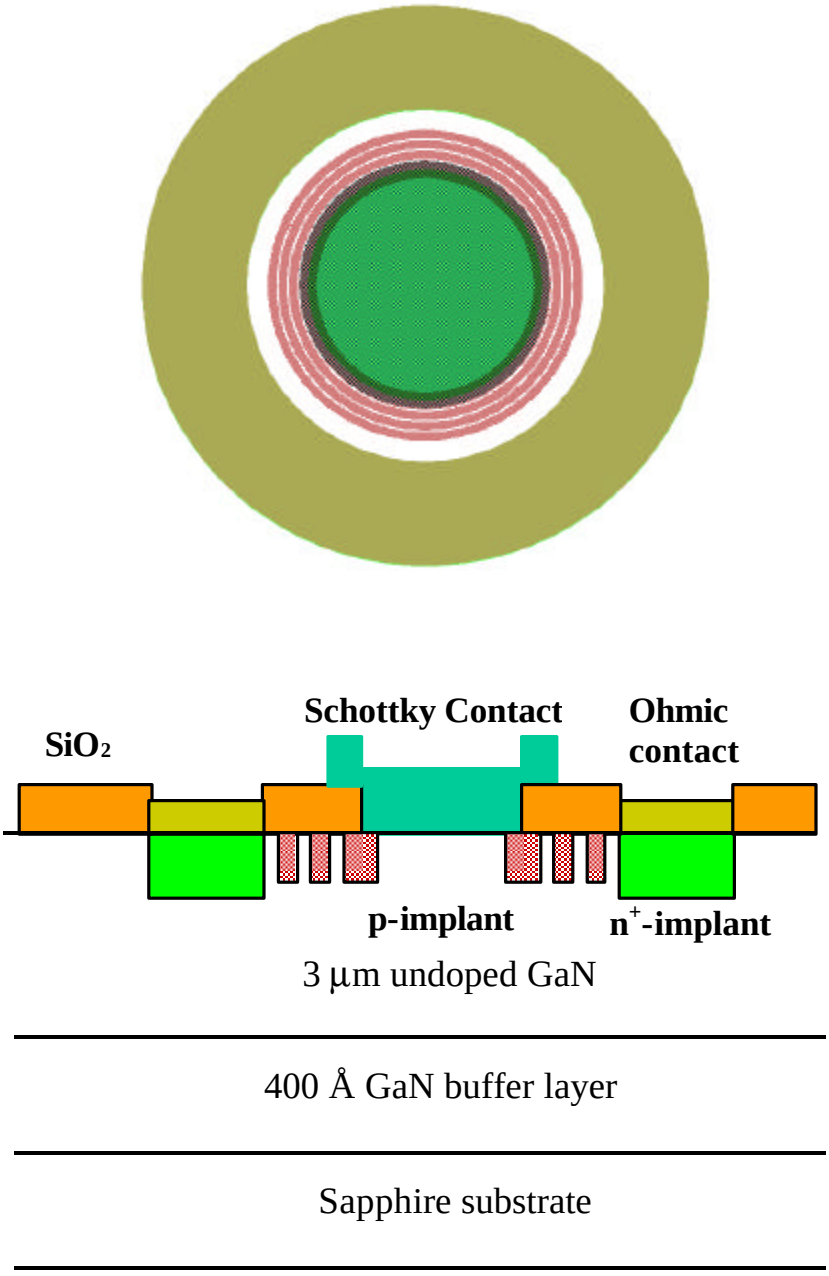

Figure 3-5 GaN power rectifiers with floating-field ring for edge terminations.

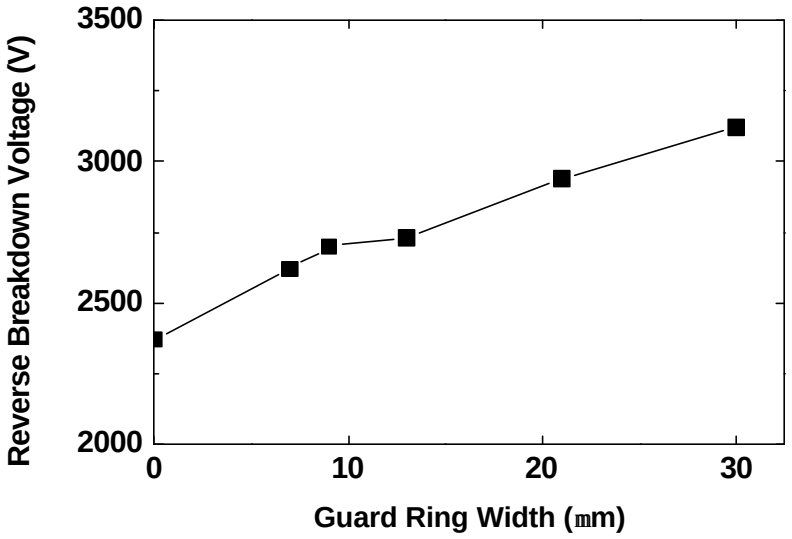

Figure 3-6 Effect of floating field ring on the reverse breakdown voltage of GaN power rectifiers.

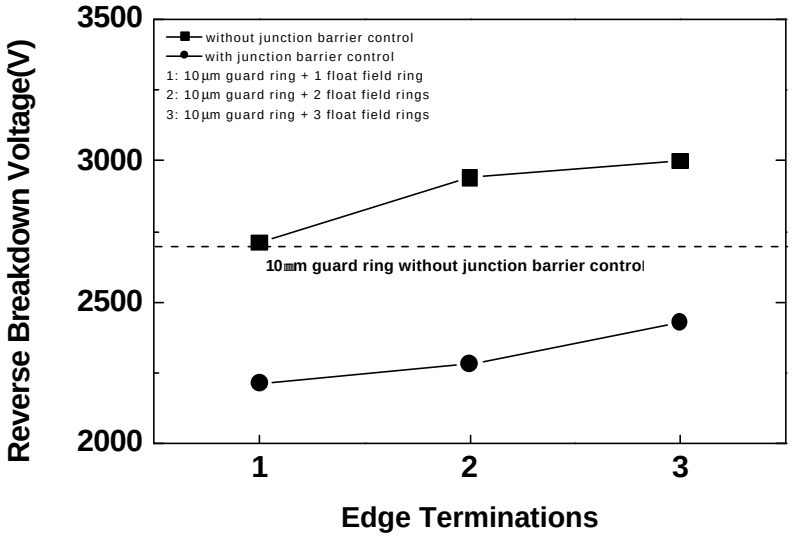

Figure 3-7 Effect of Junction Barrier Control on the reverse breakdown voltage of GaN power rectifiers.

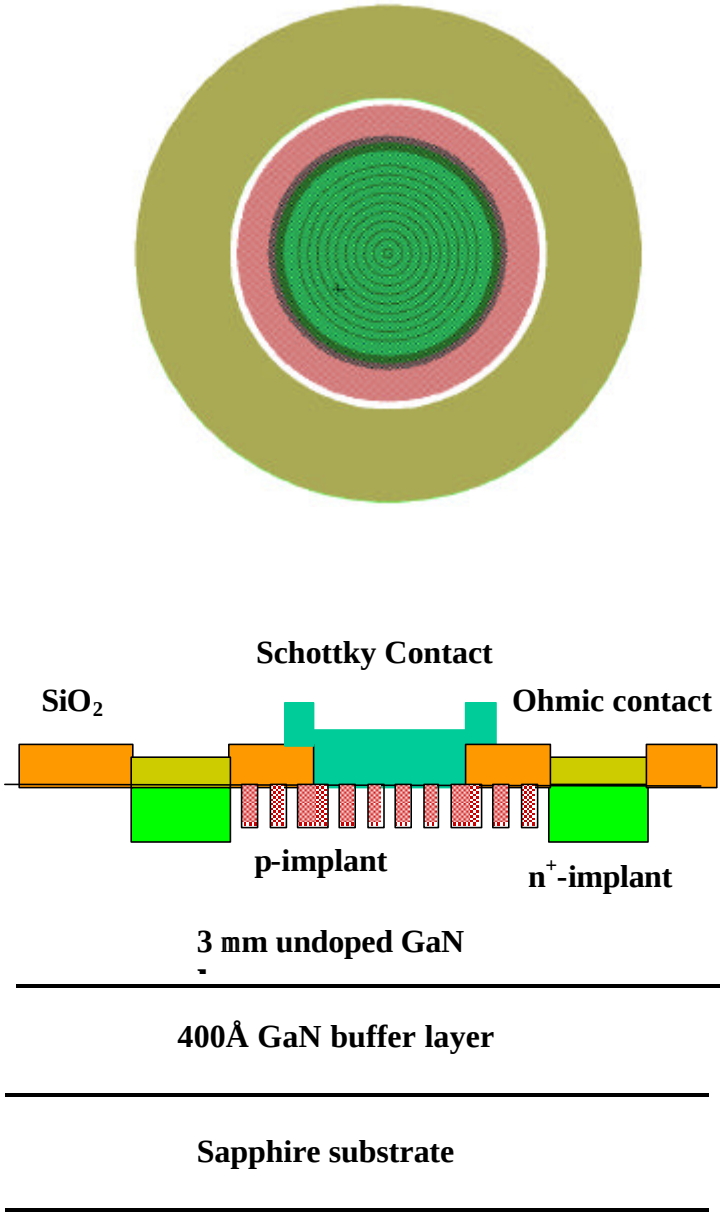

Figure 3-8 GaN power rectifiers with Junction Barrier Control.

V_B at 25 ºC. Without any edge termination, V_B is ~2300 V for these diodes. The forward turn-on voltage was in the range 15~50 V, with a best on-resistance of 0.8 Ω cm^2. The figure-of-merit $(V_B)^2/R_{ON}$ was 6.8 MW/cm^2. As the guard-ring width was increased, we observed a monotonic increase in V_B, reaching a value of ~3100 V for 30 µm wide rings (Figure 3-4). The figure-of-merit was 15.5 MW/cm^2 under these conditions. The reverse leakage current of the diodes was still in the nA range at voltages up to 90% of the breakdown value.

Figure 3-5 shows a schematic of the floating field ring structures, while Figure 3-6 shows the effect of different edge termination combinations on the resulting V_B at 25 ºC. Note that the addition of the floating field rings to a guard ring structure further improves V_B, with the improvement saturating for a three-floating field ring geometry.

Figure 3-7 shows the effect of the junction barrier control on V_B, together with a schematic of the p-n junction grid in Figure 3-8. In our particular structure we found that junction barrier control slightly degraded V_B relative to devices with guard rings and various numbers of floating field rings. We believe that with optimum design of the grid structure we should achieve higher V_B values and that the current design allows Schottky barrier lowering since the depletion regions around each section of the grid do not completely overlap. This is consistent with the fact that we did not observe the decrease in forward turn-on voltage expected for JBS rectifiers relative to conventional Schottky rectifiers.

The results of Figures 3-3 to 3-6 are convincing evidence that proper design and implementation of edge termination methods can significantly increase reverse breakdown voltage in GaN diode rectifiers and will play an important role in applications

at the very highest power levels. For example, the target goals for devices, intended to be used for transmission and distribution of electric power or in single-pulse switching in the subsystem of hybrid-electric contact vehicles are 25 kV standoff voltage, 2 kA conducting current and a forward voltage drop <2% of the standoff voltage. At these power levels, it is expected that edge termination techniques will be essential for reproducible operation.

The devices designed for vertical depletion had lower on-state voltages than the lateral diodes, due to the fact that a highly-doped n^+ contact layer can be included in the epitaxial structure, obviating the need for implantation. However, we have not yet perfected the ability to grow resistive GaN on top of conducting GaN and, therefore, the depletion layers in the vertical devices typically had lightly n-type conductivity (2×10^{16} to 5×10^{16} cm^{-3}). The typical on-state resistances were 6~10 m Ω cm^2, with reverse breakdown voltages at 25 ºC of 200~550 V (depending on doping level and layer thickness). The maximum figure-of-merit in these devices was higher than for the planar diodes, reaching values as high as 48 MW/cm^2.

In summary, GaN Schottky diodes with vertical and lateral geometries were fabricated. A reverse breakdown voltage of 3.1 kV was achieved on a lateral device incorporating p-type guard rings. Several types of edge termination were examined, with floating field rings and guard rings found to increase V_B. The best on-state resistance obtained in these lateral devices was 0.8 Ω-cm^2. In mesa diodes incorporating n^+ contact layers, the best on-state resistance was 6 m Ω-cm^2, while V_B values were in the range 200~550 V. These GaN rectifiers show promise for high power electronics applications.

3.3 Aluminum Gallium Nitride (AlGaN) Schottky Rectifiers with 4.1 kV Reverse Breakdown Volatge

3.3.1 Introduction

There is a strong interest in developing high current, high voltage switches in the AlGaN materials system for applications in the transmission and distribution of electric power and in the electrical subsystems of emerging vehicle, ship, and aircraft technology [108, 110, 111]. It is expected that packaged switches made from AlGaN may operate at temperatures in excess of 250 °C without liquid cooling, therefore reducing system complexity, weight, and cost. In terms of voltage requirements, there is a strong need for power quality enhancement in the 13.8 kV class, while it is estimated that availability of 20–25 kV switches in a single unit would cause a sharp drop in the cost of power flow control circuits. Schottky and p-i-n rectifiers are an attractive vehicle for demonstrating the high-voltage performance of different materials systems, and blocking voltages from 3–5.9 kV have been reported in SiC devices [112-114]. The reverse leakage current in Schottky rectifiers is generally far higher than expected from thermionic emission, most likely due to defect states around the contact periphery [112]. To reduce this leakage current and prevent breakdown by surface flashover, edge termination techniques such as guard rings, field plates, beveling, or surface ion implantation are necessary [115,116,3]. However, in the GaN rectifiers reported so far, there has been little effort in employing edge termination methods and no investigation of the effect of increasing the band gap by use of AlGaN.

We study on the reverse breakdown voltage (V_{RB}) of AlGaN Schottky rectifiers for different Al compositions (0–0.25) and on the effect of various edge termination

techniques in suppressing premature edge breakdown. A maximum V_{RB} of 4.3 kV was achieved for $Al_{0.25}Ga_{0.75}N$ diodes, with very low reverse current densities. At low reverse biases the rectifiers typically show currents which are proportional to the contact perimeter, whereas at higher biases the current is proportional to contact area. The forward current characteristics show ideality factors of 2 at low bias (Shockley–Read–Hall recombination) and 1.5 at higher voltage (diffusion current).

3.3.2 Experimental Methods

The undoped $Al_XGa_{1-X}N$ layers were grown by atmospheric pressure metalorganic chemical vapor deposition at 1040 °C (pure GaN) or 1100 °C (AlGaN) on (0001) oriented sapphire substrates. The precursors were trimethylgallium, trimethylgaluminum, and ammonia, with H_2 used as a carrier gas. The growth was performed on either GaN (in the case of GaN active layers) or AlN (in the case of AlGaN active layers) low temperature buffers with nominal thicknesses of 200 Å. The active layer thickness was ~2.5 µm in all cases and the resistivity of these films was of order 10^7 Ω·cm [117]. To form ohmic contacts in some cases, Si^+ was implanted at 5×10^{14} cm^{-2}, 50 keV into the contact region and activated by annealing at 1150 °C for 10 s under N_2. The contacts were then formed by lift off of e-beam evaporated Ti/Al/Pt/Au annealed at 700 °C for 30 s under N_2. The rectifying contacts were formed by lift off of e-beam evaporated Pt/Ti/Au (diameter 60–1100µm). A schematic of the planar diodes is shown in Figure 3-9. The devices were tested at room temperature under a Fluorinert® ambient.

On the GaN diodes, we also examined the use of three different edge termination methods, namely p-guard rings formed by Mg^+ implantation at the edge of the rectifying contact, use of p-type floating field rings of width 5 µm to extend the depletion boundary

along the edge of a SiO_2 passivation layer and finally, use of junction barrier controlled Schottky rectifiers (a rectifier with integrated p–n junction grid in its drift region). In all of these edge-terminated diodes the Schottky metal was extended over a SiO_2 layer at the edge to minimize field crowding.

3.3.3 Results and Discussion

Figure 3-10 shows current–voltage (I–V) characteristics from two different diodes. The GaN device employed 30 μm wide p-guard rings. This was found to be the most effective edge termination method for these structures, producing an increase in V_{RB} of ~800 V over devices without any passivation or edge termination, i.e., breakdown occurred at 2.3 kV in the control diodes and 3.1 kV in devices with guard rings. The use of guard rings or floating field rings each produced improvements in V_{RB} over the control diodes, with increases in the range 200–800 V. By sharp contrast, junction barrier control was unsuccessful in our structures, leading to decreases in V_{RB} of 300–400 V. We believe this is due to Schottky barrier lowering because of the depletion regions around each section of the grid not completely overlapping in our initial design. The best on resistance (R_{ON}) achieved for GaN diodes was 0.8 Ω-cm^2, producing a figure-of-merit $(V_{RB})^2/R_{ON}$ of 15.5 MW-cm^{-2}. Figure 3-10 also shows an I–V characteristic from an $Al_{0.25}Ga_{0.75}N$ rectifier, without any edge termination or surface passivation. In this case V_{RB} was 4.3 kV, which is far in excess of the values reported previously for GaN rectifiers, i.e., 350–450 V [116,117]. The on resistance of the AlGaN diodes was higher than for pure GaN, due to higher ohmic contract resistance. The lowest R_{ON} achieved was 3.2 Ω·cm^2, leading to a figure-of-merit of ~5.5 MW cm^{-2}.

Figure 3-11 shows the variation of V_{RB} with Al percentage in the AlGaN active

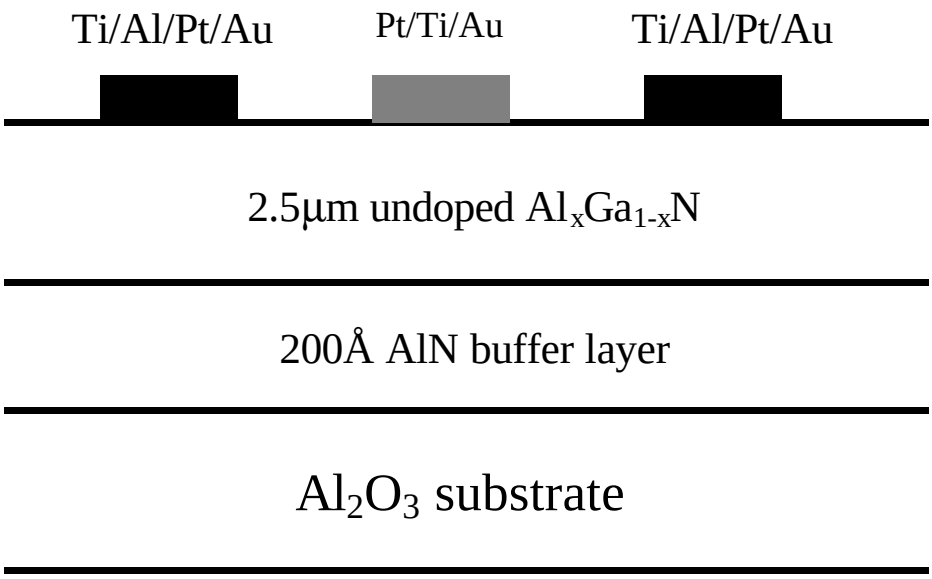

Figure 3-9 Schematic of AlGaN power rectifiers without edge termination.

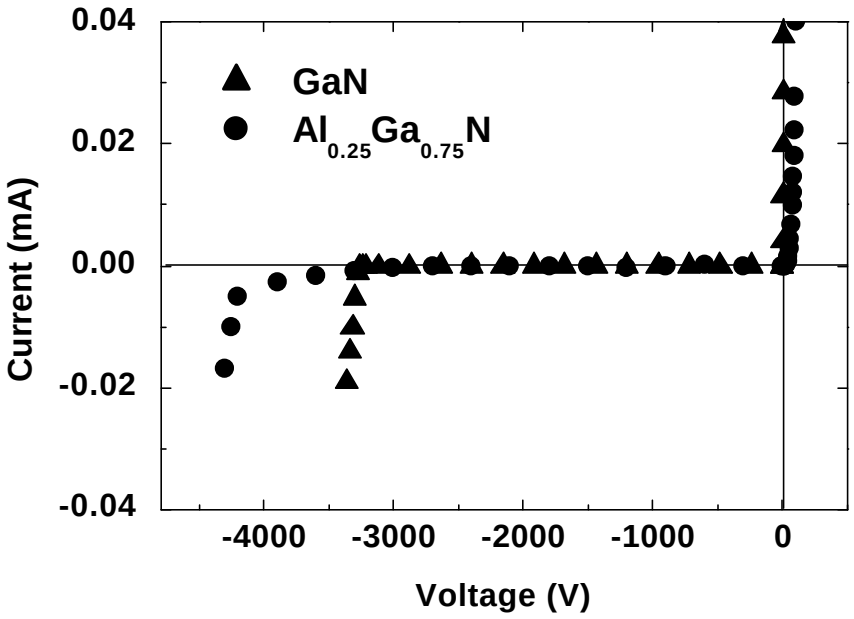

Figure 3-10 Room temperature *I – V* characteristics from an $Al_{0.25}Ga_{0.75}N$ rectifier.

layers of the rectifiers. In this case we are using the V_{RB} values from diodes without any edge termination or surface passivation. The calculated band gaps as a function of Al composition are also shown, and were obtained from the relation:

$$E_g(x) = E_{g,GaN}(1-x) + E_{g,AlN} \cdot x - bx(1-x) \qquad 3\text{-}1$$

where x is the AlN mole fraction and b is the bowing parameter with value 0.96 eV [118]. Note that V_{RB} does not increase in linear fashion with band gap. In a simple theory, V_{RB} should increase as $(Eg)^{1.5}$, but it has been empirically established that factors such as impact ionization coefficients and other transport parameters need to be considered and that consideration of Eg alone is not sufficient to explain measured V_{RB} behavior. The fact that V_{RB} increases less rapidly with Eg at higher AlN mole fractions may indicate increasing concentrations of defects that influence the critical field for breakdown.

The reverse I–V characteristics of all of the rectifiers showed $I \propto V^{0.5}$ over a broad range of voltage (50–2000 V), indicating that Shockley–Read–Hall recombination is the dominant transport mechanism. The current density in all devices was in the range $5–10\times10^{-6}$ A cm^{-2} at 2 kV. At low biases (25 V) the reverse current was proportional to the perimeter of the rectifying contact, suggesting that surface contributions are the most important in this voltage range. For higher biases, the current was proportional to the area of the rectifying contact. Under these conditions, the main contribution to the reverse current is from under this contact, i.e., from the bulk of the material. It is likely that the high defect density in heteroepitaxial GaN is a primary cause of this current. The forward I–V characteristics showed that the current density was proportional to exp(–eV/2kT) at lowest voltages (up to current densities of $\sim5\times10^{-4}$ A cm^{-2}) and to exp(–eV/1.5kT) at

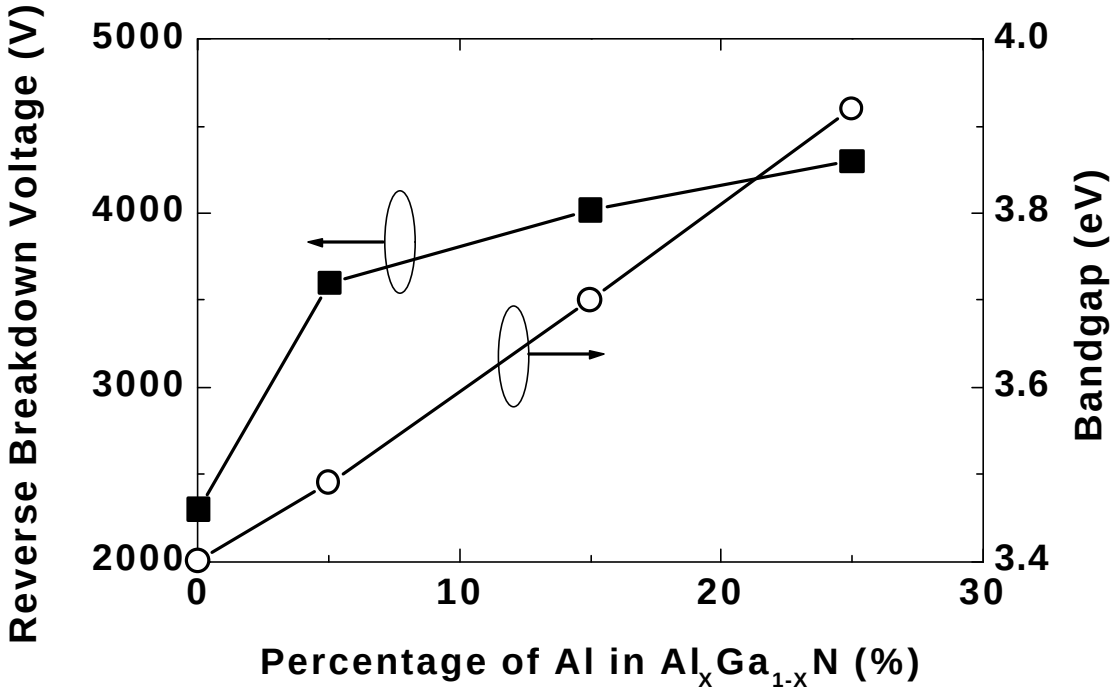

Figure 3-11 Variation of V_{RB} in $Al_XGa_{1-X}N$ rectifiers without edge termination, as a function of Al concentration. The Band gaps for the AlGaN alloys are also shown.

higher voltages (current densities in the range 10^{-3}–1.5×10^{2} A cm^{-2}). These results are consistent with Shockley–Read–Hall recombination as the dominant mechanism at low bias, followed by diffusion current at higher voltage. Qualitatively similar behavior has been reported previously for SiC Schottky rectifiers.

When pushed beyond breakdown, the diodes invariably failed at the edges of the rectifying contact, as shown in Figure 3-12. As described earlier, the use of metal field plate contact geometries with SiO_2 as the insulator and either guard rings or floating field rings significantly increased V_B. These rectifiers generally did not suffer irreversible damage to the contact upon reaching breakdown and could be re-measured many times.

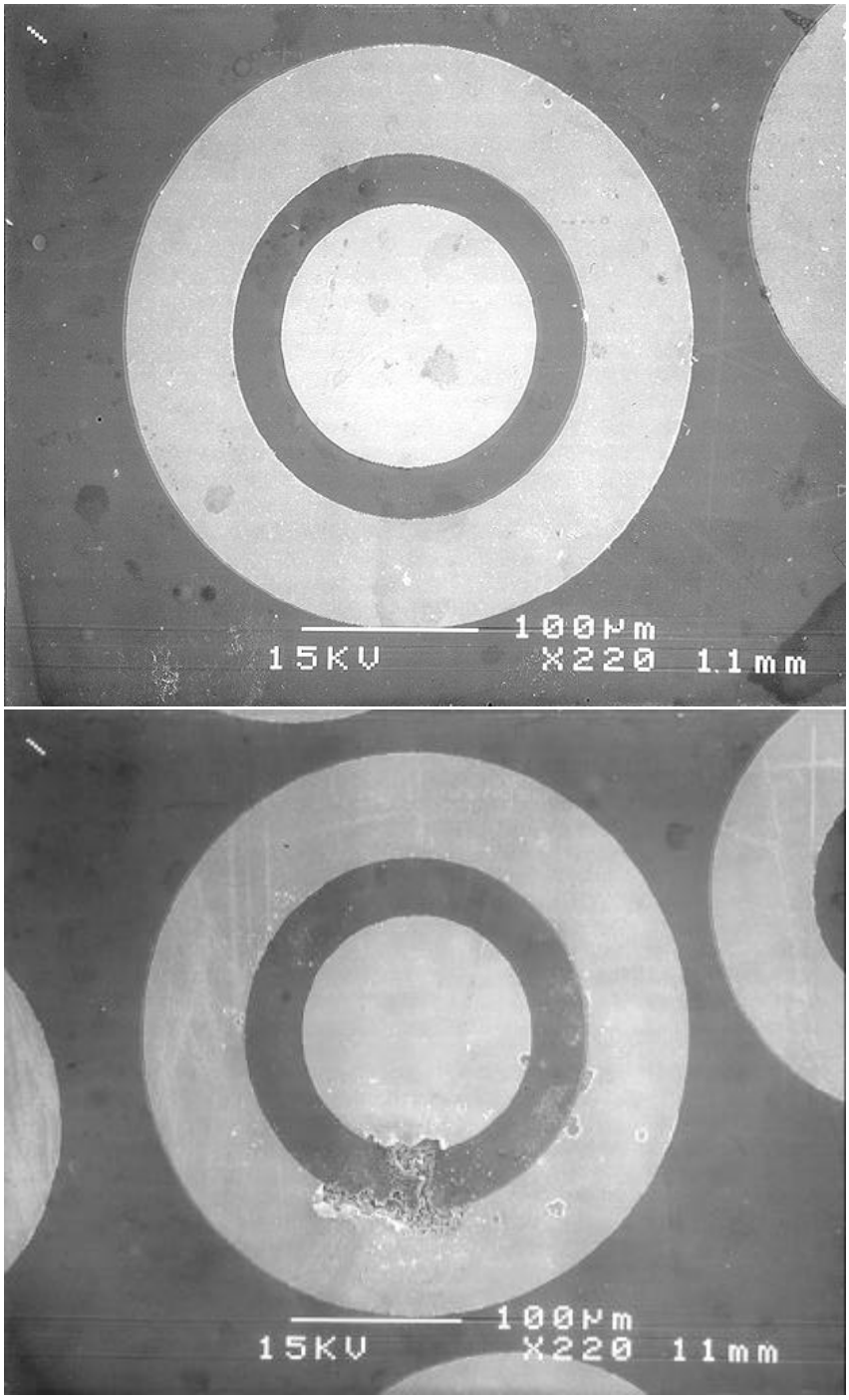

Figure 3-12 Scanning electron microscopy micrographs of AlGaN rectifiers before (top) and after (bottom) pushing the applied bias beyond the value for breakdown.

3.3.4 Summary

In summary, Schottky rectifiers on high resistivity Al_XGa_{1-X} N epi layers produced reverse breakdown voltages up to 4.3 kV for $Al_{0.25}Ga_{0.75}N$ diodes without edge termination. The current transport mechanisms were investigated as a function of bias voltage, with Shockley-Read-Hall recombination being dominant over a broad range of conditions. Minimizing electric field crowding at the corners of the rectifying contact was effective in increasing the breakdown voltage. The AlGaN materials system appears promising for high voltage applications.

3.4 Temperature Dependence and Current Transport Mechanisms in $Al_XGa_{1-X}N$ Schottky Rectifiers

3.4.1 Introduction

P-i-n rectifiers are expected to have larger reverse blocking voltages than Schottky rectifiers, but inferior switching speeds and higher forward turn-on voltages. GaN Schottky rectifiers with reverse breakdown voltage (V_{RB}) to 3.1 kV have been demonstrated when p^+ guard rings and metal overlap onto a dielectric are employed as edge termination techniques. Use of $Al_{0.25}Ga_{0.75}N$ instead of GaN produced V_{RB} values up to 4.3 kV.

Since this type of device is intended for elevated temperature operation, there is a need to understand the current transport mechanisms, the origin of the reverse leakage current and the magnitude and sign of the temperature coefficient for V_{RB}. In this section all of these properties are investigated. Over a broad range of voltages, the reverse leakage current is proportional to the diameter of the rectifying contact indicating that

surface periphery leakage is the dominant contributor. The temperature coefficient for V_{RB} was found to be negative for both GaN and AlGaN, even in edge-terminated devices.

3.4.2 Results and Discussion

The GaN and $Al_{0.25}Ga_{0.75}N$ layers were found to be resistive (~10^7 Ω cm). Each was grown on c-plane Al_2O_3 substrates by metal organic chemical vapor deposition using conventional precursors and growth temperatures of 1040 (GaN) or 1100 °C ($Al_{0.25}Ga_{0.75}N$). The layer thicknesses were 2.5–3 μm. Schematics of the completed rectifiers are shown in Fig. 3-13. The GaN devices employed p+ guard rings formed (7 μm wide) by Mg^+/P^+ implantation, n^+ source/drain region formed by Si^+ implantation (annealing was performed at 1150 °C for 10 s under N_2) and overlap of the rectifying contact onto a SiO_2 passivation layer. The AlGaN devices did not use any edge termination techniques. The contacts on all rectifiers were formed by lift-off, with the ohmic metallization annealed at 700 °C for 30 s under N_2. The rectifying contact diameters were 45–125 μm with a separation of 124 μm between these contacts and the ohmic contacts.

Current–voltage (I–V) characteristics from both types of rectifiers are shown in Figure 3-14 as a function of measurement temperature. The most obvious feature of the data is that there is a negative temperature coefficient for V_{RB}. The only previous information for GaN-based devices comes from GaN/AlGaN heterostructure field effect transistors in which a value of +0.33 $V \cdot K^{-1}$ was found [119], and from linearly graded GaN p^+pn^+ junctions, in which a value of +0.02 V K^{-1} was determined [109]. In both cases the V_{RB} values were more than an order of magnitude lower than in the present diodes.

Figure 3-15 shows the variation of V_{RB} with temperature. The data can be represented by a relation of the form:

$$V_{RB} = V_{RBO}[1 + b(T - T_0)] \quad 3\text{-}2$$

where = –6.0±0.4 V K^{-1} for both types of rectifiers. However, in Schottky and p-i-n rectifiers we have fabricated on more conducting GaN, with V_{RB} values in the 400–500 V range, the values were consistently around –0.34 V K^{-1}. Therefore, in present state-of-the-art GaN rectifiers, the temperature coefficient of V_{RB} appears to be a function of the magnitude of V_{RB}. Regardless of the origin of this effect, it is clearly a disadvantage for GaN. While SiC is reported to have a positive temperature coefficient for V_{RB} there are reports of rectifiers that display negative β values [120]. One may speculate that particular defects present may dominate the sign and magnitude of β, and it will be interesting to fabricate GaN rectifiers on bulk or quasibulk substrates with defect densities far lower than in heteroepitaxial material.

The forward turn-on voltage V_F of a Schottky rectifier can be written as

$$V_F = \frac{nkT}{e}\ln\left(\frac{J_F}{A^{**}T^2}\right) + nf_B + R_{ON} \cdot J_F \quad 3\text{-}3$$

where n is the ideality factor, k is Boltzmann's constant, T is the absolute sample temperature, e the electronic charge, J_F the forward current density (usually taken to be 100 A cm^{-2}) at V_F, A** the Richardson constant, ϕ_B the barrier height (~1.1 eV in this case), and R_{ON} the on-state resistance. The typical best VF values were ~5 V for GaN

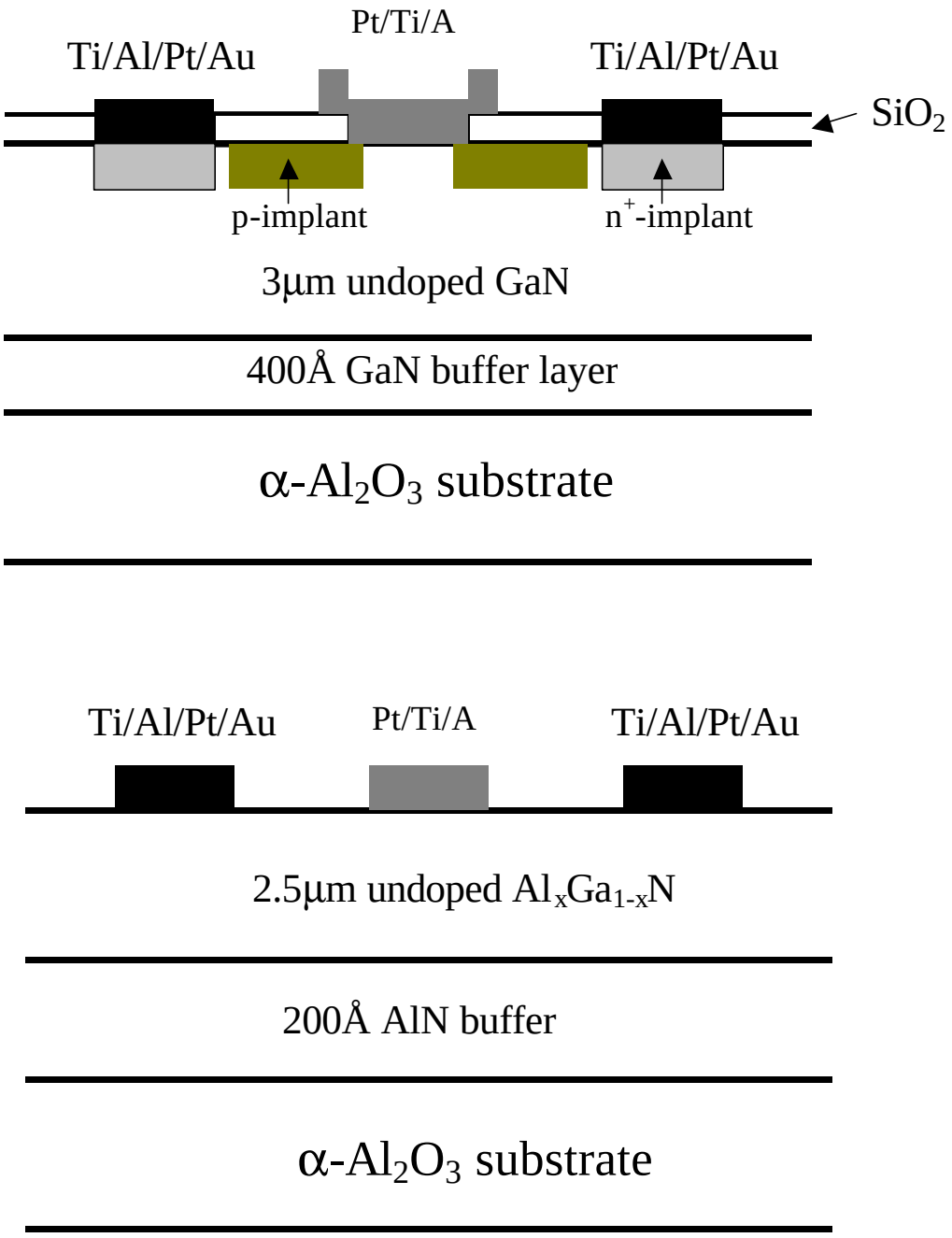

Figure 3-13 Schematic of GaN (top) and AlGaN (bottom) rectifiers. The GaN devices employ several edge termination techniques.

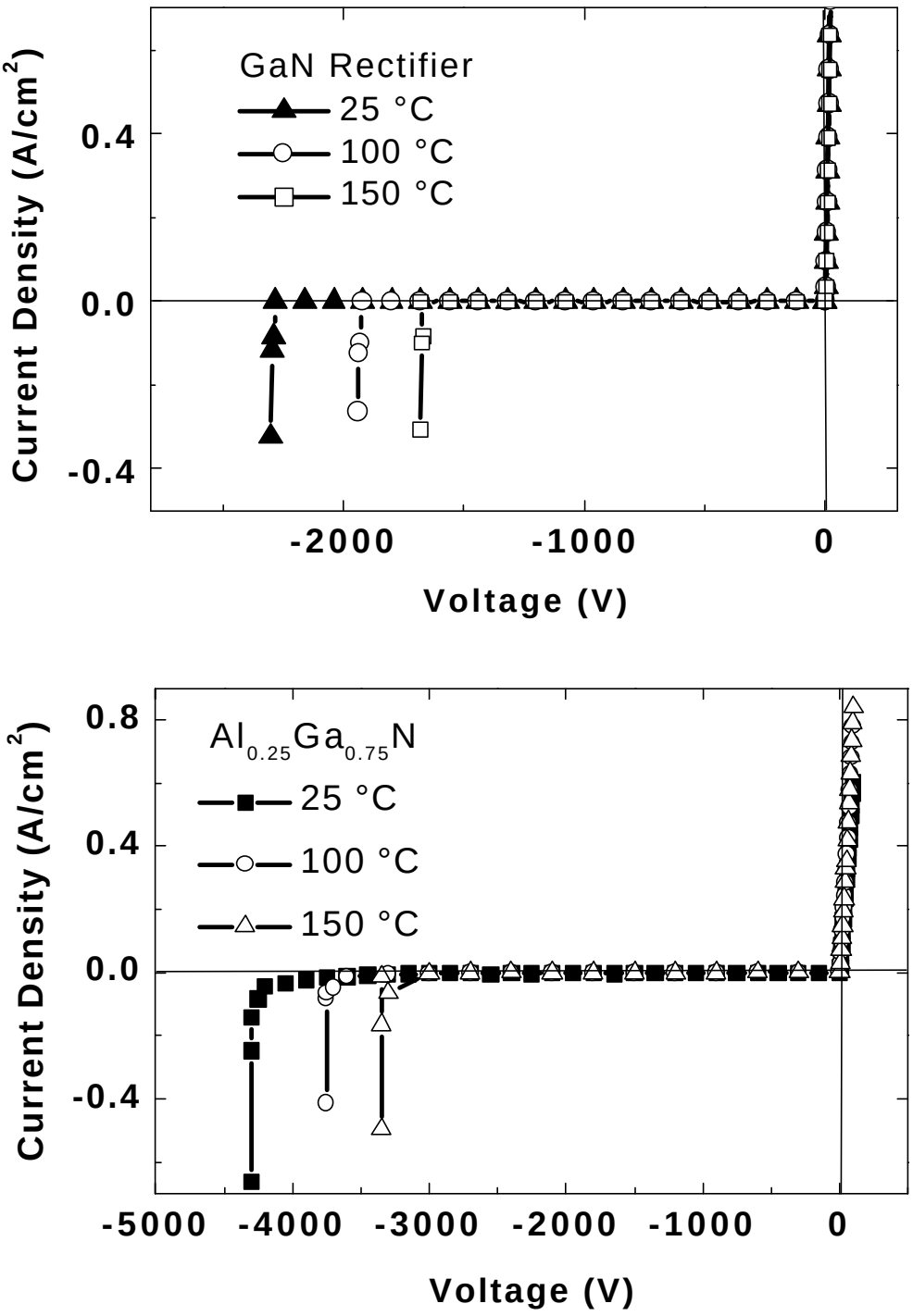

Figure 3-14 I – V characteristics as a function of temperature for GaN (top) and AlGaN (bottom) rectifiers.

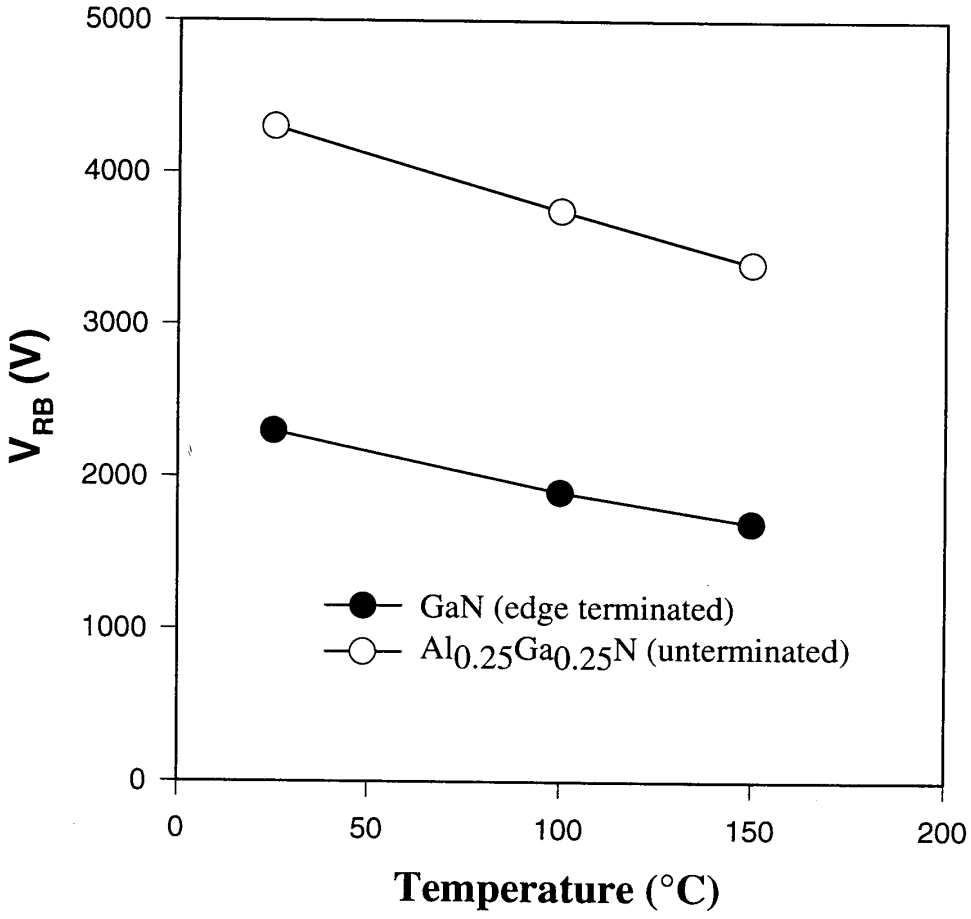

Figure 3-15 Temperature dependence of V_{RB} for GaN and AlGaN rectifiers.

and ~7.5 V for $Al_{0.25}Ga_{0.75}N$, with best R_{ON} values of 50 and 75 mΩ cm^2, respectively. The ideality factors derived from the forward I–V characteristic were typically ~2 for both GaN and $Al_{0.25}Ga_{0.75}N$ for biases up to ~2/3 of V_F. This is consistent with recombination being the dominant current transport in this bias range. At high voltages, n was typically ~1.5 for both types of rectifiers, indicating that diffusion currents were

dominant. Beyond ~2×V_F, series resistance effects controlled the current. This behavior is often reported for SiC junction rectifiers, while Schottky rectifiers in that materials system show ideality factors of 1.1–1.4. In our GaN devices, the higher ideality factors may reflect the high compensation levels in the material.

Figure 3-17 shows the reverse current (I_R) at –100 V reverse bias for GaN and AlGaN rectifiers of different contact diameter, for three different measurement temperatures. Since $I_R \propto$ contact diameter, this indicates that under these conditions the reverse current originates from surface periphery leakage. Similar results were obtained for the GaN rectifiers as shown in Figure 3-16. The activation energy for this periphery leakage was ~0.13 eV, which may represent the most prominent surface state giving rise to the current. At voltages approximately 90% of the breakdown values, the reverse current was proportional to contact area, indicating that bulk leakage is dominant under these conditions.

3.4.3 Conclusion and Summary

In conclusion, the temperature dependence of V_{RB} has been measured in high breakdown GaN and AlGaN Schottky rectifiers. The temperature coefficient is negative, which is a significant disadvantage for devices intended for high temperature operation, and there are indications that it is a function of V_{RB}. The forward current conduction makes a transition from recombination to diffusion currents. The reverse leakage current originates from surface components around the rectifying contact at modest voltages. This current is thermally activated with an energy of 0.13 eV. The yield of acceptable devices (i.e., with V_{RB} at least 90% of the maximum found on a wafer and R_{ON} within 50% of the best values obtained) was rather small (~15%), so there is still much

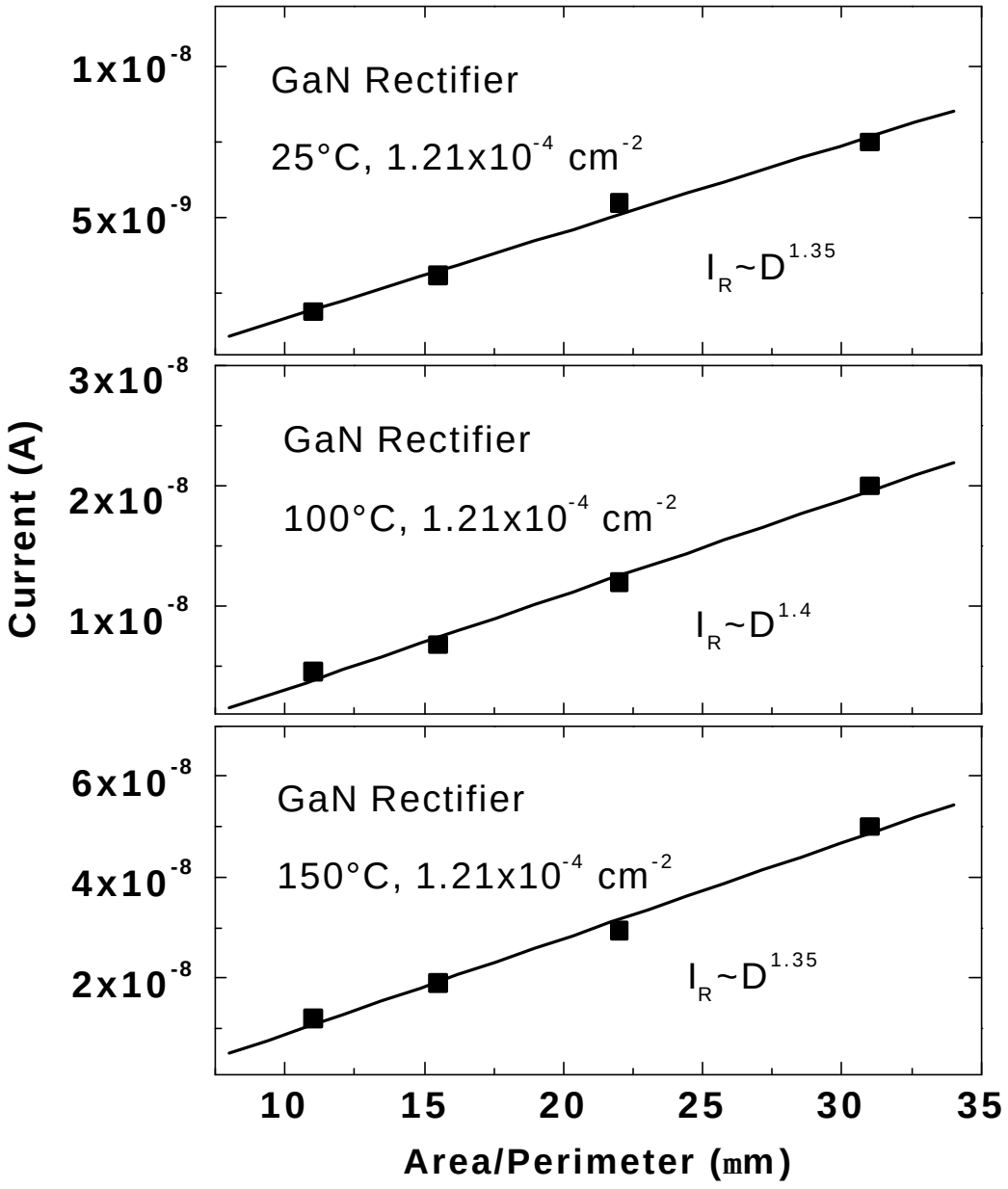

Figure 3-16 Reverse current at -100 V bias for AlGaN rectifiers measured at three different temperatures.

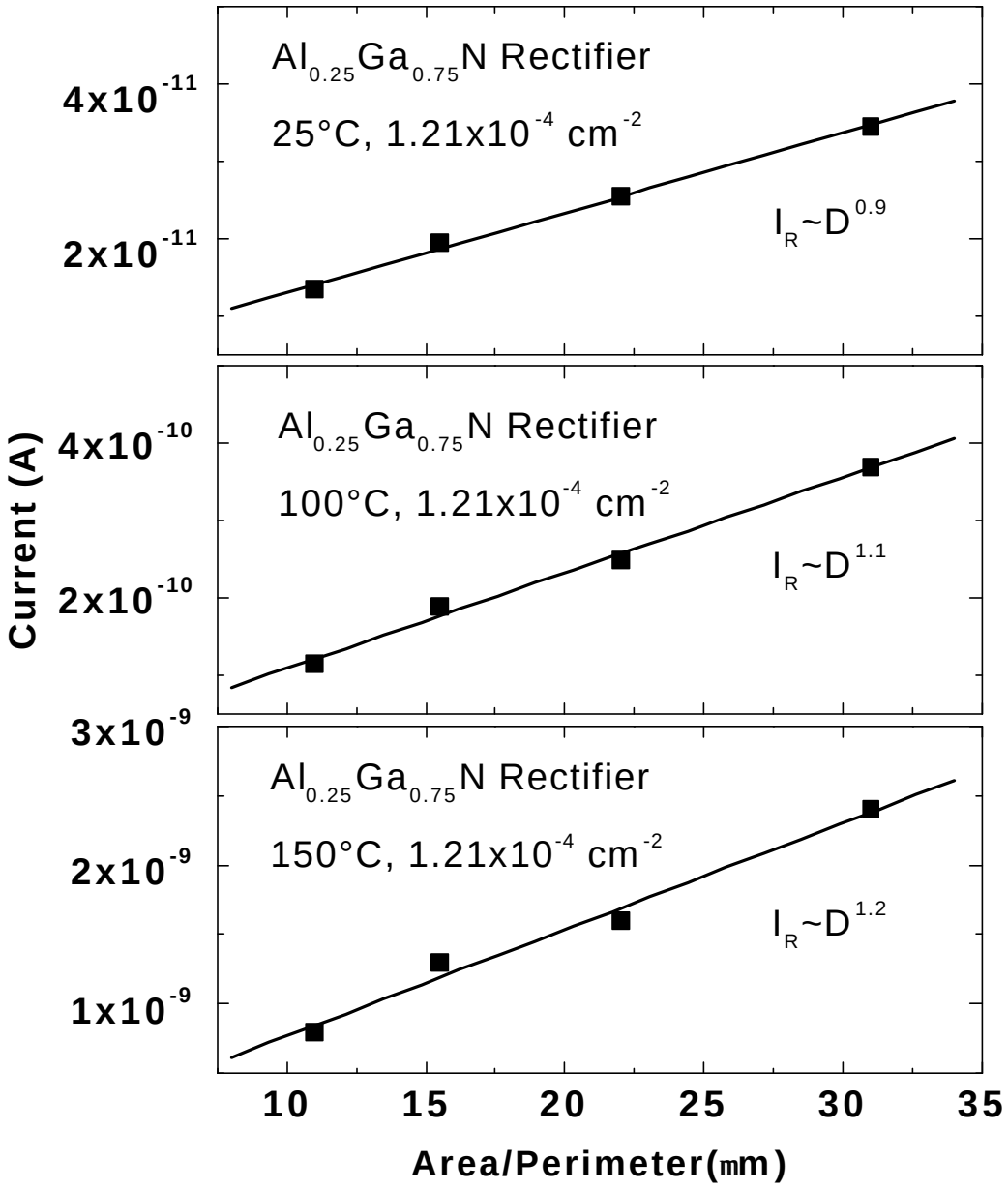

Figure 3-17 Reverse current at -100 V bias for AlGaN rectifiers measured at three different temperatures.

development needed on both materials and processing.

3.5 Lateral $Al_xGa_{1-x}N$ Power Rectifiers with 9.7 kV Reverse Breakdown Voltage

3.5.1 Introduction

There have been advances in developing GaN and AlGaN power rectifiers which are key components of inverter modules for power flow control circuits. Vertical geometry GaN Schottky rectifiers fabricated on conducting materials typically show reverse breakdown voltages (V_B) 750 V whereas lateral devices on insulating GaN and AlGaN have V_B values up to 4.3 kV.

Since the predicted breakdown field strength in GaN is of order $2–3\times10^6$ V-cm^{-1} [121, 110], there appears to be much room for improvement in rectifier performance and a need to understand the origin of reverse leakage currents, breakdown mechanisms, and the effect of contact spacing on V_B. In this letter we report on the variation of VB with Schottky-to-ohmic contact gap spacing in $Al_xGa_{1-x}N$ diodes (x = 0–0.25) employing p-guard rings and extension of the Schottky contact edge over an oxide layer for edge termination. V_B values up to 9700 kV were achieved for $Al_{0.25}Ga_{0.75}N$ rectifiers, with breakdown still occurring at the edges of the Schottky contact. The reverse leakage current just before breakdown is dominated by bulk contributions, scaling with the area of the rectifying contact.

3.5.2 Experimental Methods

The rectifiers were fabricated on resistive (~10^7 Ωcm) layers of 2.5–3 μm thick GaN or AlGaN grown on c-plane Al_2O_3 substrates at 1040–1100 °C by metalorganic chemical vapor deposition. To create n^+ regions for ohmic contacts, Si^+ ions were implanted at 5×10^{14} cm^{-2}, 50 keV, and activated by annealing at 1150 °C for 10 s under

N_2. It is important to control both the heating and cooling rates to avoid cracking of the AlGaN layer. Mg^+ implantation at 5×10^{14} cm^{-2}, 50 keV was used to create 30 μm diameter p-guard rings at the edge of the Schottky barrier metal. The rectifying contact diameter was 124 μm in most cases, while the distance of this contact from the edge of the ohmic contact was varied from 30–100 μm. The Schottky metal was extended over a SiO_2 layer deposited by plasma-enhanced chemical vapor deposition in order to minimize field crowding. Ohmic contacts were created by lift off of e-beam evaporated Ti/Al/Pt/Au annealed at 750 °C for 30 s under N_2. The Schottky contacts were formed by lift off of e-beam evaporated Pt/Ti/Au. A schematic of the completed rectifiers is shown in Fig. 3-18. Current–voltage (I–V) characteristics were recorded on a HP4145 parameter analyzer, with all testing performed at room temperature under a Fluorinert® ambient.

3.5.3 Results and Discussion

Figure 3-19 shows the measured V_B values for GaN and $Al_{0.25}Ga_{0.75}N$ rectifiers as a function of the gap spacing between the rectifying and ohmic contacts. For gaps between 40 and 100 μm, V_B is essentially linearly dependent on the spacing, with slopes of 6.35×10^5 V·cm–1 for $Al_{0.25}Ga_{0.75}N$ and 4.0×10^5 V·cm–1 for GaN. We assume the deviation from these values at shorter spacing is due to the fact that the p-guard ring almost covers this region. In vertical geometry diodes V_B is related to the maximum electric field strength at breakdown E_M, through the relation [108]:

$$V_B = E_M W_B / 2 \qquad \text{3-4}$$

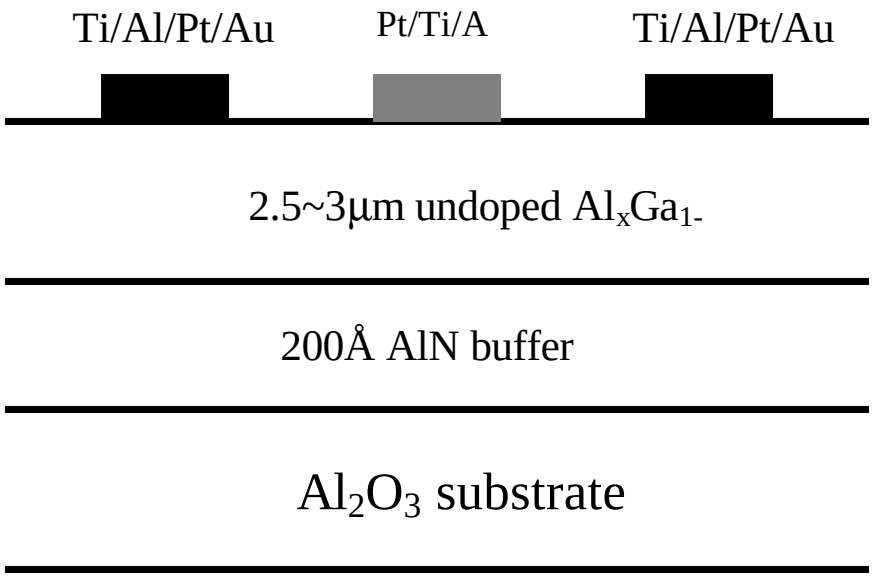

Figure 3-18 Schematic of lateral geometry AlGaN rectifiers using edge termination.

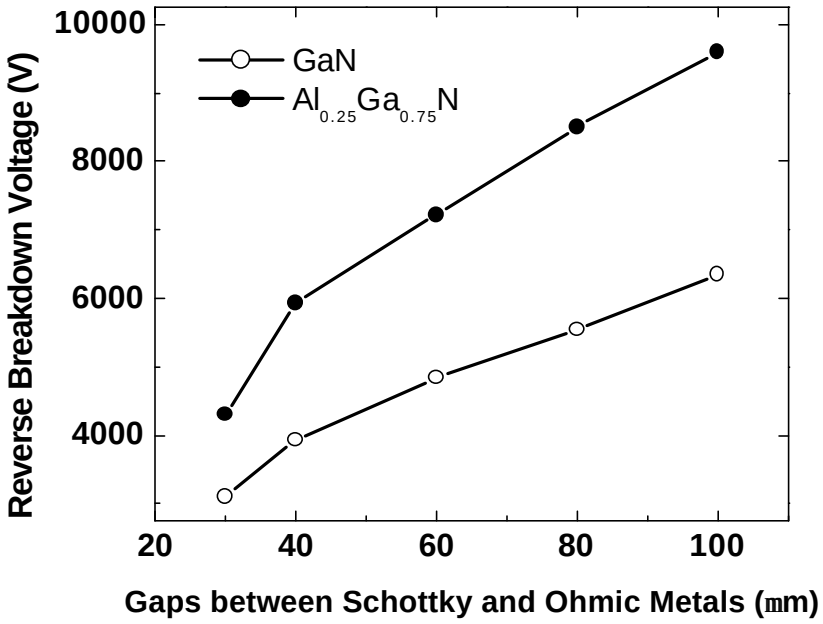

Figure 3-19 Effect of Schottky-ohmic contact gap spacing on V_B for GaN and $Al_{0.25}Ga_{0.75}N$ rectifiers.

where W_B is the depletion width at breakdown. In our laterally depleting devices the surface quality will dominate the onset of breakdown, which is reflected in the lower breakdown field observed. However, given the current state of defect densities in epitaxial GaN, the lateral geometry seems the most promising, for the time being, for achieving very high V_B values. Quasi-substrates of GaN, produced by thick epi-growth on mismatched substrates and subsequent removal of this template, are soon to be commercially available. In some cases the background doping in these is as low as 7.9×10^{15} cm^{-3} which makes feasible the use of these thick (200 μm) freestanding GaN films for vertically depleting rectifiers.

Figure 3-20 shows some I–V characteristics from the 100 μm gap spacing GaN and $Al_{0.25}Ga_{0.75}N$ rectifiers. The best forward turn-on voltages, V_F (defined as the forward voltage at a current density of 100 A cm^{-2}) was ~15 V for GaN and ~33 V for $Al_{0.25}Ga_{0.75}N$. These are much higher than the values obtained on more conducting GaN films, where V_F is typically 5–8 V. Note, however, that the ratio V_B/V_F is still very high for the resistive diodes, with values ranging from 294 to 423. The specific on-state resistance for a rectifier is given by

$$R_{ON} = (4V_B^{\,2} / e \cdot m \cdot E_M^{\,3}) + r \cdot s \cdot W_S + R_C \qquad 3\text{-}5$$

where ε is the GaN permittivity, μ the carrier mobility, S and W_S are substrate resistivity and thickness, and R_C is the contact resistance. The best on-state resistances we achieved were 0.15 Ω-cm^2 for GaN and 1 Ω-cm^2 for $Al_{0.25}Ga_{0.75}N$, leading to figure of merits $(V_B)^2/R_{ON}$ of 268 MW-cm^{-2} and 94 MW-cm^{-2}, respectively. At low reverse voltages (2000 V), the magnitude of the reverse current was proportional to contact diameter. As

the diodes approached breakdown the reverse current was proportional to contact area, suggesting bulk leakage becomes dominant.

The variation of V_B with Al percentage in the AlGaN layer of the rectifiers is shown in Figure 3-21, along with the calculated bandgaps. V_B does increase with increasing bandgap Eg, but is not proportional to $(Eg)^{1.5}$ as expected from a simple theory. The presence of bulk and surface defects will have a strong influence on V_B, and these are not well controlled at this stage of AlGaN rectifier technology.

To place our results in context, Figure 3-22, Figure 3-23 and Figure 3-24 show a compilation of R_{ON}, reverse leakage current and forward turn-on volatges versus V_B data for state-of-the-art SiC and GaN Schottky diode rectifiers, respectively, together with theoretical curves for Si, 6H, and 4H–SiC and hexagonal GaN. Our results for high breakdown GaN devices show the on resistances and forward turn-on voltages are still well above the theoretical values and more work is needed to understand current conduction mechanisms, the role of residual native oxides on contact properties, and impact ionization coefficients in GaN.

3.5.4 Summary and Conclusion

In conclusion, lateral geometry $Al_xGa_{1-x}N$ Schottky rectifiers employing edge termination show reverse breakdown voltages up to 9.7 kV. These breakdown voltages scale with contact spacing and the rectifiers appear promising for high power electronics applications.

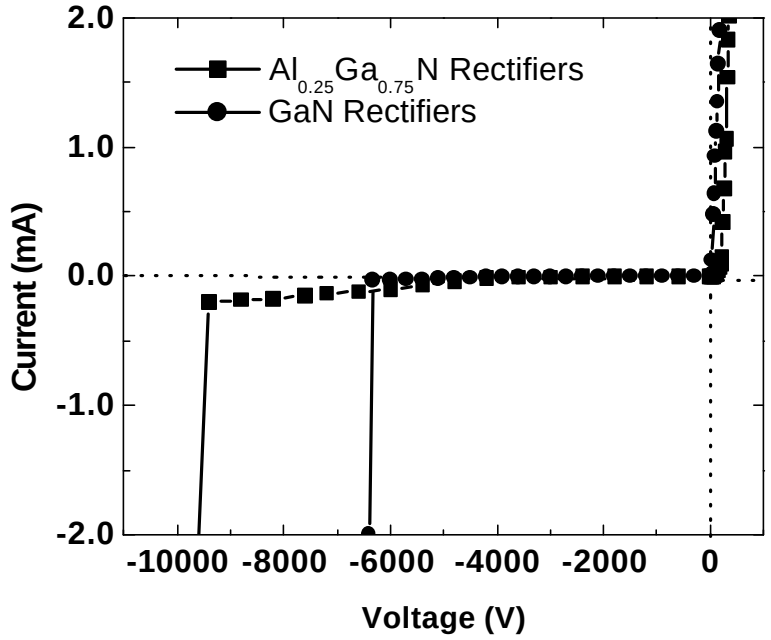

Figure 3-20 Current-voltage characteristics of GaN and $Al_{0.25}Ga_{0.75}N$ rectifiers.

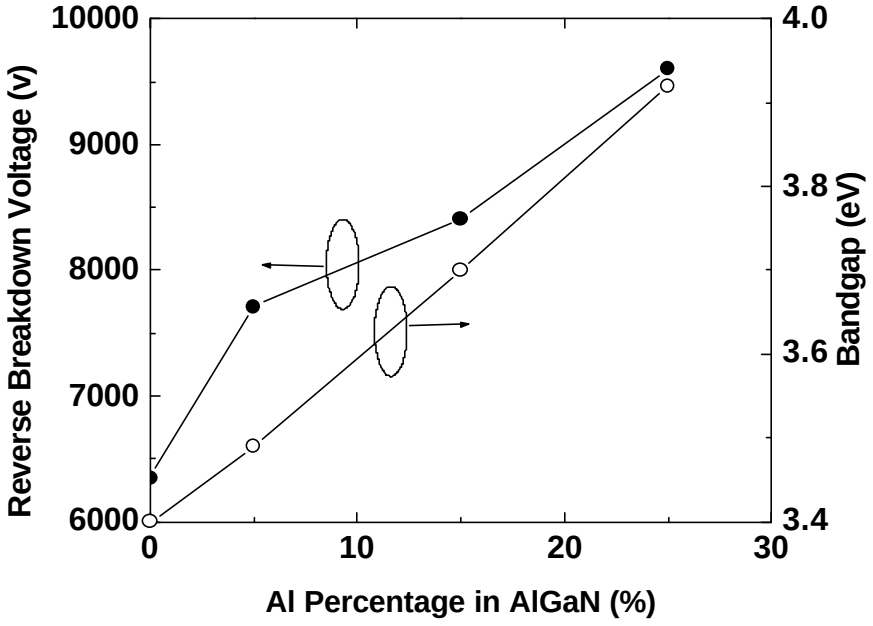

Figure 3-21 Variation of V_B with Al percentage in the AlGaN layer of the rectifiers.

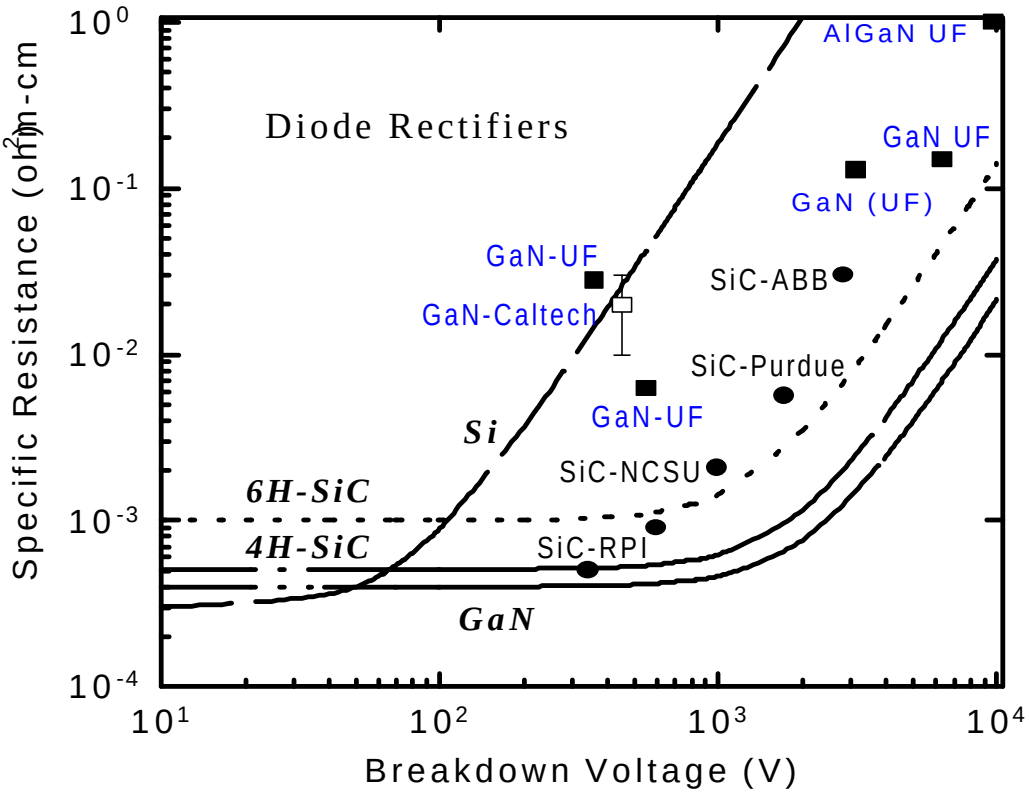

$$\bullet R_{ON} = \frac{4(V_{RB})^2}{m \in E_C^{\ 2}} + P_{sub} W_{sub} + R_C$$

Where:

V_{RB} = breakdown voltage

μ = carrier mobility

= permittivity

E_C = critical field for breakdown

P_{sub} W_{sub} = resistivity/thickness of substrate

Figure 3-22 On-state resistance vs V_B for wide band gap Schottky rectifiers. The theoretical performance limits of Si, SiC, and GaN devices are shown by the solid lines.

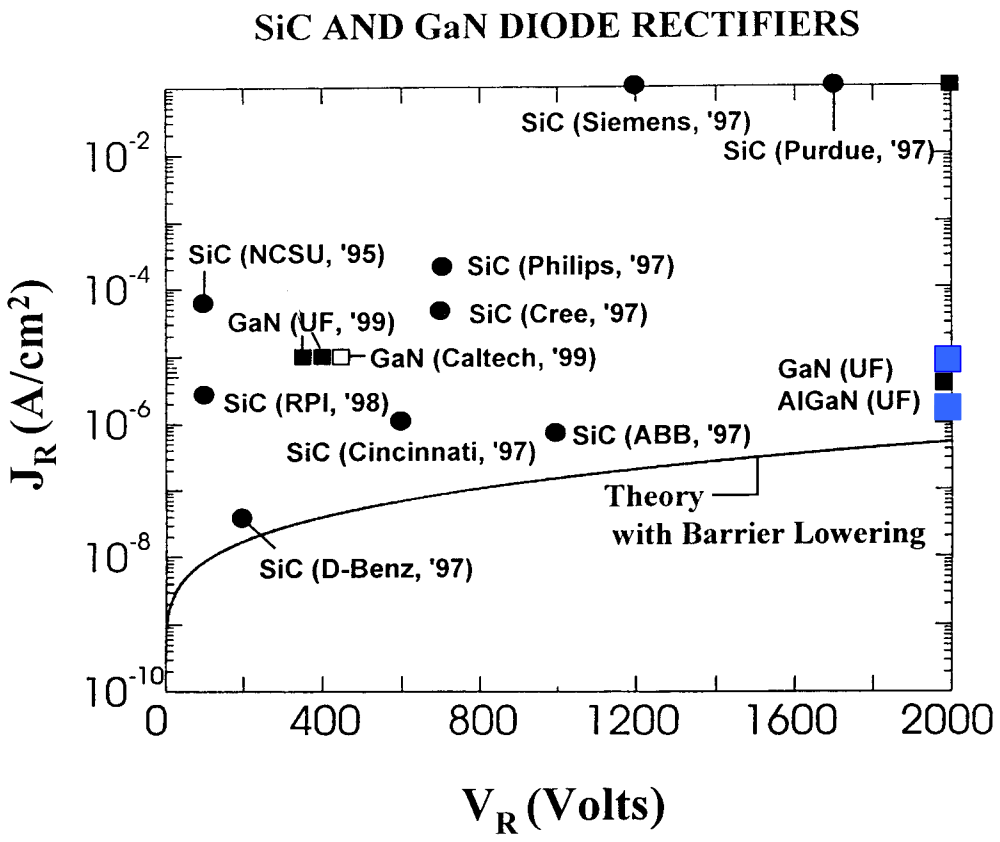

$$J_R = A^{**}T^2 \exp[\frac{-e}{kT}(f_B - \Delta f_B)]$$

Where:

J_R = reverse current density

A** = Richardson's constant

T = absolute temperature

ϕ_B = Schottky barrier height

$\Delta\phi_B$ = image-force induced barrier lowering

Figure 3-23 Reverse leakage current J_R vs V_B for wide band gap Schottky rectifiers.

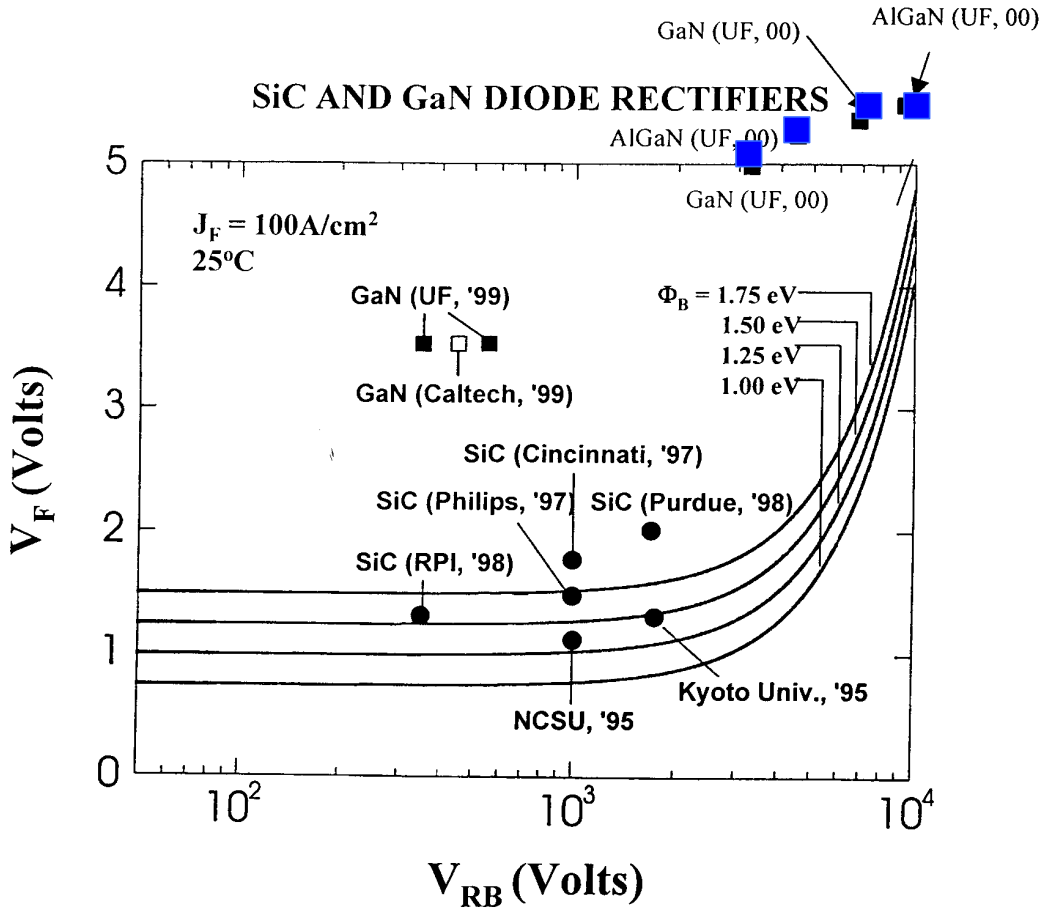

$$V_F = \frac{nkT}{e}\ln\left(\frac{J_F}{A^{**}T^2}\right) + nf_B + R_{ON}J_F$$

Where:

n = ideality factor

T = absolute temperature

A** = Richardson's constant

ϕ_B = Schottky barrier height

R_{ON} = specific on-resistance

Figure 3-24 Forward volatge drop V_F vs V_B for wide band gap Schottky rectifiers.

3.6 Vertical and Lateral GaN Rectifiers on Free-Standing GaN Substrates

Although the GaN-based power rectifiers on sapphire substrate show impressive results, there are still numerous short-comings in these devices, including higher reverse leakage current than expected from thermionic emission, high forward turn-on voltages, negative temperature coefficients for reverse breakdown voltage, non-uniformities and the low thermal condicutivity of the sapphire substrate.

Recently there have been initial reports of reverse recovery characteristics of GaN Schottky rectifiers fabricated on free-standing substrates. Those substrates have the advantages of higher thermal condiuctivity than sapphire and the potential for higher forward current densities and reverse breakdown voltages than lateral rectifiers fabricated in insulating substrates.

We investigated the effect of contact dimension and current flow direction (lateral versus vertical) on the on-state resistance and breakdown voltage of Gan Schottky rectifiers fabricated on free-standing GaN substrates. There is a dramatic effect of contact diameter on V_B, with the latter ranging from 6 to 700 V as the diameter was decresred from 7 mm to 75 μm. At the lower end of thios range the on-state resistance (R_{ON}) are exceptionally low (1.71~3.01 $m\Omega \cdot cm^{-2}$), producing maximum figure-of-merit (V_B^2/R_{ON}) above 100 $MW \cdot cm^{-2}$.

The 200 μm thick GaN quasi-substrates were grown by hydride vapor phase epitaxy on sapphire substarte, lifted-off by laser heating and then etched and polished as shown in Figure (3-25). The measured n-type doping concentration was ~10^{17} cm^{-3}. Mg^+ implantation at 5×10^{14} cm^{-2}, 50 keV, followed by annealing was used to create 30 μm

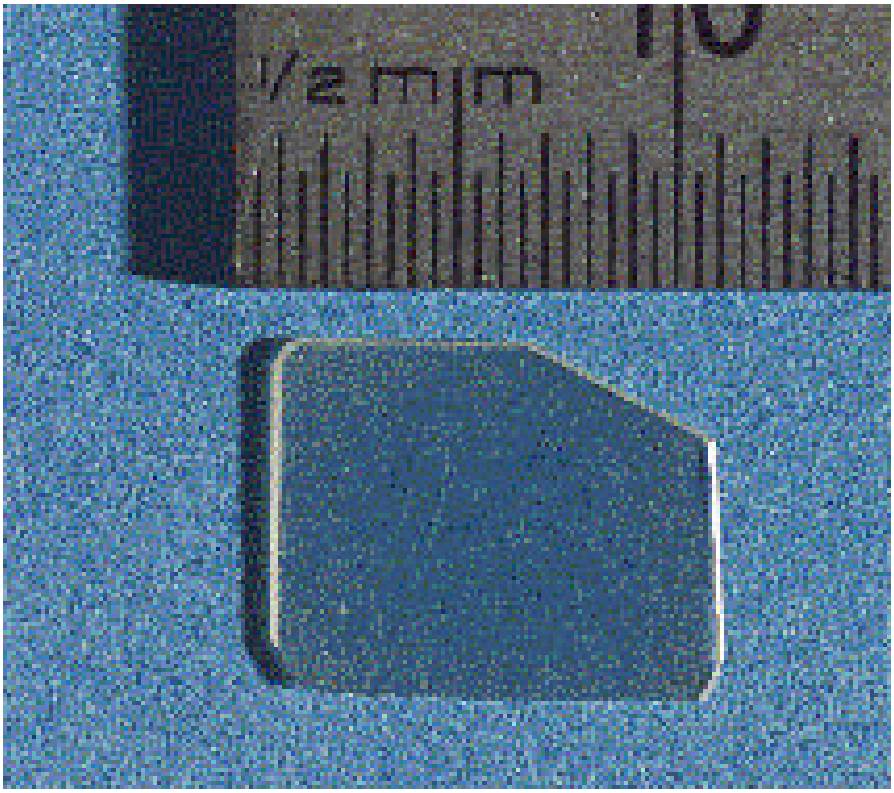

Figure 3-25 Free-standing GaN substrate grown by HVPE.

diameter p-guard rings at the edge of the Schottky contacts. The rectifying contact diamter was 75 μm for the small-area device and 7mm for the large-area devices. On these latter structures the Schottky metal was extended over a SiO_2 layer deposited by rf (13.56 MHz) plasma enhanced chemical vapor deposition using SiH_4 and N_2O as the precursors. Full-area back ohmic contacts were placed on the N-face using e-beam evaporation of Ti/Al/Pt/Au. On the small-area devices we also placed ohmic contacts on

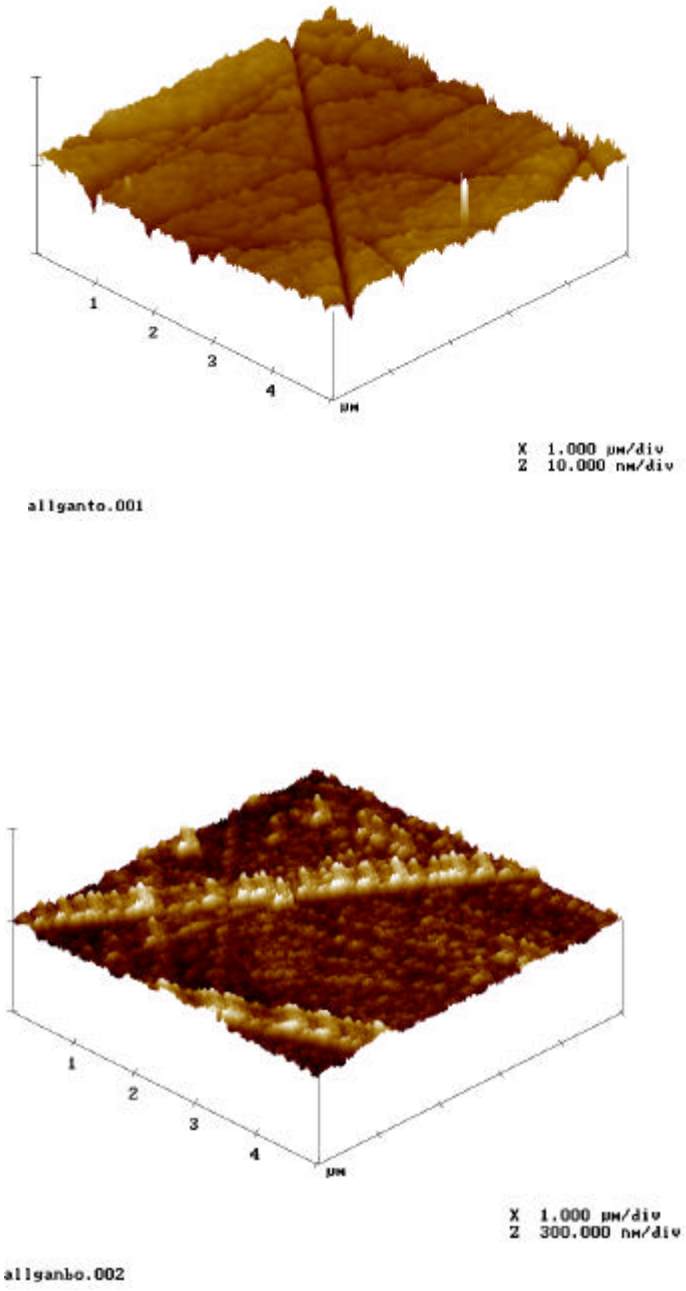

Figure 3-26 AFM images showing Ga- (front surface, top) and N- (backside surface, bottom) terminated surfaces.

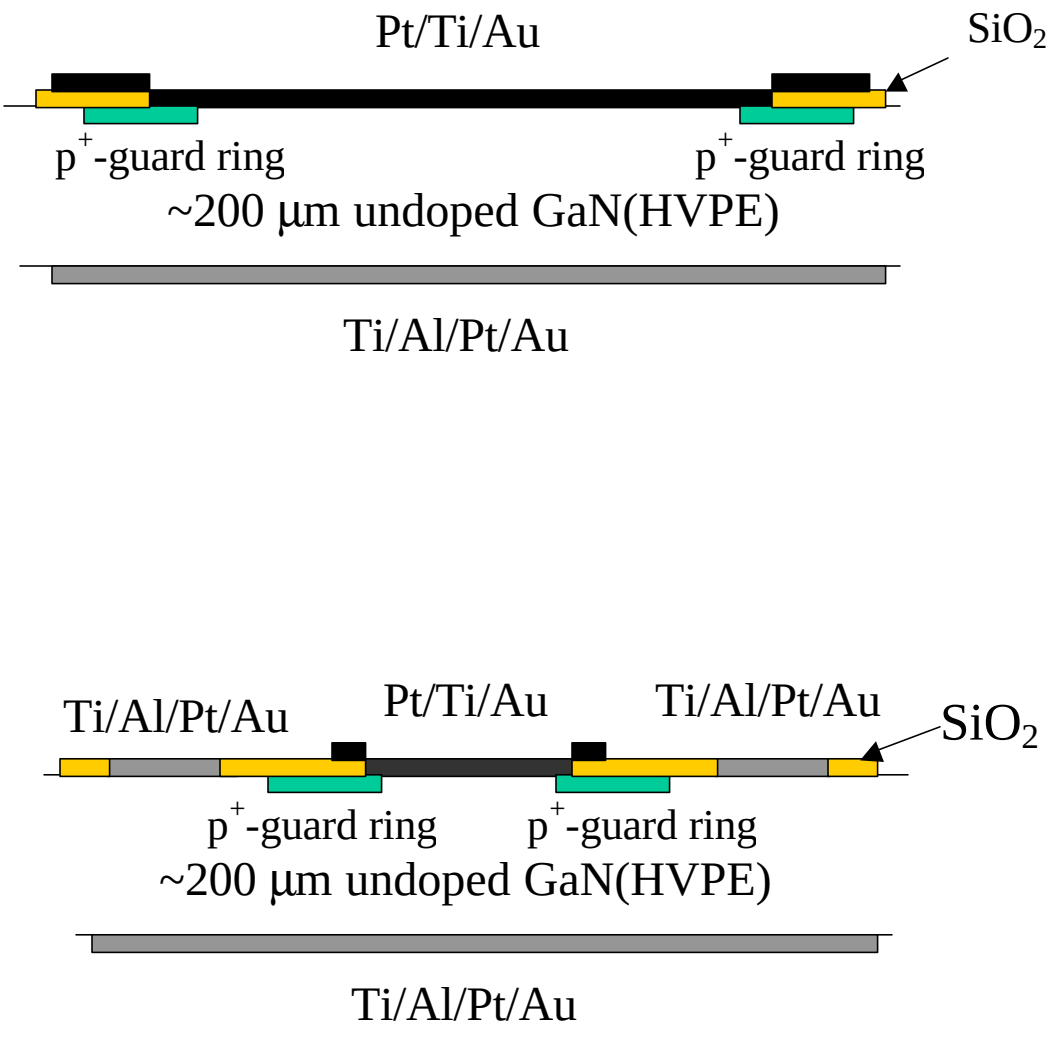

Figure 3.27. Schematic of 7 mm contact diameter (top) and 75 μm contact diameter (bottom) rectifiers.

the top (Ga-face) surface so that we could compare results from the lateral and vertical geometries. The top Schottky contacts were e-beam deposited Pt/Ti/Au in both large and small area devices. In the latter case, the Schottky-ohmic metal spacing was 30 μm. Schematics of the completed structures are shown in Fig. 3-27. Current-voltage (I-V) characteristics were recorded on an HP 4145B parameter analyzer at 25 °C for the forward part of the characteristics, while Tetronix 370A curve tracer was used for the reverse characteristics measuement.

Figure 3-28 shows the I-V characteristic from the large area rectifers. The reverse breakdown voltage (V_B) is only ~6 V and is obviously far below anything of practical use. The on-state resistance (R_{ON}) was 3.4 Ω-cm^2 for these devices. The low V_B is in stark contrast to the values achieved in smaller devices, as described below. Since the defect density in the quasi-substrate was ~10^5 cm^{-2} as measured by combined photo-chemical etching and atomic force microscopy, the large area rectifiers are highly likely to include one or more defects. Hsu et al. found that reverse bias leakage in GaN Schottky diodes occurred primarily at defects and dislocations. The figure-of-merit V_B^2/R_{ON} had a value of 10.7 W-cm^{-2} for the large area rectifiers while maximum current of ~500mA could be achieved before sample heating became a problem.

I-V characteristics from the small-area rectifers, measured in the lateral geometry are shown in Fig. 3-29. The V_B was ~250 V, with an excellent R_{ON} of 1.7 mΩ-cm^2. This on-state resistance is the lowest reported for any GaN rectifers and shows that continued improvements in surface cleaning and contact technologies for this materials system have led to a rapid maturation of our understanding of how to process these devices. The value of V_B^2/R_{ON} was 36.5 MW-cm^{-2}. Note that remarkable improvement in the electrical

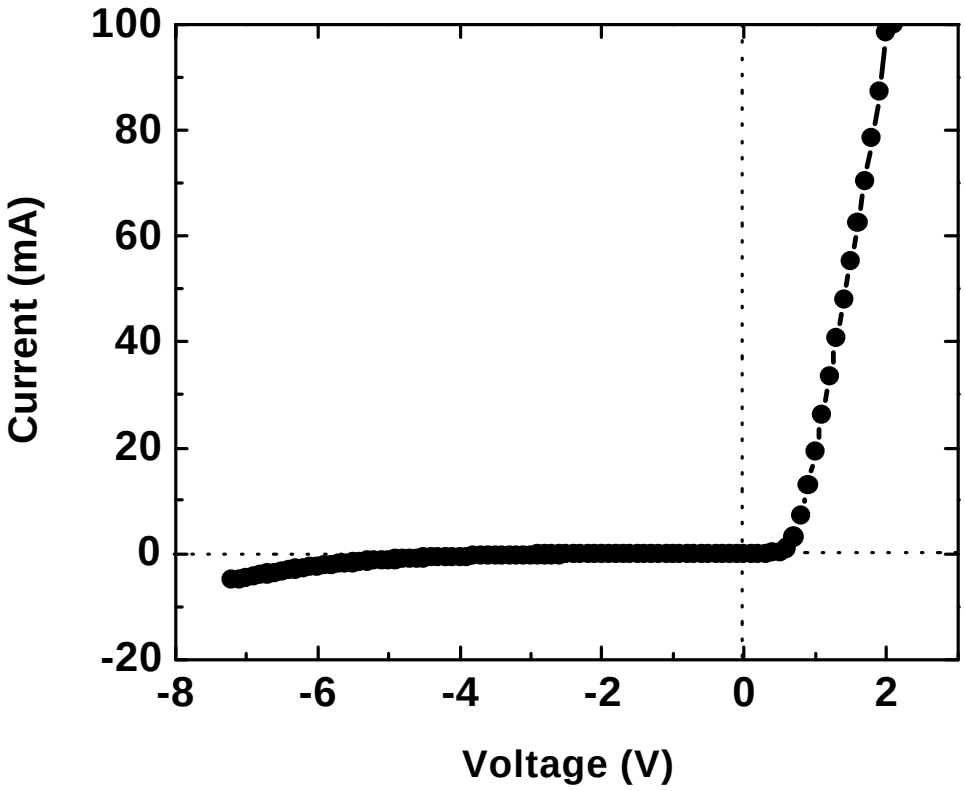

Fig. 3.28 Effect of Schottky-ohmic contact gap spacing on V_B for GaN and $Al_{0.25}Ga_{0.75}N$ rectifiers.

characteristics in the small-area rectifiers relative to the large devices fabricated on the same material. The forward turn-on voltage, V_F, defined as the forward bias at which the current density was 100 A-cm^{-2}, was 1.8 V. This is roughly half of what has been reported previously for GaN Schottky rectifersd on heterepitaxial layers. The forward turn-on voltage for Schottky rectifiers is given by

$$V_F = nkT/e(\ln[J_F / A^{**}T^2] + nf_B + R_{ON} \cdot V_F \qquad 3\text{-}6$$

Where n is the ideality factor, k is Boltzmann's constant, T the absolute diode temperature, e the electronic charge, I_F the forward current density at V_F, A** is the Richardson constant, ϕ_B the barrier height (~1.1 eV in this case for Pt on n-GaN) and R_{ON} the on-state resistance. One of the resons for the much lower V_F in these quasi-bulk rectifers is the small R_{ON} value to heteroepitaxial devices. The ideality factors were ~2 in the large area rectifers, indicating that recombination was the dominant current transport mechanism. In the small-area rectifers, n values was ~1.5, which is consistent with diffusion currents being dominant. These results can be explained by the relative probabilities for having defects in the active region of the rectifiers for the different contact diameters.

Figure 3-30 shows the I-V characteristics from the small-area diode measured from top-to-bottom, i.e. through the GaN substrate, rather than in the lateral geometry employed for the data of Figure 3-29. The VB in the vertical geometry was ~700 V, while Ron was 3.01 $m\Omega\text{-}cm^2$, leading to a figure-of-merit of 162.8 $MW\text{-}cm^{-2}$. This V_B is close to the expected maximum for the drift region doping concentrtation of ~10^{17} cm^{-3}. The forward turn-on voltage was still ~1.8 V, which is close to the minimum expected for a GaN rectifier with a V_B of 700 V and Assuming a barrier height of 1.1 eV. The ratio V_B/V_F is ~389, a record for GaN rectifers, and the forward current density could be pushed above 1000 $A\text{-}cm^{-2}$. A plausible explanation for the large improvement in V_B in the vertical geometry may be not only in the larger thickness in this direction (200 μm) compared to the 30 μm spacing between Schottky and ohmic contacts in the lateral direction, but also in the fact that the vertical depletion mode would minimize surface breakdown problems. The reverse current at bias value close to V_B was proportional to

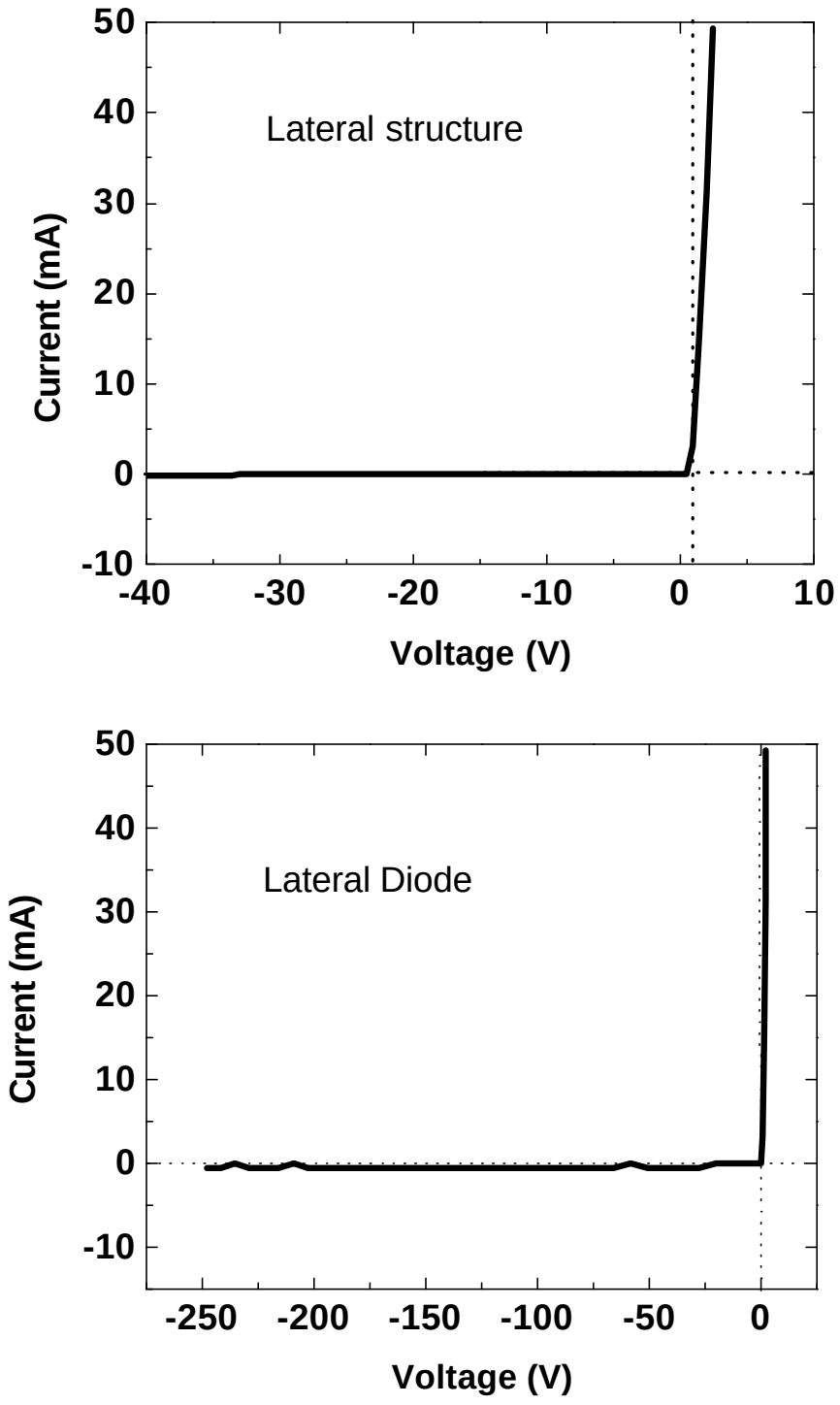

Figure 3.29. I-V characteristics from 75 μm contact diameter GaN rectifiers measured in lateral geometry.

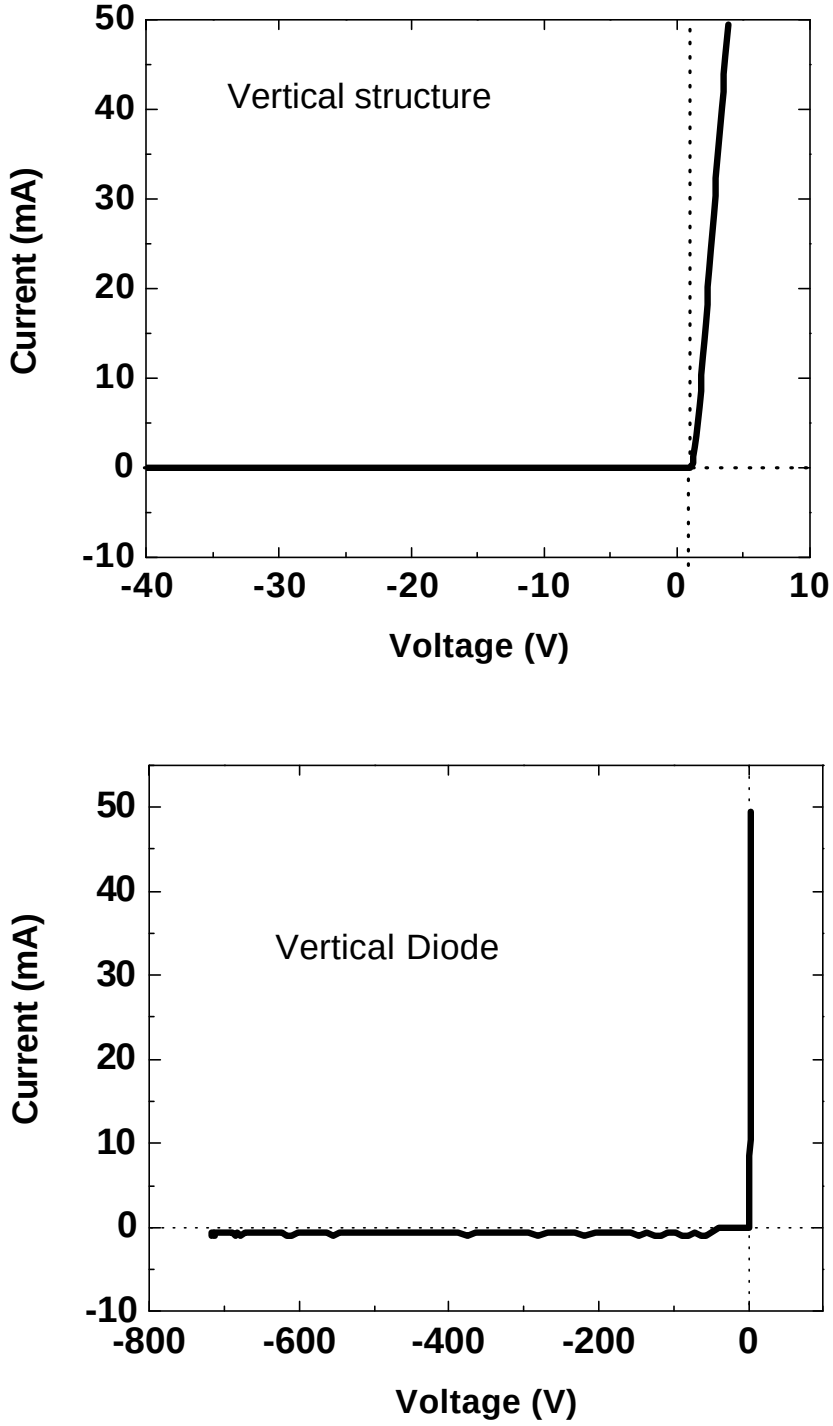

Figure 3.30. I-V characteristics from 75μm contact diameter GaN rectifiers measured in vertical geometry.

contact diameter, suggesting that the surface is playing a strong role in the origin of the leakage current.

One can expect major improvements in V_B in quasi-bulk GaN rectifiers as the background doping is decreased. For example, a 200 μm thick sample with a doping of 10^{15} cm^{-3} (which is quite feasible by reducing the background Si and O content, or by appropriate compensation) would have a predicted V_B of ~1.5×10^4 V. These would have application for power control system in the 13.8 kV class.

In summary, the size and geometry dependence of GaN Schottky rectifiers on quasi-bulk substrate has been investigated. The reverse breakdown voltage increases dramatically as contact size is decreased and is also much larger for vertically-depleting devices. The low on-state resistances produce high figure-of-merits for the rectifiers and show their potential for applications involving high power electronic control systems.

CHAPTER 4
GALLIUM NITRIDE P-I-N POWER RECTIFIERS

4.1 Comparison of GaN p-i-n and Schottky Rectifiers Performance

4.1.1 Introduction

Schottky and p-i-n diodes are employed as high-voltage rectifiers in power switching application. To suppress voltage transients when current is switched to inductive loads such as electric motors, these diodes are placed across the switching transistors. The advantage of simple metal-semiconductor diodes relative to p-n junction diodes is the faster turn-off because of the absence of minority carrier storage effects and lower power dissipation during switching. Wide bandgap semiconductors such as GaN offer additional advantages for fabrication of diode rectifiers, including much higher breakdown voltages and operating temperatures. There is much interest in developing advanced switching devices and control circuits for CW and pulsed electrical sub-systems in emerging hybrid-electric and all-electric vehicles, more-electric airplanes and naval ships and for improved transmission, distribution and quality of electric power in the utilities industry. Eventually one would like to reach target goals of 25 kV stand-off voltage, 2 kA or higher conducting current, forward drop less than 2% of the rated voltage and maximum operating frequency of 50 kHz.

Figure 4-1 shows a SIMS profile of H and other background impurities (along with intentional Si doping) in an MOCVD-grown p-i-n diode structure (left), together with the Mg profile in the structure (right). Notice once again that the H decorates the Mg

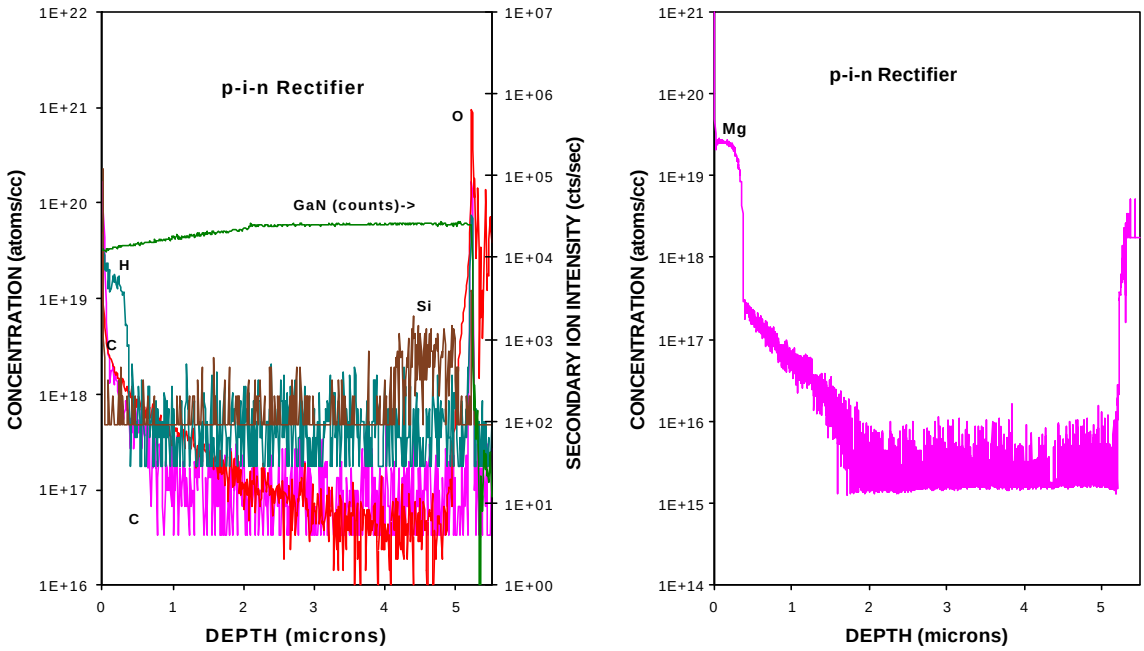

Figure 4-1. SIMS profiles of H and Si (left) and Mg (right) in an as-grown, MOCVD p-i-n rectifier structure.

due to formation of the neutral $(Mg\text{-}H)^{o}$ complexes. About 70-80% of the Mg atoms have hydrogen attached.

4.1.2 Experimental Methods

The structures were grown by MOCVD at 1050 °C onc-plane Al_2O_3 substrates. Growth commenced with a low temperature (530 °C) AlN template ~300 Å thick, followed by a 1.2 mm thick, Si-doped ($n=3\times10^{18}$ cm^{-3}) GaN layer, 4 µm of undoped ($n\times10^{16}$ cm^{-3}) GaN and 0.5 µm of Mg-doped ($N_A\sim10^{18}$ cm^{-3}) GaN. Both p-i-n and Schottky diodes were fabricated on the same wafer. This was achieved by dry etch removal of the p^{+}-GaN layer in some regions, followed by a wet etch (NaOH, 0.1 M, 80 °C) clean-up of 600 Å of material to remove residual lattice damage prior to deposition of the rectifying contact. In some cases, various amounts of material were removed by wet etching after plasma exposure and deposition of the rectifying contact.

For both p-i-n and Schottky diode structures, mesas were fabricated by dry etching down to the n^+ layer using Cl_2 /Ar ICP etching, followed by annealing at 750 ºC under N_2 to remove sidewall damage. Ohmic contacts to the n^+ layer were prepared by lift-off of Ti/Al/Pt/Au alloyed at 700 ºC, while rectifying contacts to the undoped GaN were formed by lift-off of Ni/Pt/Au. To form an Ohmic contact to the p^+ layer, we used the same metallization. Schematics of the p-i-n and Schottky rectifier structures are shown in Figure 4-2. A scanning electron micrograph of a typical diode is shown in Figure 4-3.

4.1.3 Results and Discussion

Current-voltage (I-V) measurements were recorded on a HP 4145B parameter analyzer. Figure 4-4 shows the I-V characteristics at 25 ºC for p-i-n and Schottky rectifiers fabricated side-by-side on the same wafer. There is a clear difference in the V_{RB} of the two devices (~490 V for the p-i-n versus ~347 V for the Schottky). For very high blocking voltages (typically in excess of ~3 kV) or forward current densities (>100 A cm^{-2}) the p-i-n is expected to have the advantage because of the prohibitive leakage and resistance of the drift region in a Schottky diode. However, for high frequency operation the Schottky has an advantage in switching speed due to the absence of minority carriers. The on-state characteristics of the Schottky and V_{RB} characteristics of the p-n junction can be achieved in junction barrier controlled Schottky rectifiers.

The forward voltage drop (V_F) of the two types of rectifiers can be written as

$$V_F = \frac{nkT}{e}\ln\left(\frac{J_F}{A^{**}T^2}\right) + nf_B + R_{ON}\cdot J_F \qquad \text{(Schottky)} \tag{4-1}$$

and

$$V_F = \frac{kT}{e}\ln\left(\frac{n_- n_+}{n_i^{\,2}}\right) + V_m \qquad \text{(p-i-n)} \tag{4-2}$$

where n is the ideality factor, k the Boltzmann's constant, T the absolute temperature, e the electronic charge, J_F the forward current density at V_F , A^{**} the Richardson constant, ϕ_B the barrier height, R_{ON} the on-state resistance, n_- and n_+ the electron concentrations in the two end regions of the p-i-n (the p^+-n and n^+-n regions) and V_m is the voltage drop across the i-region.

The typical values of V_F were ~5 V for the p-i-n rectifiers and ~3.5 V for the Schottky rectifiers, both measured at 25 °C and defining V_F as the forward voltage at which the current density was 100 A/cm^2. Both of these values are still well above the theoretical minima, which should be of the order of the barrier height for the Schottky metal (between 1 and 1.5 eV in our case) or the bandgap for the p-i-n diode (3.4 eV for GaN). A similar situation occurs in SiC rectifiers, although there have been reports of V_F values relatively close to the theoretical values. In general it is expected that V_F will remain fairly constant for GaN p-i-n's and Schottky rectifiers to breakdown voltages in the 3~5 kV range, at which point there is a sharp increase due to the increase in on-state resistance.

Forward I-V characteristics for p-i-n rectifiers of different contact areas are shown in Figure 4-5. It is often found for SiC p-I-n rectifiers that the Sah-Noyce-Shockley model for forward current conduction cannot be applied due to the presence of a multiple number of deep and shallow impurity levels in the bandgap, which can act as recombination sites. The I-V characteristic of Figure 4.4 corresponds well to the four different exponential regimes predicted by this model, with ideality factors close to 1 at

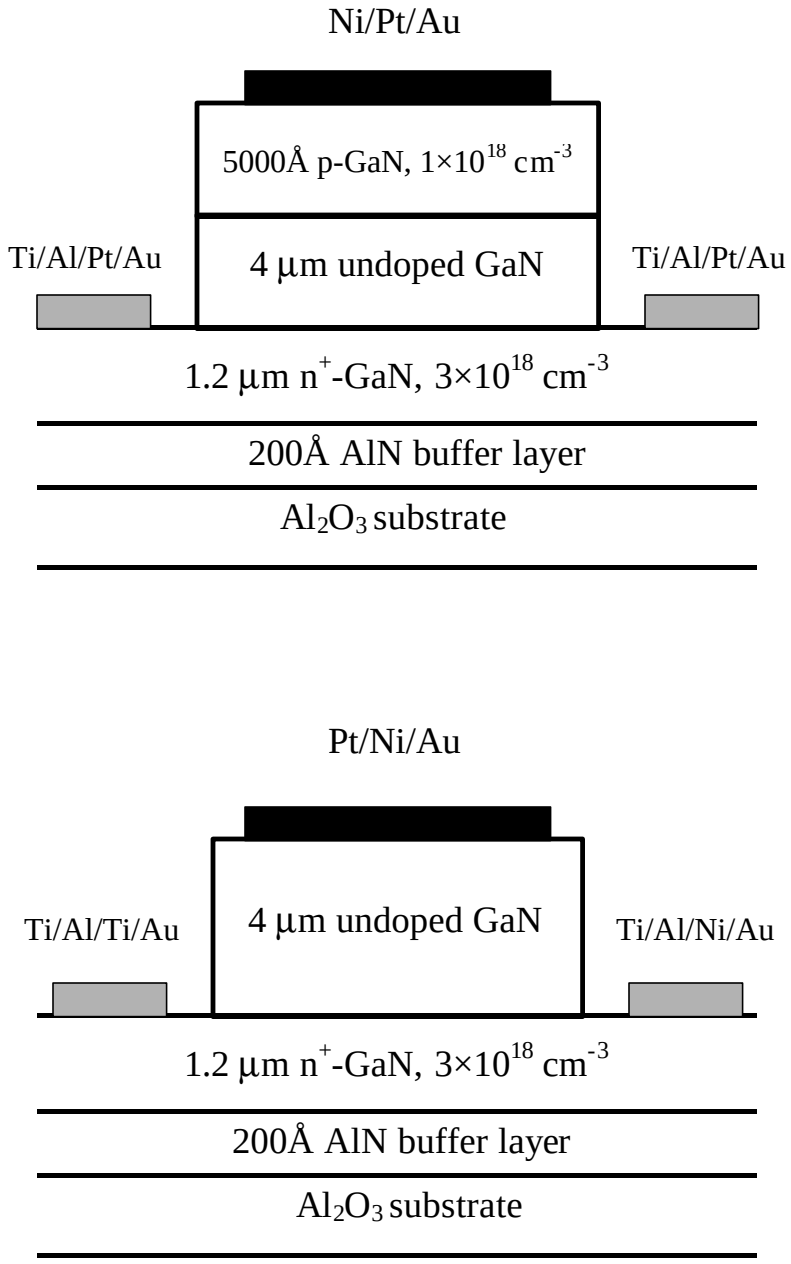

Figure 4-2 Schematic of p-i-n (top) an Schottky (bottom) rectifiers.

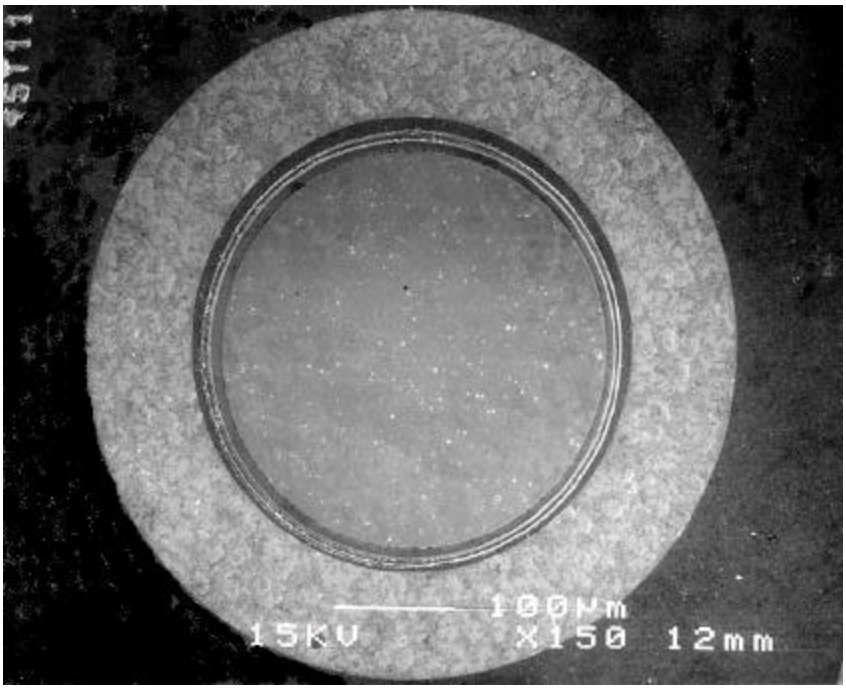

Figure 4-3 Schematic of p-i-n (top) an Schottky (bottom) rectifiers.

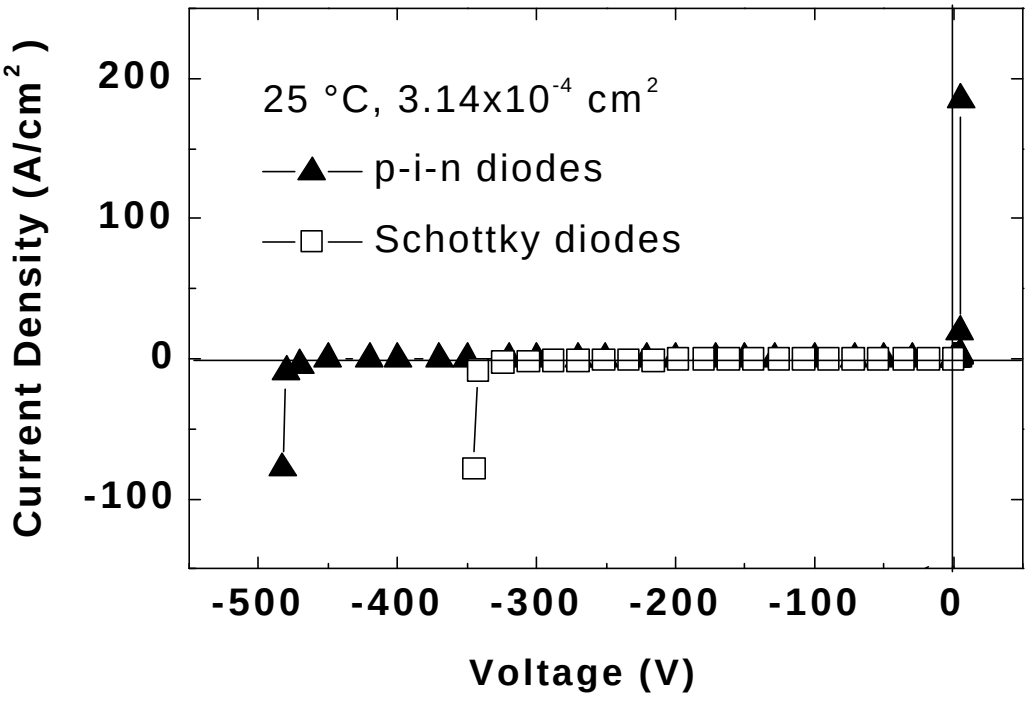

Figure 4-4 I-V Characteristicss from p-i-n and Schottky rectifiers.

low bias (< 0.6 V), ~2 at higher bias (0.6-5 V), dependent on the number of deep and shallow levels (around 5 V) and then ~2 at higher bias. In the latter case our characteristic becomes dominated by series resistance effects. In the multi-recombination center model, the forward current density J_F can be written as:

$$J_F = J_{01}\exp(\frac{eV}{2kT}) + J_{02}\exp(\frac{eV}{nkT}) + J_{S2}\exp(\frac{eV}{kT}) \qquad 4\text{-}3$$

where the first two terms represent the recombination current components and the third represents the diffusion current component originating from the recombination of electrons and holes in neutral regions outside the space-charge region. When we measure the forward I-V characteristics at elevated temperatures (150~250ºC) for the p-i-n diodes, the shape of the curves became more simplified and appeared to revert to the more common Sah-Noyce-Shockley form. This is probably a result of the fact that recombination through multiple deep and shallow levels becomes far less effective at elevated temperature. The Schottky diodes typically showed ideality factors in the range 1.3~1.6 at V_F=2.5~4 V and n=2 at V_F > 4 V, consistent with recombination at low bias and diffusion current at higher bias.

Figure 4-6 shows the reverse current measured at 100 V bias for p-i-n diodes with different contact diameters. For all the temperatures employed in these measurements, the reverse current was directly proportional to the diameter of the contact, indicating the dominance of surface perimeter leakage. If bulk leakage were dominant then we would obtain a slope of 2 for the plot of reverse current versus contact diameter. Note again that all of our devices are unpassivated and unterminated, thus no effort was made to minimize surface contributions to the leakage current. However, one of the expected

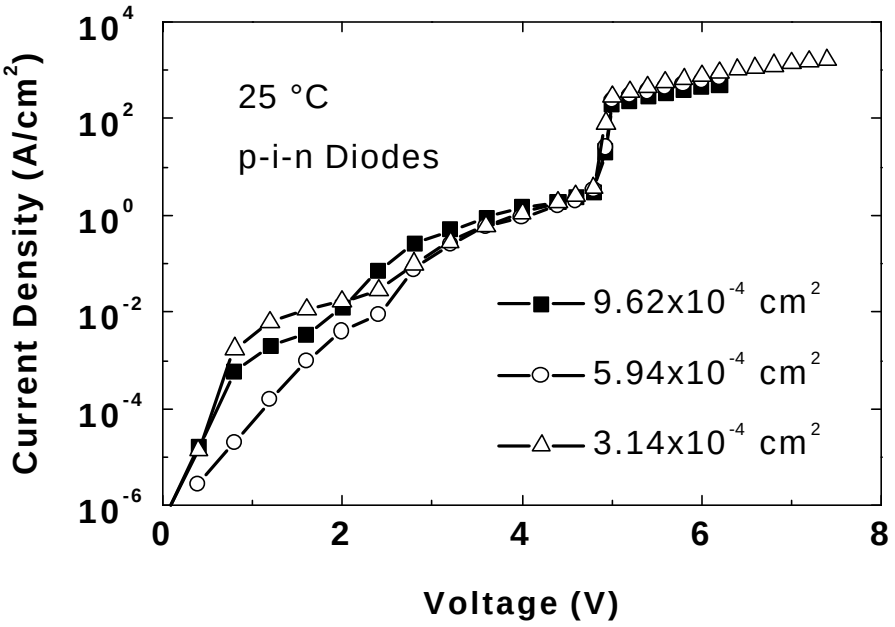

Figure 4-5 Forward I-V characteristics at 25 °C from p-i-n rectifiers of different contact areas.

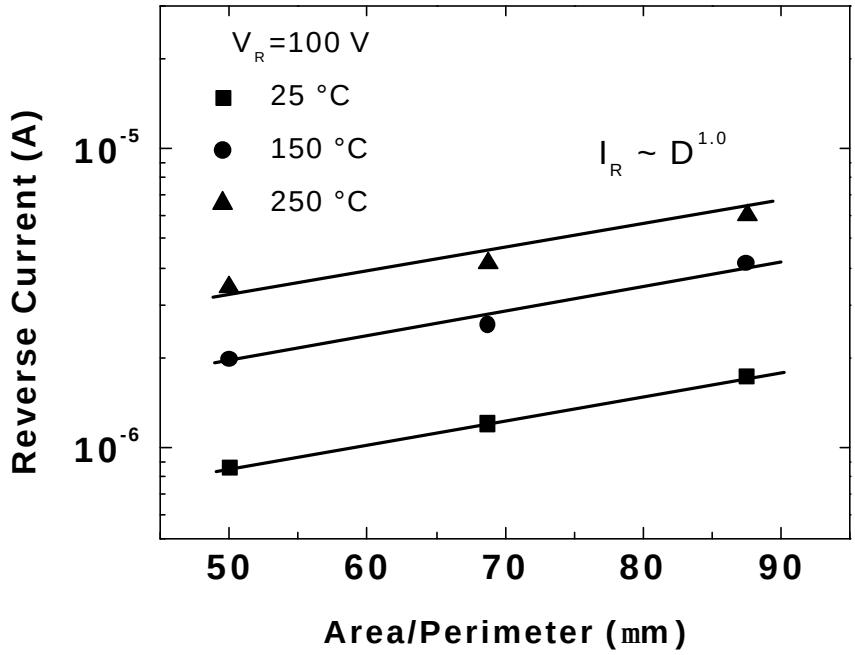

Figure 4-6 Reverse current as a function of contact diameter for p-i-n rectifiers at different temperatures.

attributes of GaN for electronic devices was a relative insensitivity to surface effects. We have consistently observed to the contrary that the GaN surface is easily disrupted during plasma processing or thermal annealing, usually through the preferential loss of nitrogen. Figure 4-7 shows the I-V characteristics from a p-i-n diode at three different temperatures. It is clear that there is a negative temperature coefficient for the reverse breakdown voltage. We observed similar behavior for Schottky diodes and a compilation of such data is shown in Figure 4.7. Here we have also included results from several other GaN Schottky rectifiers we have fabricated on n-type material. Note that in all cases the measured breakdown voltage decreases with temperature as:

$$V_{RB} = V_{RBO}(1 + \beta \cdot (T - T_0)) \qquad 4\text{-}4$$

where $\beta = -0.34 \pm 0.05$ V/K. Other reports have found positive temperature coefficients for AlGaN-GaN high electron mobility transistors (+0.33 V/K) and GaN p^+-p-n^+ linearly-graded junctions (+0.02 V/K). In separate experiments we have found that use of edge termination techniques (floating field rings, junction barrier control or metal overlap onto a dielectric on the surface) also produced negative temperature coefficients of V_{RB} in GaN Schottky rectifiers.

A direct comparison of GaN p-i-n and Schottky rectifiers fabricated on the same GaN wafer showed higher reverse breakdown voltage for the former (490 V versus 347 V for the Schottky diodes), but lower forward turn-on voltages for the latter (~3.5 V versus ~5 V for the p-i-n diodes). The forward I-V characteristics of the p-i-n rectifiers show behavior consistent with a multiple recombination center model. For the Schottky rectifiers, the forward I-V characteristics were consistent with Shockley-Read-Hall

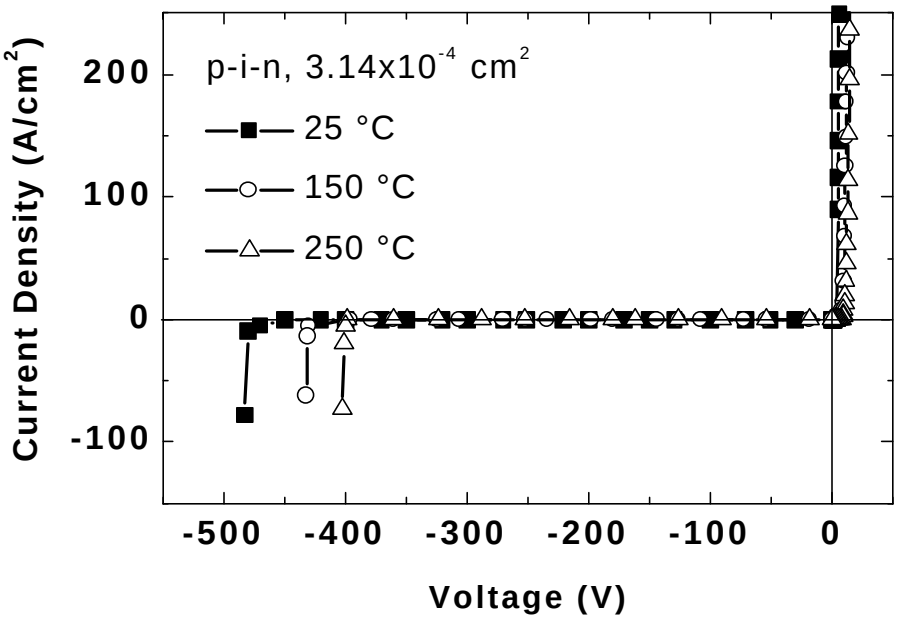

Figure 4-7 I-V characteristics from p-I-n rectifiers as a function of temperature.

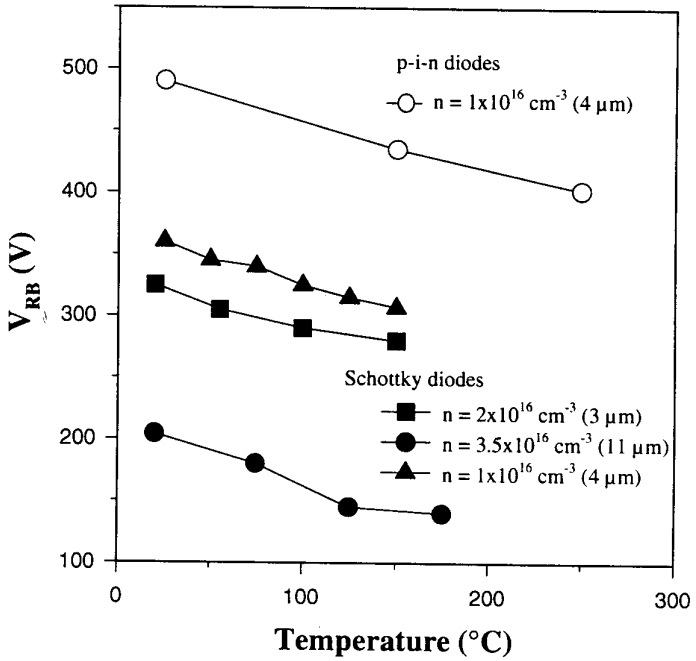

Figure 4-8 Temperature dependence of V_{RB} in p-i-n and Schottky rectifiers.

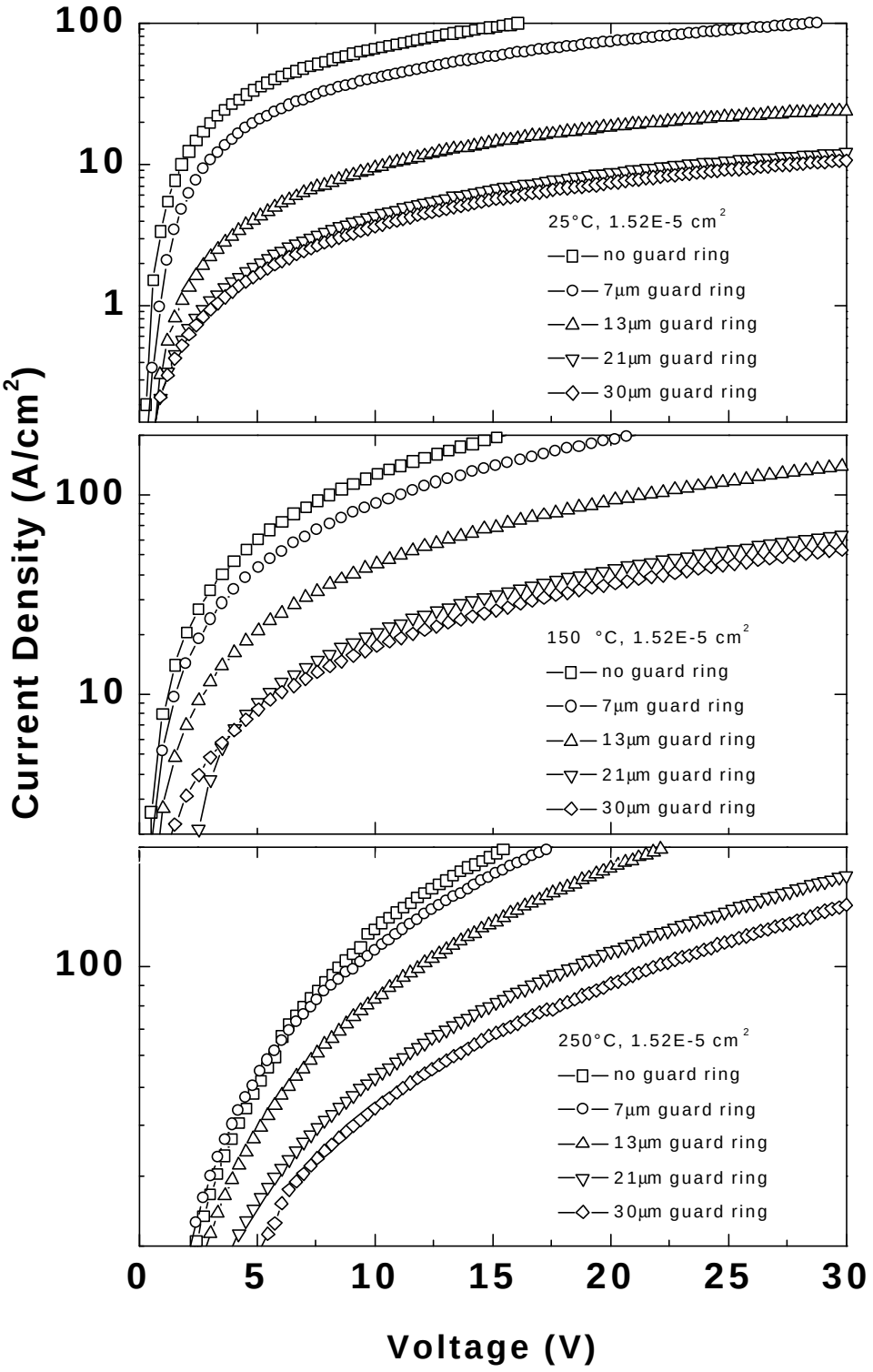

Figure 4-9 Forward I-V characteristics at 25 °C, 150°C and 250°C from GaN Schottky rectifiers employing p^+ guard rings of different widths.

recombination at low bias and diffusion currents at higher bias. The reverse current in both types of rectifiers was dominated by surface perimeter leakage at moderate bias. Finally, all of the devices we fabricated showed negative temperature coefficients for reverse breakdown voltage, which is a clear disadvantage for elevated temperature operation.

Figure 4-9 (top) shows the $J_F \sim V_F$ characteristics at 25 ºC from lateral geometry GaN rectifiers with different p^+ guard-ring widths. The series resistance effects are more obvious when the guard rings are employed, especially for widths beyond 7 μm. When we also used floating field rings of 5 μm width or junction barrier control we also observed an increase in the series resistance in the rectifiers. Even though edge termination techniques improved V_{RB} (from 2.3 kV in unterminated diodes to 3.1 kV with optimized edge termination), they produced a deterioration of the forward current conduction. We believe that more work needs to be done to optimize the design and implementation of the implanted p-guard rings. In currently available GaN it is difficult to activate implanted acceptor dopants because of the presence of compensating defects and impurities and the difficulty in avoiding nitrogen loss from the surface during annealing.

Figure 4-9 (center) shows the forward J_F -V_F characteristics at 150°C from the lateral GaN rectifiers with guard rings of different widths. The series resistance effect is less evident at this temperature and current densities of 100 A/cm^2 are reached at lower forward biases. Similarly, the use of blocking rings and junction barriers control deteriorated the current conduction, but in all cases the current densities were much higher than at 25 ºC.

Similar data are also shown in Figure 4-9 for measurement at 250 °C. The same trend holds, namely that lower forward voltages were needed to reach high current densities. The best on-resistances obtained at different temperatures were 0.13 Ωcm2 at 25°C, 0.075 Ωcm^2 at 150°C and 0.067 Ω-cm^2 at 250°C. The figure-of-merit V_{RB}^2/R_{ON} was 73.9 W/cm^2 at 25°C, 64.5 MW/cm^2 at 150°C and 38.2 MW/cm^2 at 250°C. Thus, even though R_{ON} decreased with temperature, so did V_{RB} because of a negative temperature coefficient for this parameter of ~6 V/K in these high breakdown rectifiers.

A compilation of data for V_F versus V_{RB} for GaN and SiC Schottky rectifiers is shown in Figure 4-10. The solid lines are theoretical values for SiC, assuming different barrier heights. While SiC rectifiers have achieved V_F values close to the theoretical values, the GaN devices are still well below their optimal performance. This clearly indicates that much more work is needed in the areas of thermally stable rectifying contacts, surface cleaning and preparation, and material quality. On the positive side, all of the GaN results have been reported only in the past year or so, and represent excellent progress in this field.

Figure 4-11 shows a compilation of published results for R_{ON} versus V_{RB} for SiC and GaN Schottky rectifiers. The lines on the plot represent theoretical values for Si, 4H-SiC, 6H-SiC and GaN. The first reports on GaN (V_{RB} values of ~500 V) show performance similar to that expected for Si. The more recent results, with V_{RB} values of >3 kV at R_{ON} values <1 Ωcm2, show performance well in excess of that possible with Si. Note that SiC has achieved performance close to its theoretical values, emphasizing its more mature state of development.

The reverse current density for SiC and GaN Schottky rectifiers is shown in Figure 4-12 as a function of reverse bias. Note that this is not reverse breakdown voltage, but simply reverse bias. The solid line represents values calculated for SiC, assuming barrier lowering due to image-force effects. Once again, these are some reports for SiC rectifiers with J_R values close to the theoretical minimum. However, most wide bandgap rectifiers show reverse currents well above the predicted values, which indicates the role of crystal defects and surface leakage in influencing the device performance. In all of our GaN diodes we find $I_R \propto V_R^{0.5}$, which is indicative of Shockley-Read-Hall recombination being the dominant current mechanism.

To date there have not been any published reports on p-i-n GaN rectifiers intended for high voltage applications, at least to our knowledge. Figure 4-13 shows the Mg profile in our p-i-n structure, in which the turn-on of the acceptor begins well before the p^+ contact layer. However, the overwhelming majority of the dopant is sharply confined to the top 0.5 μm of the structure. It is not clear if the low concentration tail represents in-diffusion of interstitial Mg or a build-up of Mg prior to growing the p^+ layer.

Figure 4-14 shows a compilation of V_F versus V_{RB} data for SiC p-i-n rectifiers, as well as our GaN result. The solid lines represent theoretical values for Si, 4H-SiC and 6H-SiC p-i-n rectifiers. As time has progressed, the SiC devices have produced performance relatively close to the theoretical values; by contrast, our GaN result is quite respectable, given the fact that the theoretical values will be slightly higher than for SiC because of the layer bandgap of GaN. It is expected that p-i-n diodes will have larger

VRB values than do Schottky rectifiers, but higher V_F values and slower switching speeds. The latter is a result of the presence of minority carriers in the device.

4.1.4 Summary and Conclusion

We have presented a summary of results for GaN Schottky and p-i-n diode rectifiers. In particular the forward turn-on voltages of these devices are ~3.5 and 5 V, respectively. Reverse blocking voltages of 350-550 V are typical at present for rectifiers fabricated on conducting GaN, while lateral diodes fabricated on resistive GaN produce VRB values above 3 kV with proper edge termination. The results are still inferior to theoretically predicted values for this materials system, but show the rapid progress over the last 2 years. The current transport in GaN Schottky rectifiers is still mainly by Shockley-Read-Hall recombination. The forward I-V characteristics of p-i-n rectifiers show a number of slope changes, which are consistent with a multiple-recombination-level model.

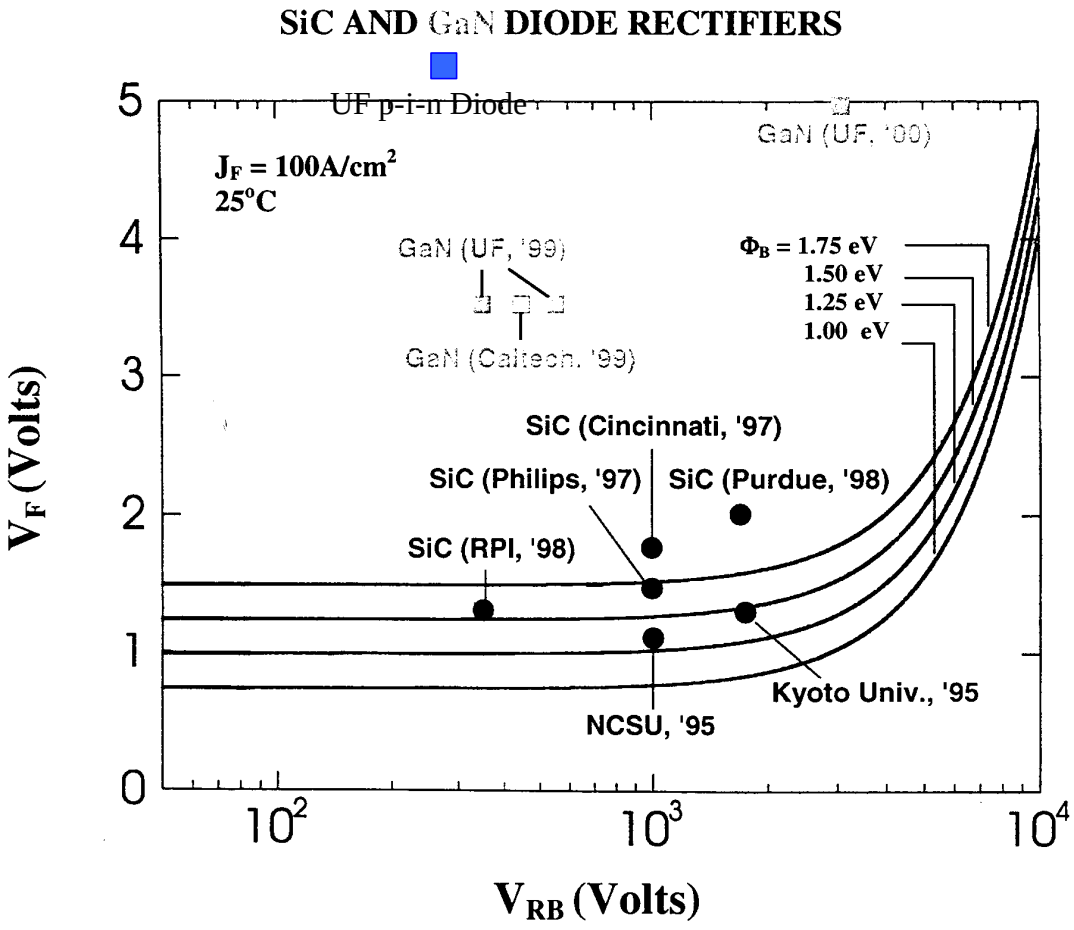

Figure 4-10 V_F versus V_{RB} for GaN and SiC Schottky rectifiers in the literature.

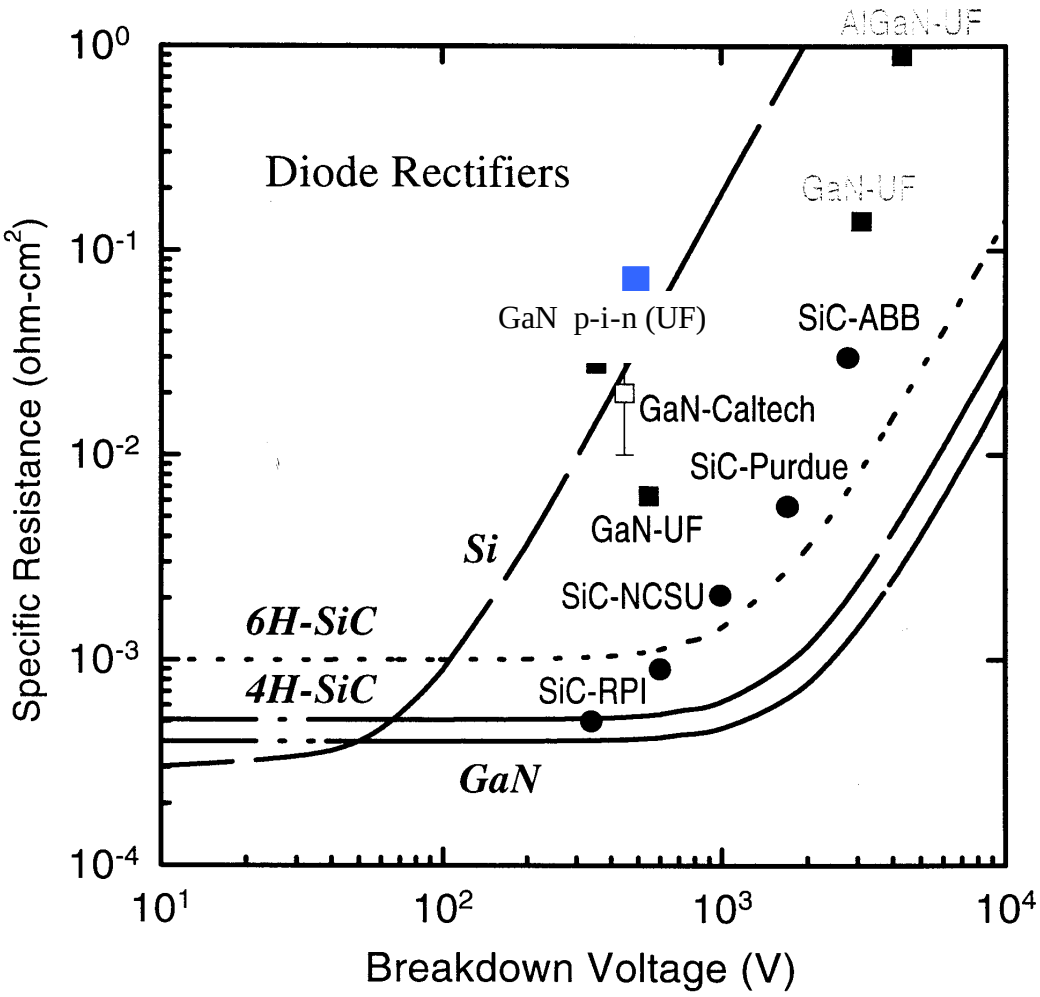

Figure 4-11 R_{ON} versus V_{RB} for GaN and SiC Schottky rectifiers reported in the literature.

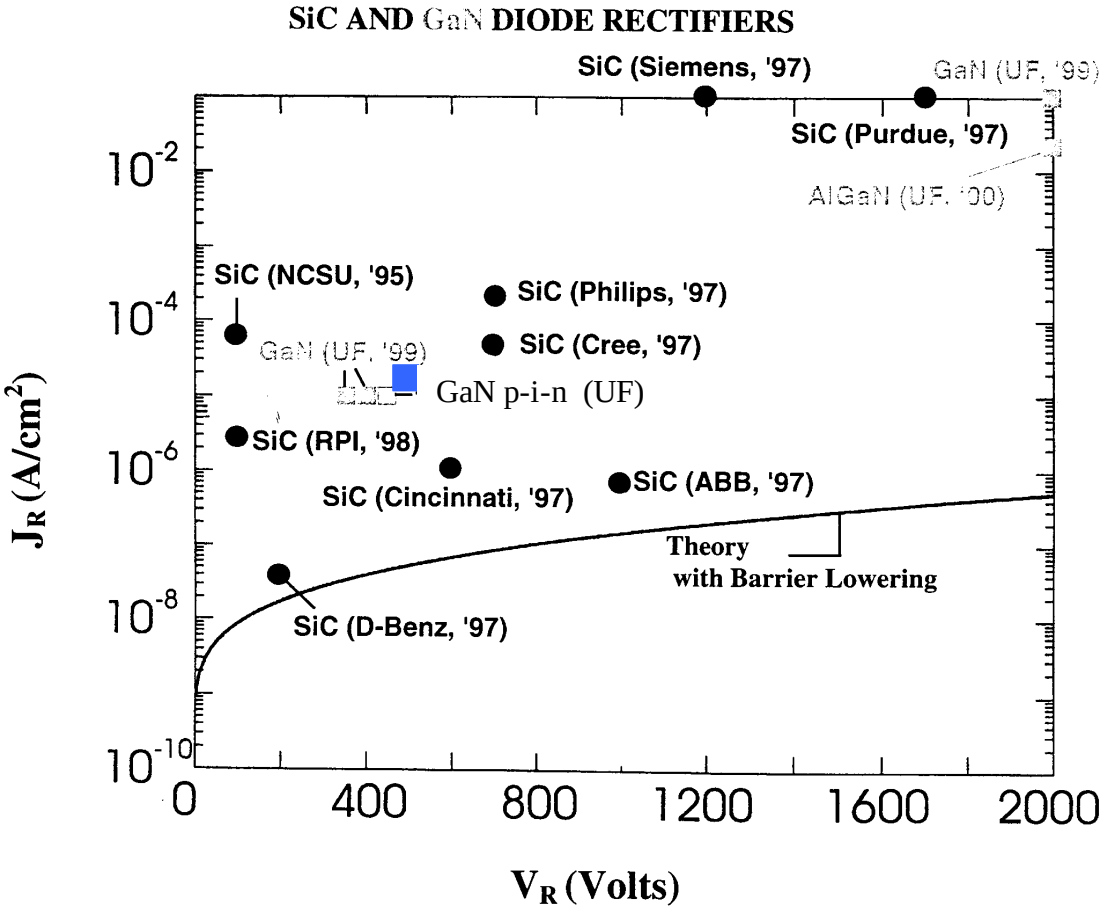

Figure 4-12 J_R versus V_{RB} for GaN and SiC Schottky rectifiers reported in the literature.

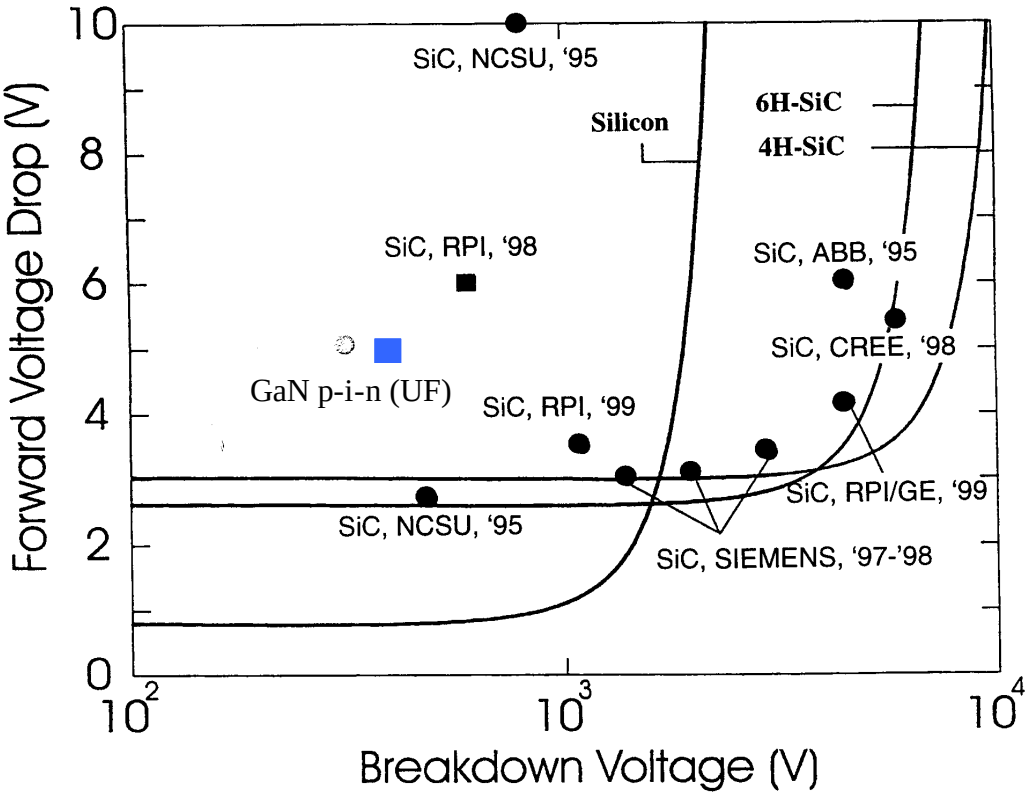

Figure 4-13 V_F versus V_{RB} for GaN and SiC p-i-n rectifiers reported in the literature.

CHAPTER 5
GALLIUM NITRIDE-BASED BIPOLAR DEVICES

5.1 Gallium Nitride pnp Bipolar Junction Transistors Operated to 250 °C

5.1.1 Introduction

There is strong interest in the development of GaN bipolar transistors for high temperature (>400 °C), higher power (>100 W) applications involving space and terrestrial communications links and phased array radar. To this point there has been one report of a GaN bipolar junction transistor (BJT) and three reports of GaN/AlGaN heterojunction bipolar transistors (HBTs). All of these have been npn devices, which suffer from high base resistance due to the relatively low hole concentrations obtained in GaN(Mg). An attractive alternative is the pnp configuration, since it is easier to achieve heavy base doping in n-GaN and the higher carrier mobility in n-type material would reduce base resistance. In HBT structures there would also be larger emitter-base energy bandgap differences and band discontinuities than in the npn configuration.

We demonstrated the first GaN pnp BJT. The device shows efficient emitter injection efficiency over a broad range of operating conditions and little discernable change in dc performance at temperatures up to 250 °C.

5.1.2 Experimental Methods

The layer structure was grown by Metal Organic Chemical Vapor Deposition (MOCVD) at ~1050 °C on (0001) c-plane sapphire substrates. The growth was initiated

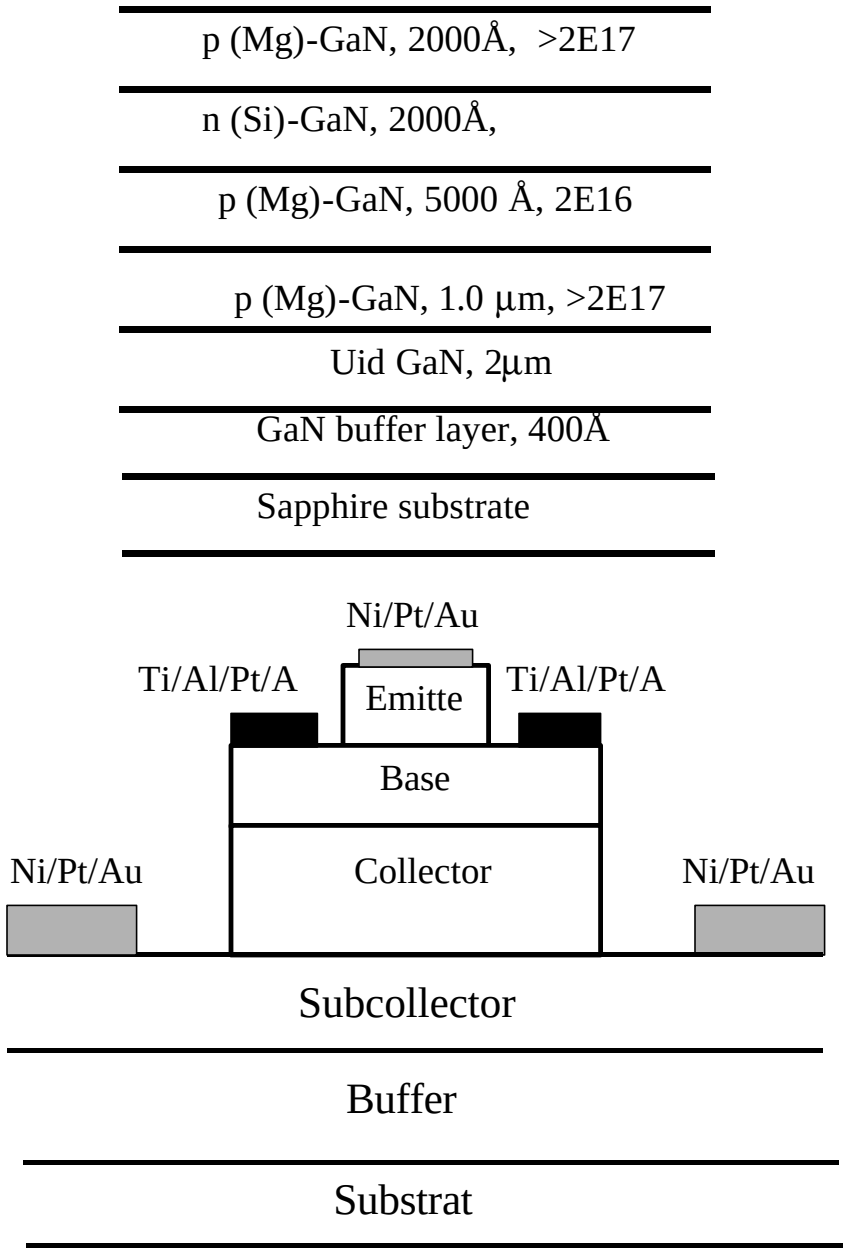

Figure 5-1 Layer structure (top) and schematic (bottom) of GaN pnp BJT.

with a low temperature (500 ^{o}C) GaN buffer prior to ramping to the final growth temperature. A p-type (Mg-doped) subcollector was followed by a lightly p-type (Mg-doped) collector, on n-type (Si-doped) base and a p-type (Mg-doped) emitter, as shown at the top of Figure 5-1. Secondary Ion Mass Spectrometry profiling showed good demarcation of the individual layers in the structure. The base and sub-collector layers were exposed for contacting using Inductively Coupled Plasma etching using a Cl_2/Ar discharge at 300 W source power and –85 V dc self-bias. The GaN etch rate under these conditions is ~1,000 Å $^{-1}$. Etch damage was removed by annealing at 750 ^{o}C for 30 secs under N_2. Device isolation was also achieved by dry etching to the substrate. The-e-beam deposited metallization was Ni/Pt/Au for the emitter and subcollector and Ti/Al/Pt/Au for the base. These contacts were patterned by lift-off, with emitter diameters of 50-100 μm and were annealed at 400^{o}C for 20 secs. A schematic of the completed devices is shown in Figure 5-1 (bottom). The SEM images of fabricated devices are shown in Fig. 5-2. The specific contact resistivities were ~10^{-2} for p-type and 10^{-5} Ω for n-type. Device testing was performed with an HP 4145A parameter analyzer and a higher temperature probe station.

5.1.3 Results and Discussion

Figure 5-3 shows common-base characteristics at 25 ^{o}C (top) and 250 ^{o}C (bottom) from a 90 μm diameter BJT. Note that at both temperatures the collector current is approximately equal to the emitter current, which indicates a high emitter injection efficiency. In addition there is little change in the characteristics at elevated temperature, emphasizing the promise of the BJT for high temperature applications. The offset voltage is ~2 V at 25 ^{o}C, which is similar to the value reported by Yoshida and Suzuki for

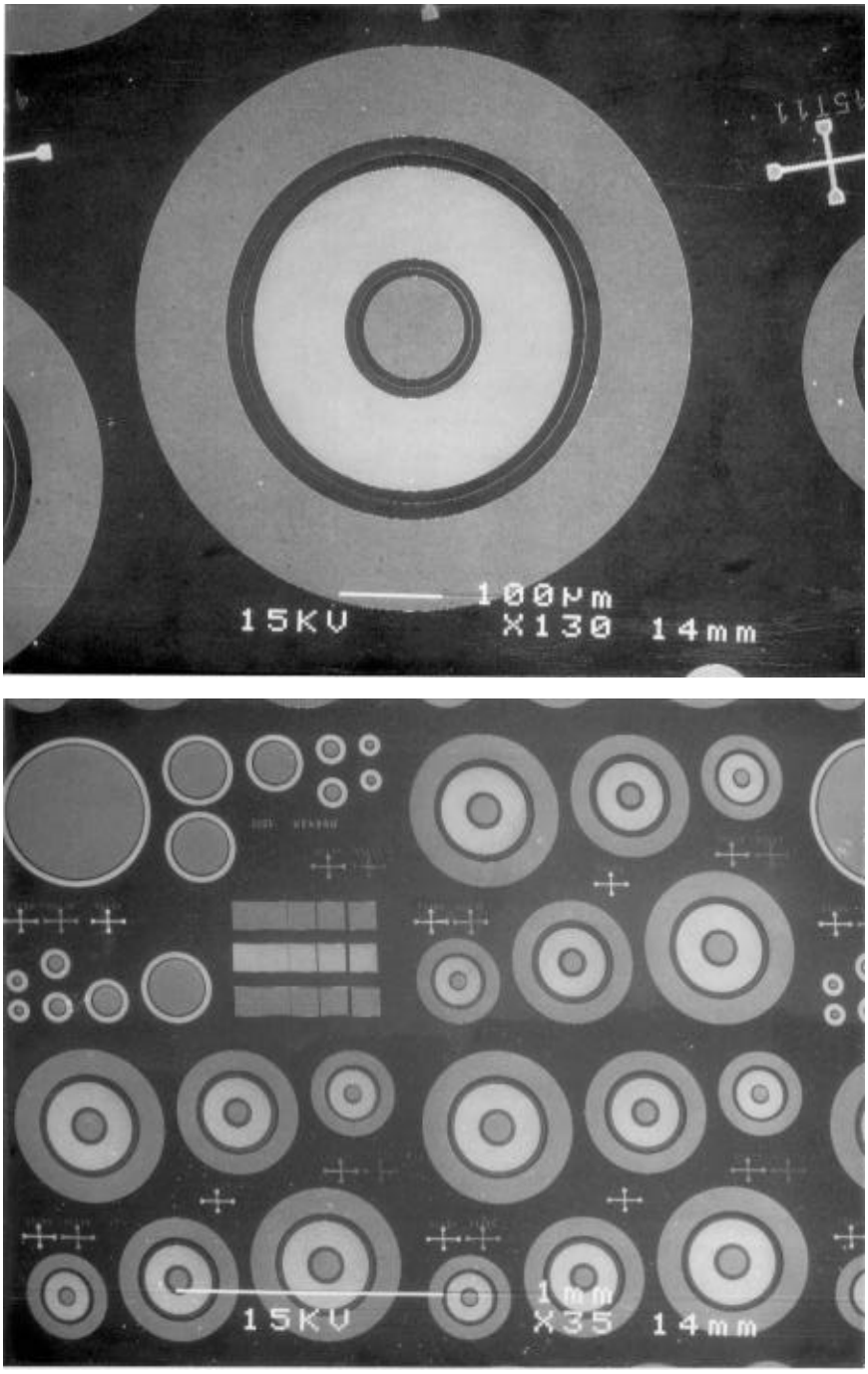

Figure 5-2 SEM images of fabricated GaN pnp BJT.

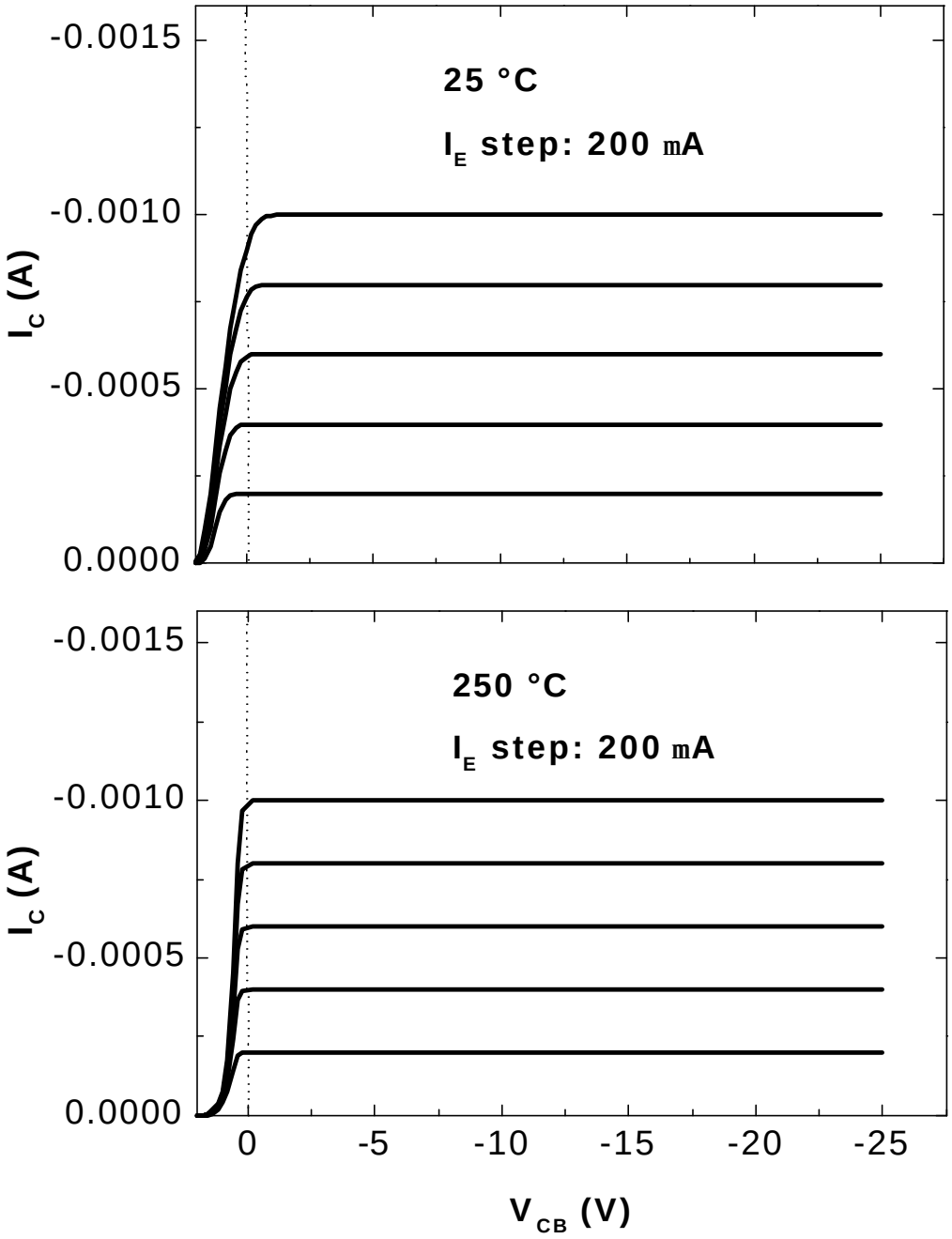

Figure 5.3 Common base I-V characteristics at 25°C (top) and 250°C (bottom) for GaN pnp BJT. The emitter current was stepped in 200 μA steps from 200 μA.

npn BJTs at 250 ^{o}C, the offset voltage was ≤ 1 V, whereas in npn structures the value remained at ~ 2 V.

To explore the limits of operation of the pnp BJTs, we tested the devices at higher voltages. Figure 5-4 shows the collector-base breakdown voltage, V_{BCB}, is ~ 65 V at 25 ^{o}C. A stable current density of 204 A·cm^{-2} was run at this voltage, leading to a power density of 13.0 kW·cm^{-2}. These values can clearly be increased by optimized design of the layer structure and mask layout and this will be an area of future work. At 250 ^{o}C we observed a slight reduction in V_{BCB} to ~60 V. Several previous reports have found a positive temperature coefficient for breakdown voltage in GaN, but we have invariably observed a reduction in breakdown of devices such as GaN diode rectifiers at elevated temperature. This may result from the presence of surface states and suggests that attention needs to be paid to passivation and edge termination methods for GaN.

Figure 5-5 shows I-V characteristics from the e-b (top) and b-c (bottom) junctions as a function of measurement temperature. The forward turn-on voltage decreases significantly with temperature, at least partially due to the higher hole concentrations in the emitter and subcollector. The Mg acceptor has a large ionization level (~170 meV) and from Fermi-Dirac statistics the relative ionization efficiency is 10% at 25 ^{o}C and 48% at 250 ^{o}C.

The common base configuration for bipolar transistors is advantageous for microwave power amplifiers because of the possibility of significant power gain through the impedance transformation offered by the amplifier. In future work we will also discuss common-emitter and dc current gain characteristics of the pnp BJTs.

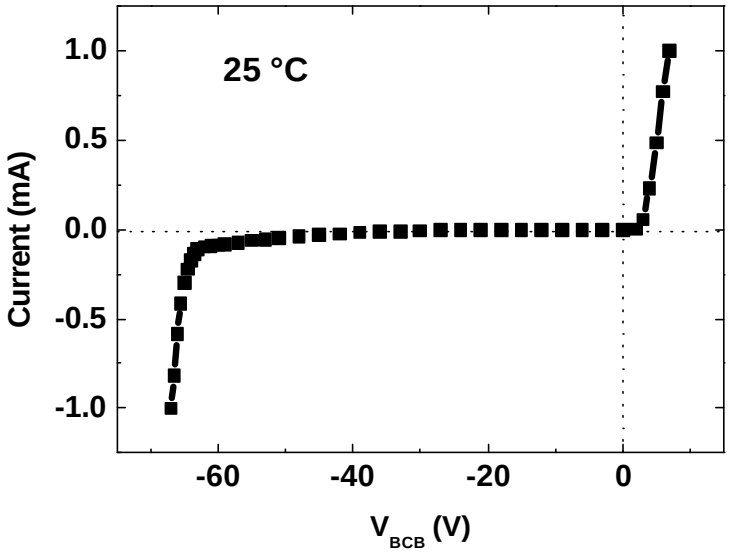

Figure 5-4 Common base I-V characteristics of GaN BJT at 25°C, showing a V_{BCB} value of 65 V.

5.1.4 Summary and Conclusion

In conclusion large area GaN pnp BJTs have been fabricated using a low damage dry etch process. At 25 °C, V_{BCB} was 65 V with power densities of 13.9 kW·cm^{-2}. The devices showed little fall-off in performance at temperatures up to 250 °C.

5.2 Direct-Current Characteristics of pnp AlGaN/GaN Heterojunction Bipolar Transistors

5.2.1 Introduction

There are numerous advantages of the AlGaInN materials system for high power electronics, including wide band gaps for high voltage and temperature operation, good carrier transport properties, the availability of heterostructures, and finally the processing experience base accumulated during the development of nitride light-emitting diodes and

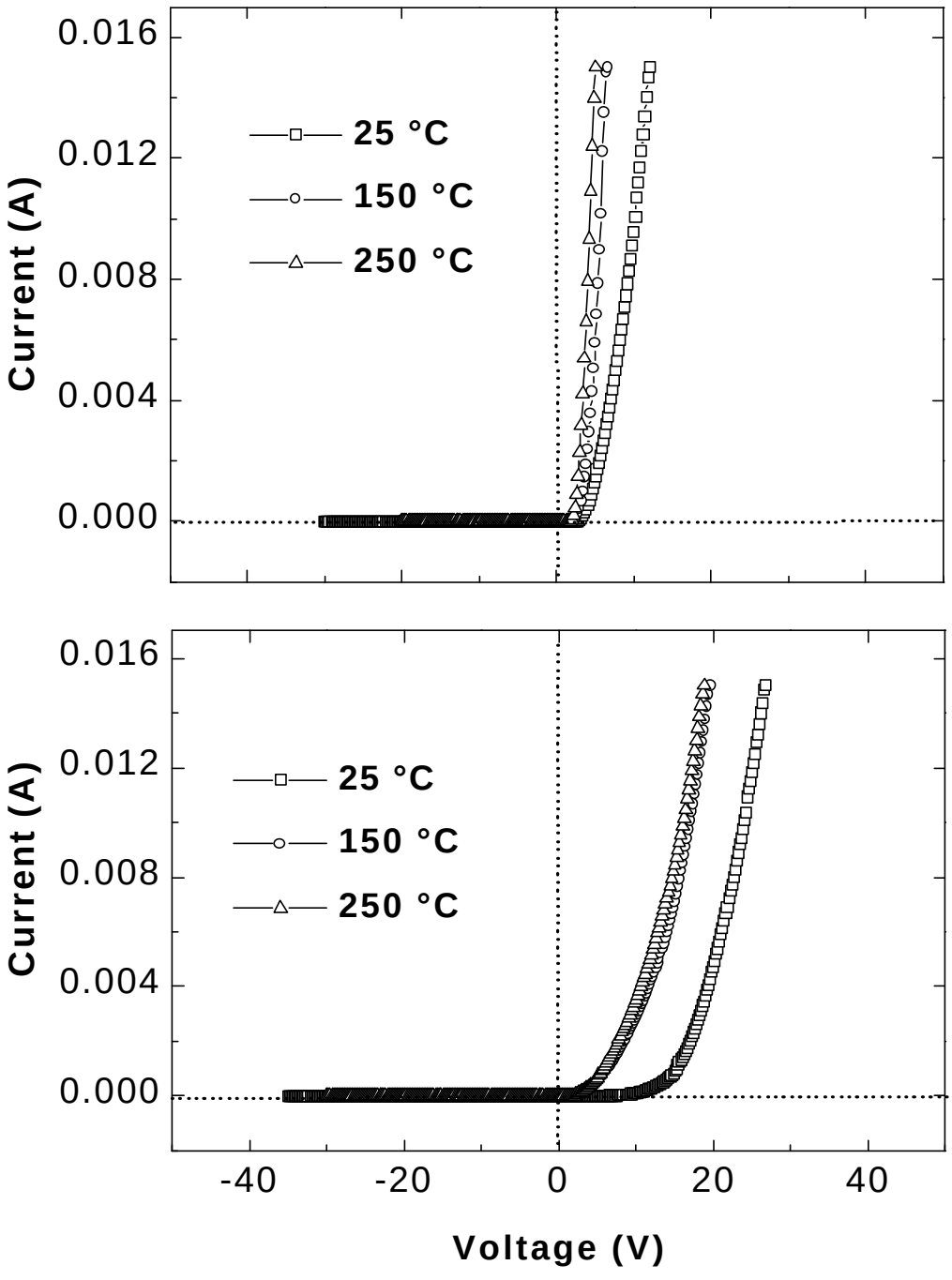

Figure 5-5 Emitter-base (top) and collector-base (bottom) junction I-V characteristics as a function of temperature.

lasers. Most of the work on nitride-based electronics has focused on AlGaN/GaN high electron mobility transistors, but there are potential advantages to the use of heterojunction bipolar transistors (HBTs) in some applications because of their higher transconductance, better linearity, and more uniform threshold voltages.4 Several groups have reported demonstrations of npn AlGaN/GaN HBTs, in which the dc performance was limited by the high base resistance. This is due to the large ionization level for the Mg dopant (~170 meV) and the consequently low hole density available at room temperature.

There are two advantages to the pnp configuration for AlGaN/GaN HBTs. First, there is a larger emitter–base valence band offset than conduction band offset, and second the base resistance will be much lower due to the higher doping level achievable in n-type material. In this letter we report on the dc characteristics of the first pnp AlGaN/GaN HBT. Under all conditions the collector current was approximately equal to the emitter current, indicating high emitter injection efficiency.

5.2.2 Experimental Methods

The layer structure for these devices was grown by metal-organic chemical vapor deposition on c-plane sapphire substrates. The growth temperature was ~500 °C for the GaN buffer and ~1050 °C for the active layers. The structure is shown schematically at the top of Figure 5-6. An unintentionally doped 2-µm-thick buffer of GaN was grown on the low temperature buffer (200 Å) in order to decrease the defect density in subsequent layers. A 1-µm-thick Mg-doped GaN subcollector with hole concentration $>2\times10^{17}$ cm^{-3} was followed by a 5000-Å-thick Mg-doped collector with hole concentration 2×10^{16} cm^{-3}. The GaN base was Si-doped (~10^{18} cm^{-3}) and was 1000 Å thick. The resistivity of

material grown under the same conditions is ~2.5×10 ^{2} Ωm, leading to a sheet resistivity of 2.5 k Ω /€ for a 1000-Å-thick base. This is approximately a factor of 125 times lower than for a p-type GaN base with typical hole concentration 2×10^{17} cm^{-3} and hole mobility of 10 cm^2 V^{-1} s^{-1}. The layer structure was completed with a p-type (Mg-doped, 2000 Å thick) $Al_{0.1}Ga_{0.9}N$ emitter with hole concentration ~2×10^{17} cm^{-3} and a Mg-doped GaN (5000 Å thick) emitter contact layer with hole concentration >2×10^{17} cm^{-3}. Figure 5-7 shows a TEM image from the grown pnp GaN/AlGaN structure and the interfaces are very sharp and smooth, although the defect density was very high, on the order of 10^{8} cm^{-2}.

The device fabrication process was similar to that reported previously for GaN bipolar junction transistors. In brief summary, the base and subcollector were exposed for contacting using Cl_2/Ar dry etching in an inductively coupled plasma (ICP) reactor, followed by annealing under N_2 at ~800 °C to remove residual plasma damage. Lift-off of e-beam deposited Ni/Pt/Au for p-type and Ti/Al/Pt/Au for n-type contacts was followed by annealing at 400 °C to produce the lowest specific contact resistivities. A schematic of the processed device cross-section is shown at the bottom of Figure 5-6. Emitter contact diameters were 50–100 μm and the mask also contained transmission line method patterns for measurement of the specific contact resistivity (~10^{-2} Ω-cm^2 for p type and ~10^{-5} Ω-cm^2 for n type). Testing was performed up to 250 °C using a high temperature probe station and a parameter analyzer.

5.2.3 Results and Discussion

Common–base characteristics from a 50 μm diameter HBT are shown in Fig. 5.8 as a function of measurement temperature. Over this temperature range (25–250 °C) the

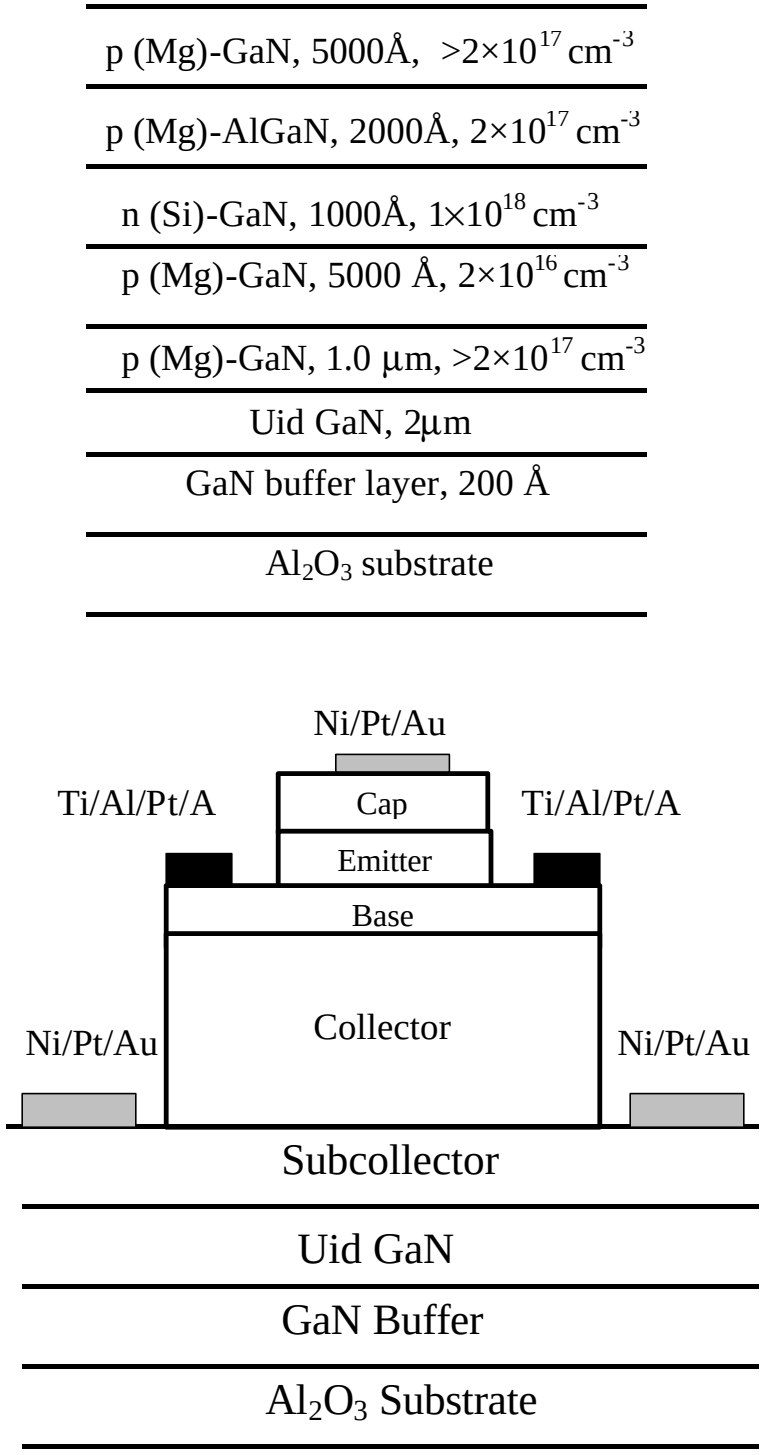

Figure 5-6 Layer structure (top) and schematic (bottom) of GaN/AlGaN pnp HBT.

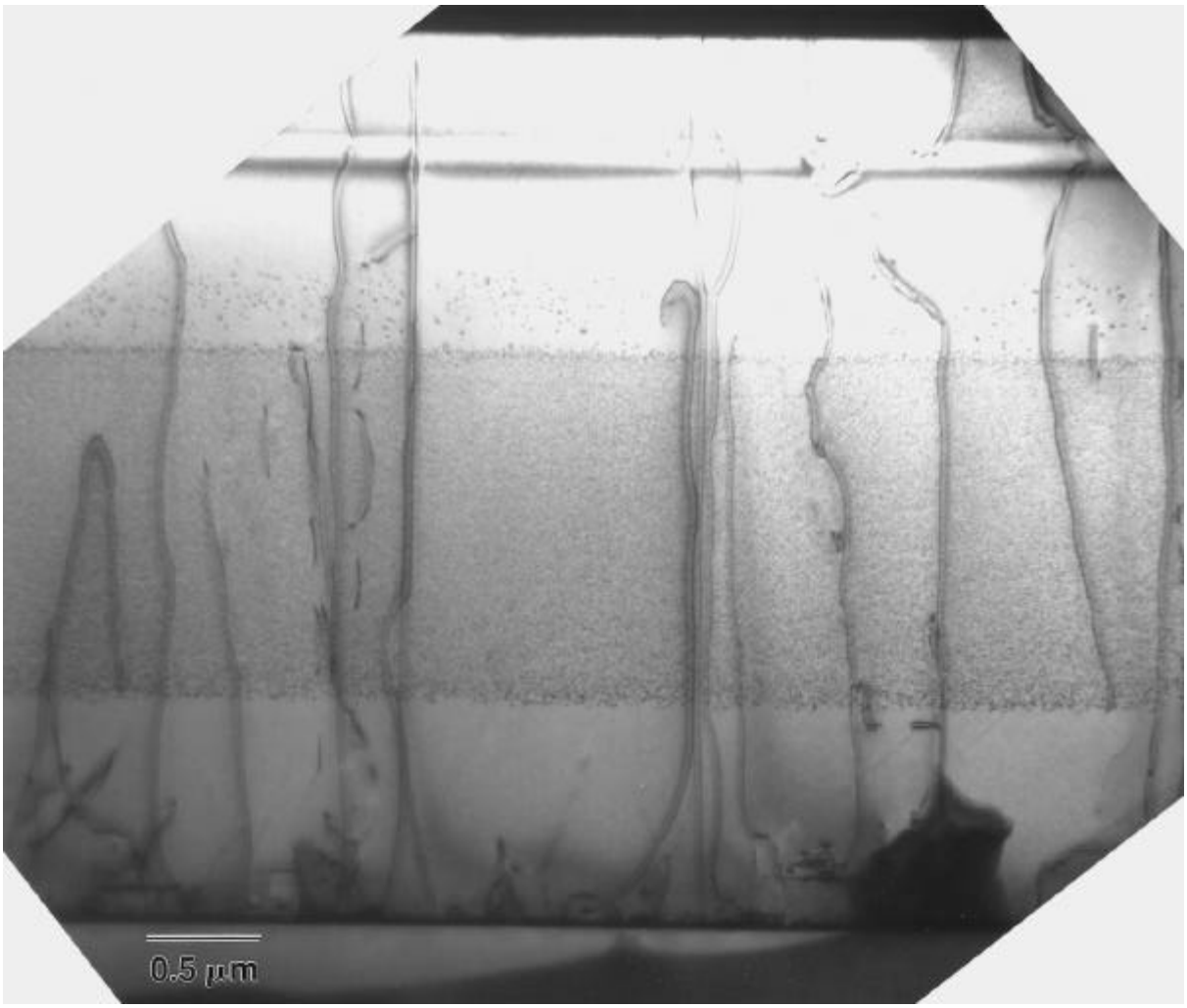

Figure 5-7 TEM of GaN/AlGaN pnp HBT structure, showing very sharp and smooth interface.

collector current IC is approximately equal to the emitter current IE, indicating high efficiency for injection of holes from the emi tter. The offset voltage is of order 2 V, similar to the value reported for GaN npn BJTs, but lower than the 5 V reported for GaN npn HTBs. Note that the breakdown voltage decreases with increasing temperature, consistent with reports of negative temperature coefficients for breakdown in GaN rectifiers.18 This may result from the effect of bulk or surface states in the HBTs, since defect-free GaN would be expected to have a positive temperature coefficient for breakdown voltage. Previous reports of temperature dependent performance of pnp and npn GaN BJTs have shown little change in the common–base current–voltage (I–V) characteristics at elevated temperatures. More work is needed to understand the larger changes observed in the HBT structures and whether they are related to the presence of additional defects associated with the AlGaN emitter. The common–base configuration is attractive for microwave power amplifier applications because of the possibility of gain obtained through the impedance transformation offered by the amplifier. Due to leakage in the collector–base junction, the common–emitter characteristics were problematic, with inconsistent results across the wafer. In the best devices Gummel plots showed dc current gains of 20–25 at room temperature. A plot from one of these devices is shown in Figure 5-9. The offset is still quite high at 4–4.5 V, while collector currents up to several mA were achieved. When we opened the base contact, no collector current was observed. This confirms the transistor modulation.

Figure 5-10 shows I–V characteristics from the emitter–base (top) and base–collector (bottom) junctions for measurement temperatures of 25, 150, or 250 °C. As this temperature is increased the forward turn-on voltage tends to decrease, which is due in

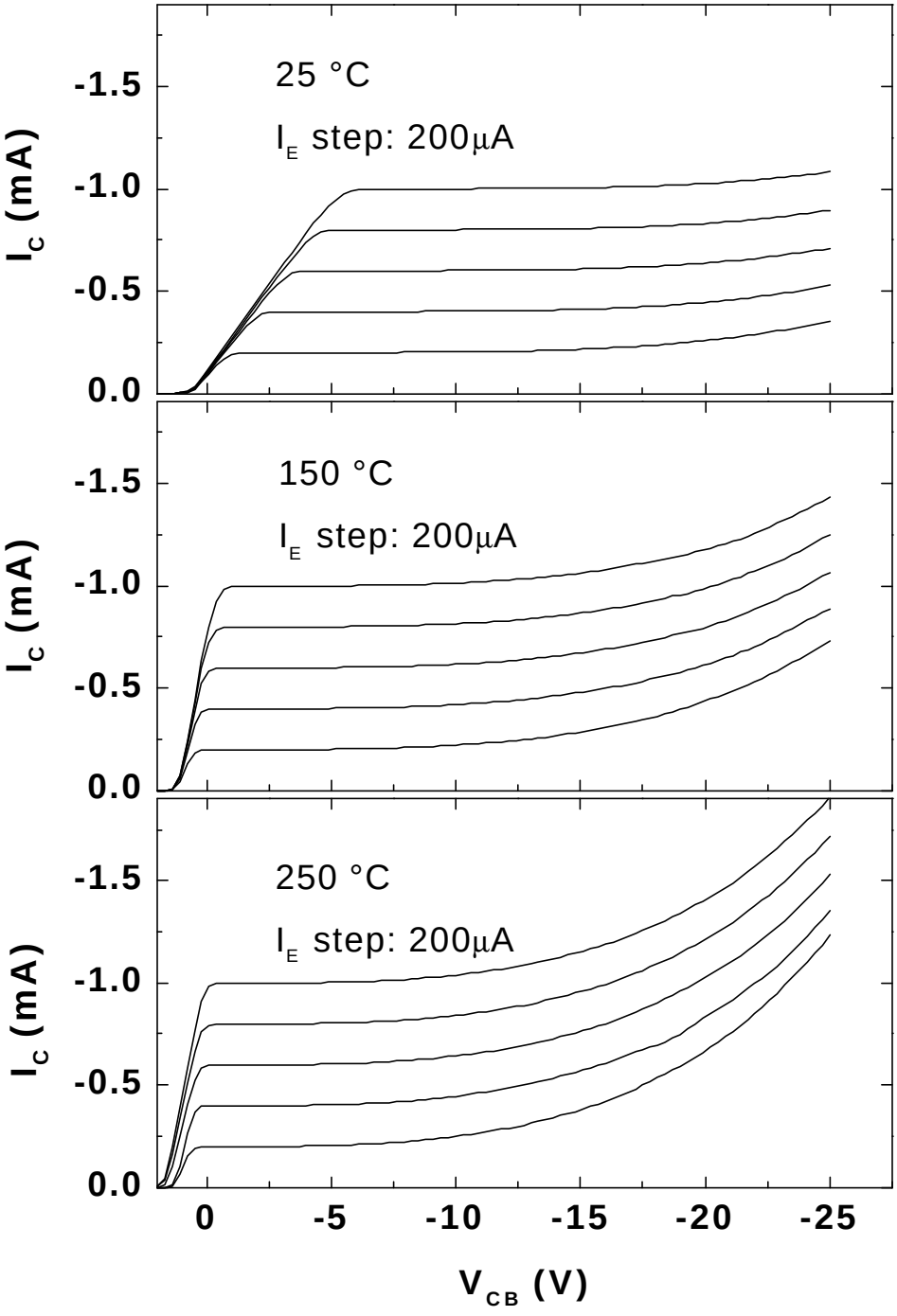

Figure 5-8 Common–base I–V characteristics at 25, 150, and 250 °C for AlGaN/GaN pnp HBTs. The emitter current was stepped in 200 steps from 200 μA.

part to the higher hole concentrations in the emitter contact and subcollector regions producing lower contact resistance. A small reduction (~2 V between 25–250 °C) in reverse breakdown voltage with increasing temperature was also evident. In the common–base mode the devices were operated up to a maximum current density of 2.05 kA-cm^{-2} at 25 V, corresponding to a power density of 51.25 kW-cm^{-2}. The devices are not optimized for power operation, and this will be an area for future development.

5.2.4 Summary and Conclusion

In conclusion, pnp AlGaN/GaN HBTs have been fabricated and show high emitter injection efficiency. The reverse breakdown voltage shows a negative temperature coefficient, while the ideality factors for both emitter– and collector–base junction were close to 2 at low bias, indicating that recombination is dominant. These devices are promising for microwave power amplifiers.

5.3 Self-Aligned Small-Area GaN/AlGaN Heterojunction Bipolar Transistors

5.3.1 Introduction

Heterojunction Bipolar Transistors (HBT) have a number of advantages over heterostructure field effect transistor (HFETs), including higher power density capability, better linearity, more uniform threshold voltages and higher transconductance. In the GaN/AlGaN materials system there are several factors currently limiting the performance of HBTs including the low p-type doping achieved in the base region of npn devices, the low electron lifetime in the neutral base, high leakage currents in the collector-emitter junction and high recombination rates. Some of these limitations may be alleviated with use of pnp structures, but the microwave performance of these would be expected to be inferior to npn devices.

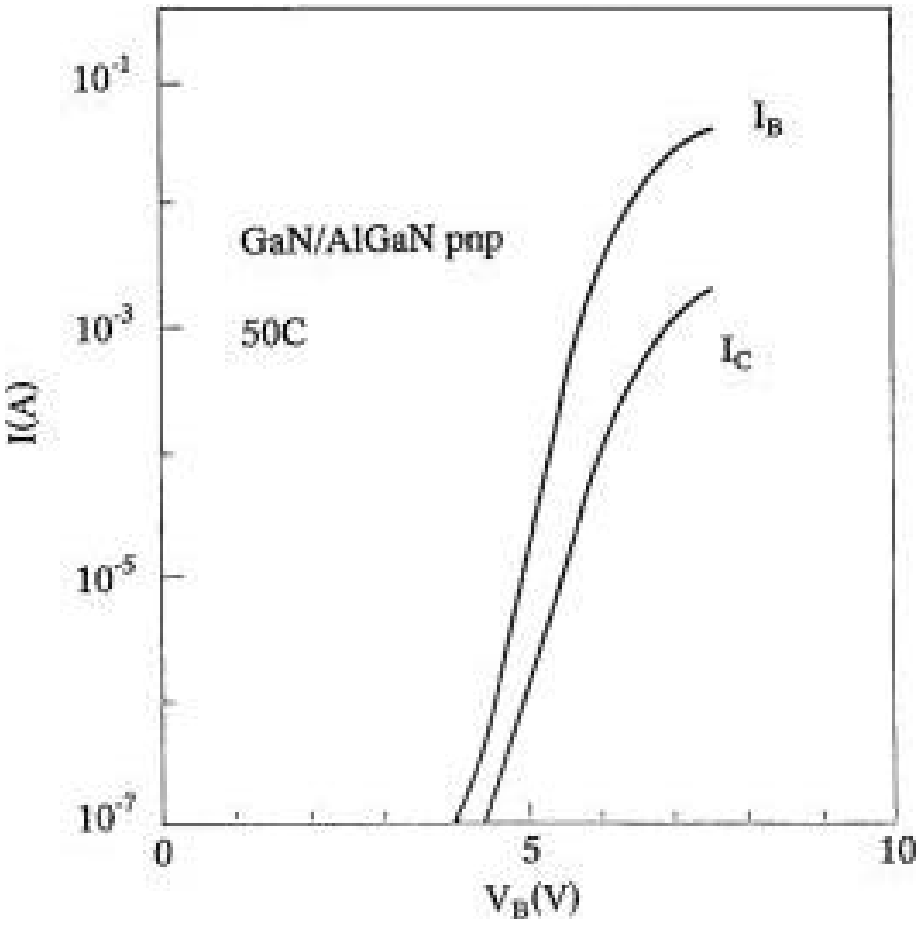

Figure 5-9 Gummel plot of HBT with $V_{CB} = 0$.

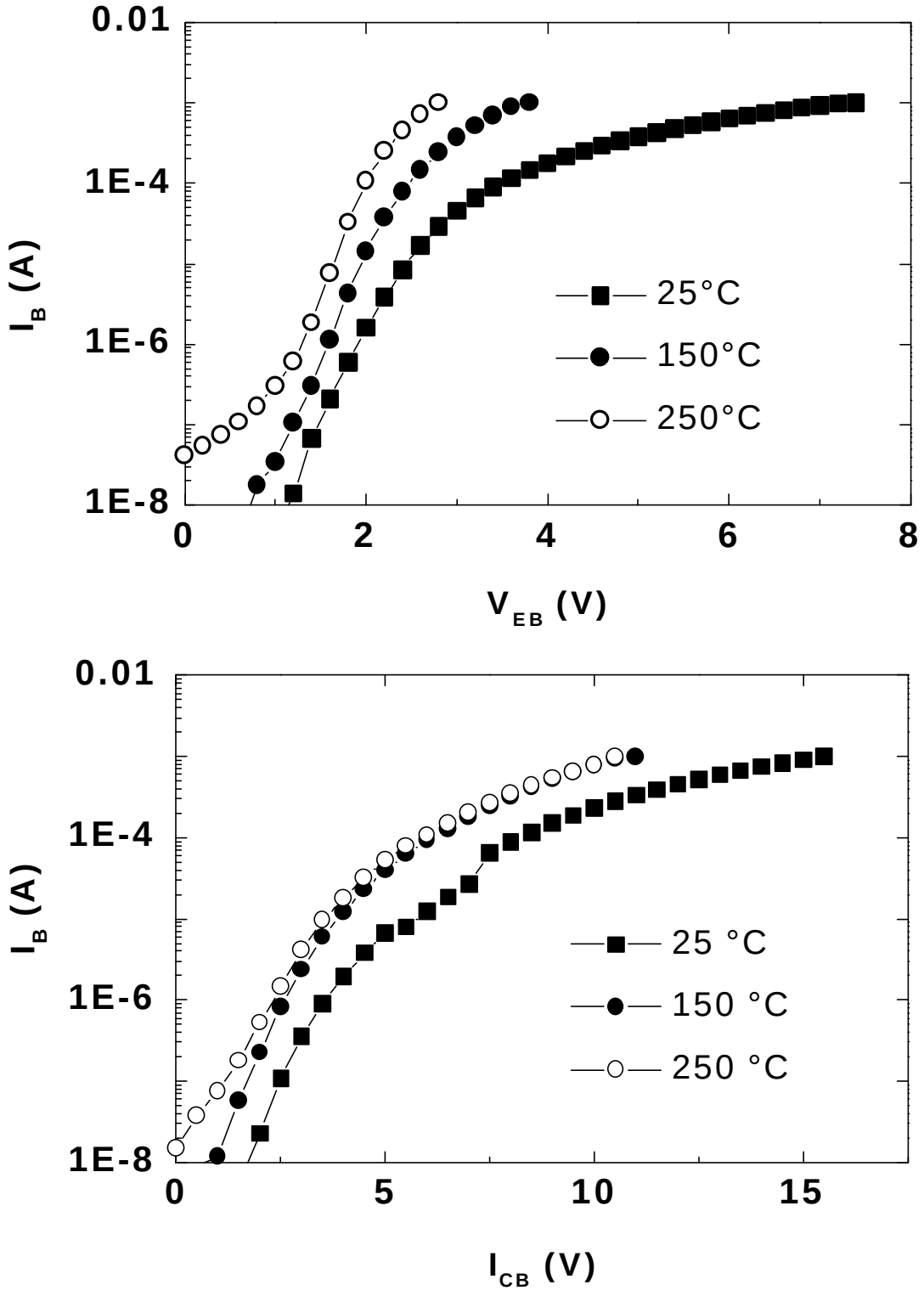

Figure 5-10 Emitter– (top) and collector–base (bottom) forward I–V characteristics as a function of temperature.

While GaN/AlGaN HBTs are attractive candidates for high frequency switching and communications applications, the main interest is in microwave power amplifiers in the 1-5 GHz frequency range and with operating temperature >400 °C. To fulfill the frequency requirement, devices with small emitter –contact areas are necessary (i.e.<10 μm^2). To date, all of the reported GaN/AlGaN HBTs have had much larger active areas. In this paper we describe a self-aligned fabrication process for these devices that includes dielectric sidewall spacers and selected –area growth of GaAs(C) on the base region to decrease contact resistance. The resulting device performance is compared with large –area devices fabricated as the same wafer.

5.3.2 Experimental Methods

The layer structure was grown by metal-organic chemical vapor deposition (MOCVD) in c-plane sapphire substrates, as described previously. The structure consisted of a 2 μm undoped GaN buffer, a 1.44 μm thick $n^+(3\times10^{18}\,cm^{-3})$ GaN subcollector, a 0.5 μm thick n $(3\times10^{16}\,cm^{-3})$ GaN collector, a 0.2 μm thick p $(3\times10^{17}\,cm^{-3})$ GaN base , and 10 pairs of p-$Al_{0.15}Ga_{0.85}N$/p-GaN superlattice layer used for base contact layer. To avoid the dry etching damage to the base, a regown emitter region was used. The SiO_2 was used as regown mask. The emitter region was opened by dry etching and day etching damage was removed by thermal annealing and wet etch. The regown emitter consisted of a 0.2 μm thick $n^+(5\times10^{17}\,cm^{-3})$ $Al_{0.15}Ga_{0.85}N$ emitter and a 0.3 μm n^+ $(8\times10^{18}\,cm^{-3})$ GaN contact layer as shown in Fig. 5-11.

All etching was performed in a Plasma Therm 770 series Inductively Coupled Plasma (ICP) system, using an ICP source power of 300 W (2MHz), a chuck power of 40W(13.56MHz), process pressure of 5 mTorr and gas mixture of $10Cl_2/5Ar$. The self-bias was –95 V under these conditions. SiO_2 deposition was performed in a Plasma Therm system at 300 mTorr and 300ºC, using gas mixtures of SiH_4/N_2O. The emitter and collector metallization was Ti(200 Å)/Al(600 Å)/Pt (400 Å)/Au (3000 Å) and was annealed at 800 ºC for 30 secs under nitrogen ambient., while the base metallization was Ni(300 Å)/Au(1500 Å) , alloyed at 500 ºC for 30 secs under air ambient.

5.3.3 Results and Discussion

Figure 5-12 shows the schematic of finished device. Prior to metal deposition, the GaN surface was cleaned in HCl/H_2O (1:20) for 1 min, followed by DI water rinse and drying in filtered nitrogen.

Figure 5-13 shows the hole concentration as a function of well width of p-$Al_{0.15}Ga_{0.85}N$/p-GaN superlattice. For the best case, the hole concentration can be increased by an order of magnitude. For a well width of 50 Å, a hole concentration enhancement of a factor of 6 was achieved.

Figure 5-15 (top) shows the scanning Electron Micrographs (SEM) of the completed device. These micrographs illustrate some of the problems with the process, namely that alignment needs to be very precise for these small-area devices, which is difficult given the topography and the fact that lift-off is employed to define the metal contact. In addition, there is no dry etch selectivity between the AlGaN emitter and underlying GaAs base and it is very difficult to remove the resist after high density

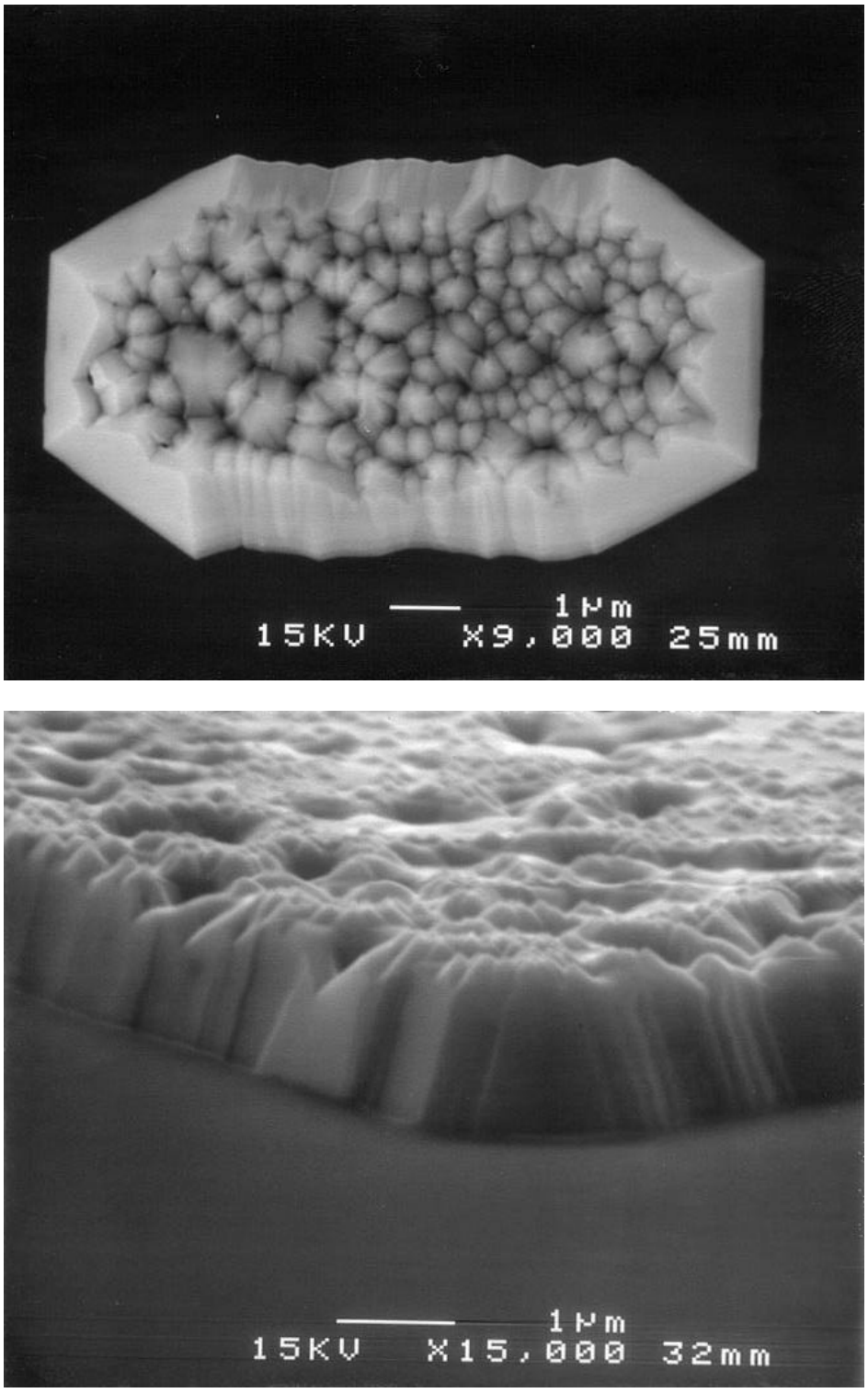

Figure 5-11 Schematic of finished small area self-aligned GaN/AlGaN HBT.

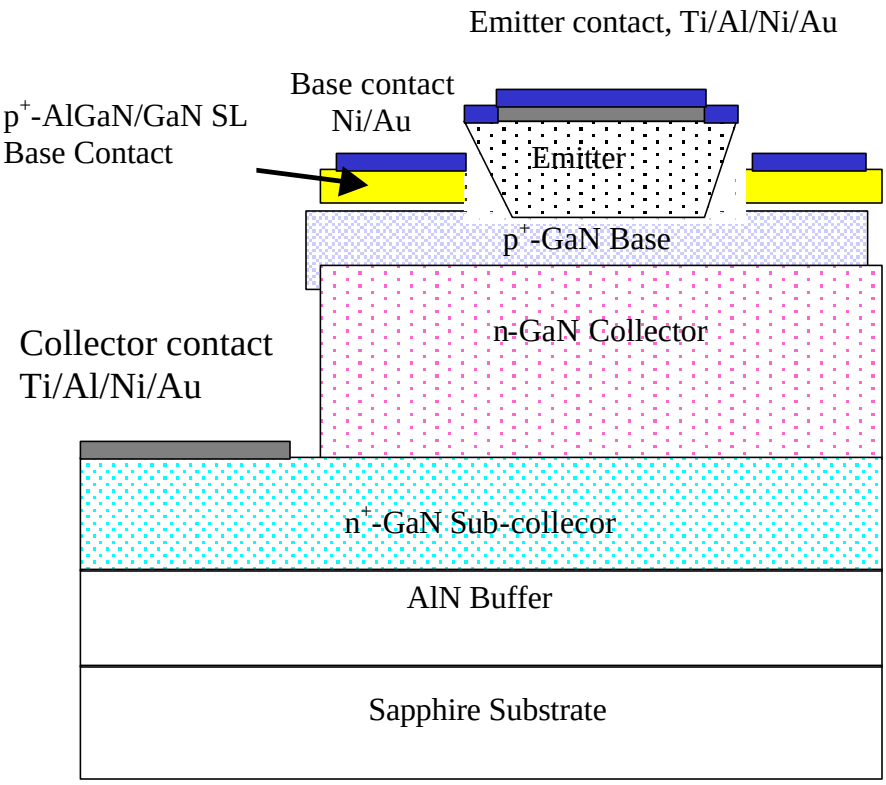

Figure 5-12 Schematic of finished small area self-aligned GaN/AlGaN HBT.

plasma etching . The GaN surface morphology is also relatively rough compared to conventional homoepitextial compound semiconductors employed for HBTs. This is illustrated in the SEM micrographs of Fig. 5-15 (bottom), which shows the devices after collector metallization but prior to etching of the collector mesa.

The dc performance of large area (emitter) devices fabricated using the simple non-self – aligned process repored previously is shown in Figure 5-16. At top are the common –base characteristics measured at 25 ºC. A maximum current density of 2.55 $kA \cdot cm^{-2}$ at 10 V was measured, corresponding to a power density of 20.4 kW/cm^{-2}. This measurement was limited by our test set-up and can be expected to improve with optimized devices and a true power maskset. Note that $I_C \sim I_E$, indicating a high emitter injection efficiency. The offset volatge was in the range of 2-3 V, similar to the buit-in junction potential. The collector-base breakdown voltage, V_{BCB} was ≥10 V, while the Early voltage was too large to measure accurately. Not all devices showed common-emitter characteristics, due most likely to the poor quality of regown emitter region and high defect level in the material.

5.3.4 Summary and Conclusion

In summary, a self-aligned process for small-area GaN/AlGaN HBTs has been developed. Further work is needed on a better emitter region regrowth, surface morphology, etch selectivity and device yield in addition to improvements in material quality.

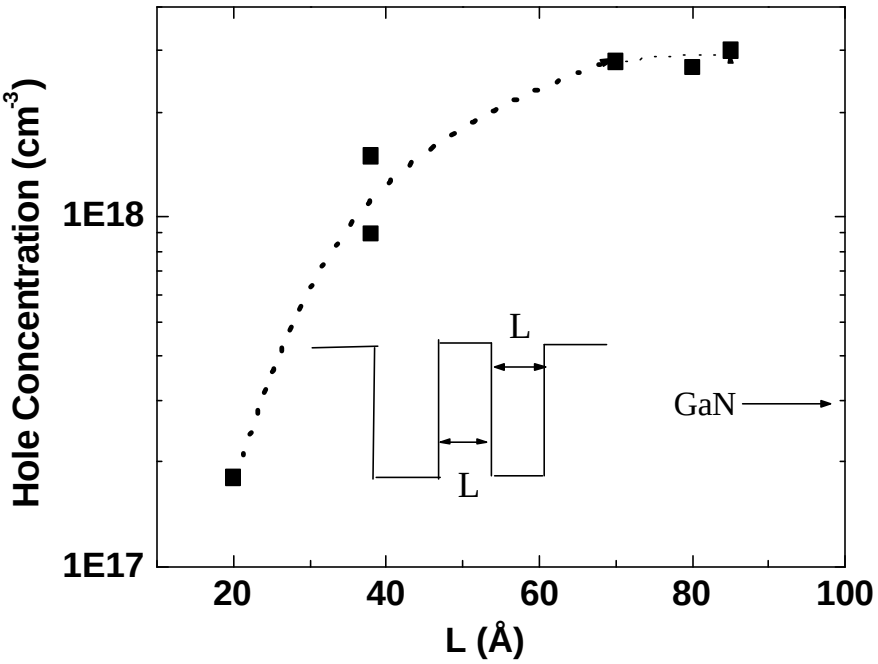

Figure 5-13 Hole concentration as a function of p-AlGaN/p-GaN superlattice well width.

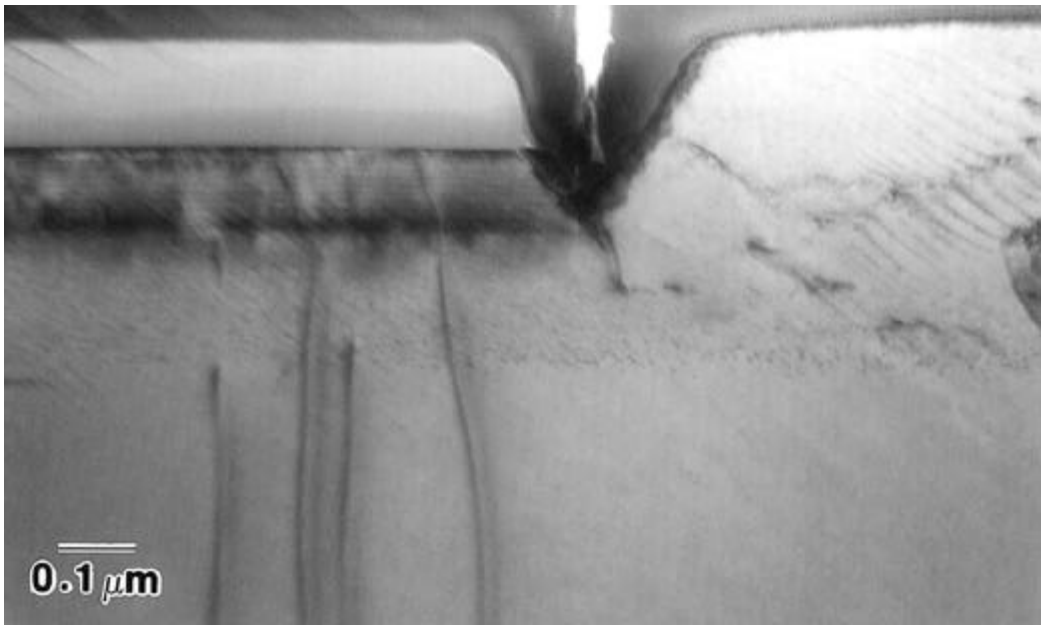

Figure 5-14 TEM image of regrown Emitter region.

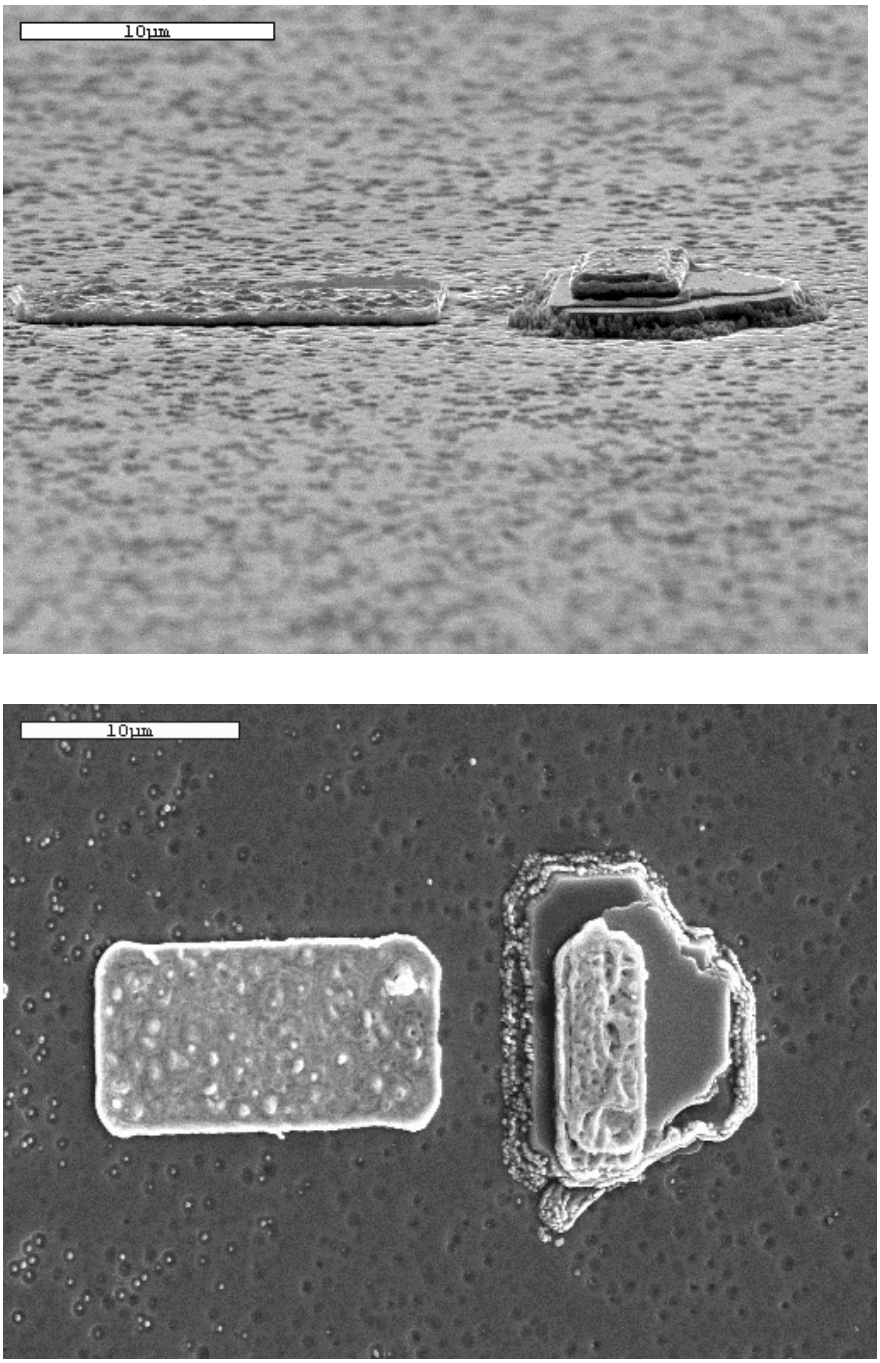

Figure 5-15 SEM images of regrown Emitter region.

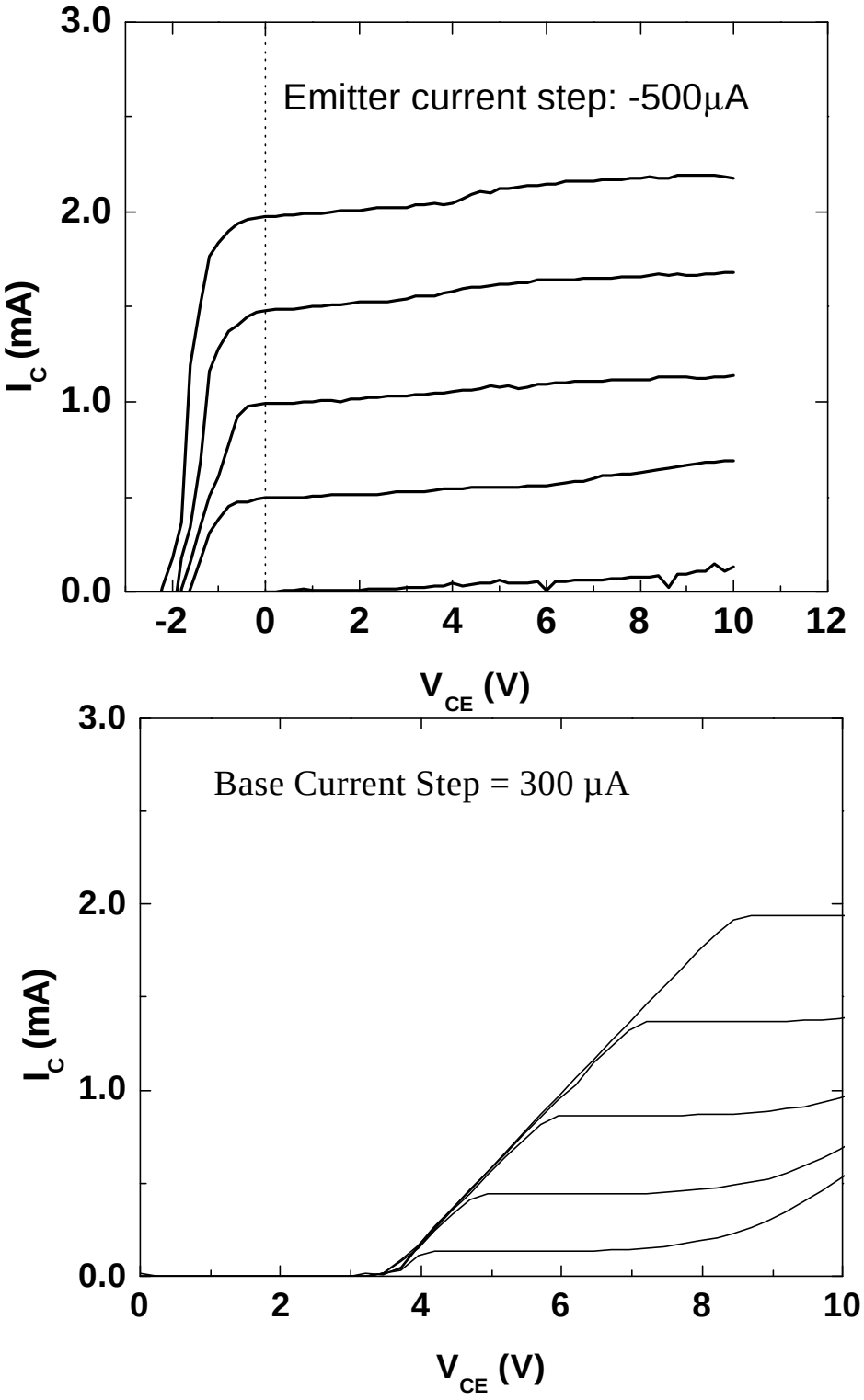

Figure 5-16 Common-base and common-emitter characteristics of self-aligned small-area GaN/AlGaN HBT.

REFERENCES

[1] H. Morkoc, S. Strite, G.B. Gao, M.E. Lin, B. Sverdlov, M. Burns, J. Appl. Phys. 76 (1994) 1363.

[2] S.M. Sze, Semiconductyor Devices: Physics and Technology, John Willy & Sons, 1985

[3] W. Liu, Fundametals of III-V Devices: HBTs,MESFETs, and HFETs/HEMTs, John Willy & Sons, 1999

[4] B. J. Baliga, Modern Power Devices, Krieger Publishing Company, 1987

[5] T.P. Chow, R. Tyagi, IEEE Trans. Electron. Dev. 41 (1994) 1481.

[6] Z.Z. Bandic, P.M. Bridger, E.C. Piquette, T.C. McGill, R.P. Vaudo, V.M. Phanse, J.M. Redwing, Appl. Phys. Lett. 74 (1998) 1266.

[7] R. Gaska, J.W. Yang, A. Osinsky, Q. Chen, M.A. Khan, A.O. Orlov, G.L. Snider, M.S. Shur, Appl. Phys. Lett. 72 (1998) 707.

[8] S.J. Pearton, J. C. Zolper, R. J. Shul, F. Ren, J. App. Phys. 86(1999) 1; S. J. Pearton, F. Ren, A. P. Zhang, K. P. Lee, Mater. Sci & Eng Reports, R30 (2000) 53.

[9] Y. Uzawa, Z. Wang, A. Kawakami, B. Komiyama, Appl. Phys. Lett. 66 (1995) 1992.

[10] O. Ambacher, J. Phys. D 31 (1998) 2653.

[11] S. Fischer, A. Gisbertz, B.K. Meyer, M. Topf, S. Koynov, I. Dirnstorfer, D. Volm, R. Ueckev, P. Reiche, Symp. Proc. EGN-1, 1996.

[12] P. Kung, A. Saxler, X. Zhang, D. Walker, R. Lavado, M. Razaghi, Appl. Phys. Lett. 69 (1996) 2116.

[13] W. Gotz, L.T. Romano, J. Walker, N.M. Johnson, R.J. Molnar, Appl. Phys. Lett. 72 (1998) 1214.

[14] C. Wetzel, D. Volm, B.K. Meyer, K. Pressel, S. Nilsson, E.N. Mokhov, P.G. Baranov, Appl. Phys. Lett. 65 (1994) 1033.

[15] Y.A. Vodakov, E.N. Mokhov, A.D. Roenkov, M.E. Boiko, P.G. Baranov, J. Cryst. Growth 10 (1998) 183.

[16] T.D. Moustakas, T. Lei, R.J. Molnar, Physica B 185 (1993) 39.

[17] J.M. Van Hove, R. Hickman, J.J. Klaassen, P.P. Chow, P.P. Ruden, Appl. Phys. Lett. 70 (1997) 282.

[18] M. Ilegems, J. Cryst. Growth 13/14 (1972) 360.

[19] M. Morita, S. Isogai, N. Shimizu, K. Tsubouchi, N. Mikohiba, Jpn. J. Appl. Phys. 19 (1981) L173.

[20] H. Amano, N. Sawaki, I. Akasaki, Y. Toyada, Appl. Phys. Lett. 48 (1986) 353.

[21] S. Keller, P.B. Keller, Y.F. Wu, B. Heying, D. Kapolnek, J.S. Speck, U.K. Mishra, S.P. DenBaars, Appl. Phys. Lett. 68 (1996) 1525.

[22] S. Nakamura, T. Mukai, M. Senoh, Appl. Phys. Lett. 64 (1994) 1687.

[23] Y. Kato, S. Kitamura, K. Hiramatsu, N. Sawaki, J. Cryst. Growth 144 (1994) 133.

[24] H. Marchand, J.P. Ibbetson, P.T. Fini, P. Kozodoy, S. Keller, S. DenBaars, J.S. Speck, U.K. Mishra, Mater. Res. Soc. Int. J. Nitride Semi Res. 3 (1998) 3.

[25] R. Madar, G. Jacob, J. Hallais, R. Frucgart, J. Cryst. Growth 31 (1975) 197.

[26] J. Karpinski, S. Porowski, S. Miotkowska, J. Cryst. Growth 56 (1982) 77.

[27] J. Burm, K. Chu, W. Davis, W.J. Schaff, L.F. Eastman, T.J. Eustis, Appl. Phys. Lett. 70 (1997) 464.

[28] D.L. Rode, D.K. Gaskill, Appl. Phys. Lett. 66 (1995) 1972.

[29] J.D. Albrecht, R.P. Wang, P.P. Ruden, M. Farahmand, K.F. Brennan, J. Appl. Phys. 83 (1998) 4777.

[30] R.J. Molnar, T.D. Moustakas, Bull. Am. Phys. Soc. 38 (1993) 445.

[31] W. Gotz, N.M. Johnson, J. Walker, D.P. Bour, H. Amano, I. Akasaki, Appl. Phys. Lett. 67 (1995) 2606.

[32] H. Amano, M. Kito, K. Hiramatsu, I. Akaski, Jpn. J. Appl. Phys. 28 (1989) L2112.

[33] S. Nakamura, T. Muskai, M. Senoh, N. Iwasa, Jpn. J. Appl. Phys. 31 (1992) L139.

[34] S.J. Pearton, C.R. Abernathy, C.B. Vartuli, J.C. Zolper, C. Yuan, R.A. Stall, Appl. Phys. Lett. 67 (1995) 1435.

[35] J.C. Zolper, R.G. Wilson, S.J. Pearton, R.A. Stall, Appl. Phys. Lett. 68 (1996) 1945.

[36] O. Brandt, H. Yang, H. Kostal, K. Ploog, Appl. Phys. Lett. 69 (1996) 2707.

[37] S. Nakamura, T. Muskai, M. Senoh, Appl. Phys. Lett. 67 (1995) 1868.

[38] S. Nakamura, M. Senoh, N. Iwasa, S. Nagahama, T. Yamada, T. Muskai, Jpn. J. Appl. Phys. 10B (1995) L1332.

[39] S. Nakamura, M. Senoh, S.I. Nagahama, N. Iwasa, T. Yamada, T. Matsushita, H. Kiyoku, Y.S. Ugimoto, Jpn. J. Appl. Phys. 35 (1996) L217.

[40] S. Nakamura, M. Senoh, S.I. Nagahama, N. Iwasa, T. Yamada, T. Matsushita, H. Kiyoku, Y.S. Ugimoto, Appl. Phys. Lett. 68 (1996) 2105.

[41] S. Nakamura, M. Senoh, S.I. Nagahama, N. Iwasa, T. Yamada, T. Matsushita, H. Kiyoku, Y.S. Ugimoto, T. Kozaki, H. Umemoto, M. Sano, K. Chocho, Appl. Phys. Lett. 72 (1998) 211.

[42] M.A. Khan, A.R. Bhattarai, J.N. Kuznia, D.T. Olson, Appl. Phys. Lett. 63 (1993) 1214.

[43] M.A. Khan, J.N. Kuznia, D.T. Olson, W. Schatt, J. Burm, M.S. Shur, Appl. Phys. Lett. 65 (1994) 1121.

[44] S.T. Sheppard, K. Doverspike, W.L. Pribble, S.T. Allen, J.W. Palmour, L.T. Kehias, T.J. Jenkins, IEEE Electron. Dev. Lett. 20 (1999) 161.

[45] L. Daumiller, C. Kirchner, M. Kamp, K.J. Ebeling, L. Pond, C.E. Weitzel, E. Kohn, in: Proceedings of the 56th Development Research Conference, Charlottesville, VA, 1998.

[46] B.E. Foutz, http://iiiv.tn.cornell.edu/www/foutz/ganhfet.html.

[47] P.M. Asbeck, E.T. Yu, S.S. Lau, G.J. Sulliran, J.M. Van Hove, J. Redwing, Electron. Lett. 33 (1997) 1230.

[48] B.E. Foutz, L.F. Eastman, U.V. Bhapkar, M.S. Shur, Appl. Phys. Lett. 70 (1997) 2849.

[49] M.A. Khan, T.N. Kuznia, A.R. Bhattaraia, D.T. Olson, Appl. Phys. Lett. 62 (1993) 1786.

[50] S.C. Binari, L.B. Rowland, W. Kruppa, G. Kelner, K. Doverspike, D.K. Gaskill, Electron. Lett. 30 (1994) 1248.

[51] J.C. Zolper, R.J. Shul, A.G. Baca, R.G. Wilson, S.J. Pearton, R.A. Stall, Appl. Phys. Lett. 68 (1996) 2273.

[52] S.C. Binari, Electrochem. Soc. Proc. 95±21 (1995) 136.

[53] F. Ren, M. Hong, S.N.G. Chu, M.A. Marcus, M.J. Schurman, A.G. Baca, S.J. Pearton, C.R. Abernathy, Appl. Phys. Lett. 73 (1999) 3893.

[54] L.S. McCarthy, P. Kozodoy, M.J.W. Rodwell, S.P. DenBaars, IEEE Electron. Dev. Lett. 20 (1999) 277.

[55] J. Han, A.G. Baca, R.J. Shul, C.G. Willison, L. Zhang, F. Ren, A. Zhang, G. Dang, S.M. Donovan, X.A. Cao, H. Cho, K.B. Jung, C.R. Abernathy, S.J. Pearton, R.G. Wilson, Appl. Phys. Lett. 74 (1999) 2702.

[56] R.J. Shul, "Dry etching of GaN", in GaN and Related Materials, ed. S.J. Pearton (Gordon and Breach, NY 1997), Chapter 12

[57] A.T. Ping, A.C. Schmitz, I. Adesida, M.A. Khan, Q. Chen and J. Yang, "Characteristics of RIE damage to GaN using Schottky diodes", J. Electron. Mater., 26 266(1997)

[58] S.J. Pearton, J.W. Lee, J.D. MacKenzie, C.R. Abernathy and R.J. Shul, "Dry etch damage in InN, InGaN and InAlN", Appl. Phys. Lett., 67 2329(1995)

[59] H.P. Gillis, D.A. Choutov, K.P. Martin, M.D. Bremser and R.F. Davis, "Highly anisotropic dry etching of GaN by LE4 in DC plasma", J. Eletron. Mater., 26 301(1997)

[60] A.S. Usikov, W.L. Lundin, U.I. Ushakov, B.V. Pushnyi, N.M. Schmidt, J.M. Zadiranov and T.V. Shuhtra, "Electrical and optical properties of GaN after dry -14, 57(1998)

[61] A.T. Ping, Q. Chen, J.W. Yang, M.A. Khan and I. Adesida, "The effects of RIE damage on ohmic contacts to n-GaN", J. Electron. Mater., 27 261(1998)

[62] J.Y. Chen, C.J. Pan and G.C. Chi, "Electrical and optical changes in the near-surface of GaN", Solid-State Electron., 43 649(1999)

[63] Z.F. Fan, S.N. Mohammad, W. Kim, O. Aktas, A.E. Botchkarev and H. Morkoc, "Effect of Reactive Ion Etching on ohmic contacts to n-GaN", Appl. Phys. Lett., 69 1672(1996)

[64] J.M. Van Hove, R. Hickman, J.J. Laasen, P.P. Chow and P.P. Ruden, "Growth of high quality GaN by rf-MBE", Appl. Phys. Lett., 70 282(1997)

[65] C.R. Eddy and B. Molnar, "The effect of H2-based etching on GaN", Mat. Res. Soc. Symp. Proc., Vol 395 745(1996)

[66] C.R. Eddy and B. Molnar, "Plasma etch-induced conductivity changes in GaN", J. Electron. Mater., 28 314(1999)

[67] S.J. Pearton, "Implant isolation of compound semiconductors", Mat. Sci. Rep., 4, 313(1990)

[68] J.-Y. Duboz and M.A. Khan, in Group III Nitride Semiconductor Compounds, ed. B. Gil (Clarendon Press, Oxford, 1998)

[69] Z. Fan, S. N. Mohammad, Ö. Aktas, A. E. Botchkarev, A. Salvado Appl. Phys. Lett. 69 1229 (1996)

[70] Y.-F. Wu, B.P. Keller, O.Fini, S. Keller, T.J. Jenkins, L.T. Kehias, S.P. DenBaars and U.K. Mishra, IEEE Electron. Dev. Lett. 19 50 (1998)

[71] M.S. Shur, Solid State Electron. 42 2119 (1998)

[72] S.C. Binari, J.M. Redwing and W. Kruppa, Electron. Lett. 33 242 (1997)

[73] R. Gaska, J.W. Yang, A. Osinsky, Q. Chen, M.A. Khan, A.O. Orlov, G. L. Snider, and M. S. Shur, Appl. Phys. Lett. 72 707(1998)

[74] A.T. Ping, Q. Chen, J.W. Yang, M.A. Khan and I. Adesida, IEEE Electron. Dev. Lett. 19 54 (1998)

[75] G.J. Sullivan, M.Y. Chen, J.A. Higgins, J.W. Yang, Q. Chen, R.L. Pierson and B.T. McDermott, IEEE Electron. Dev. Lett. 19 198 (1998)

[76] for example, S. J. Pearton, J. C. Zolper, R. J. Shul, and F. Ren, J. Appl. Phys. 86 1 (1999) and references therein

[77] L.F. Eastman, K. Chu, W. Schaff, M. Murphy, N.G. Weimann and T. Eustis, MRS Internet J. Nitride Semicond. Res. 2 17 (1997)

[78] J.S. Foresi and T.D. Moustakas, Appl. Phys. Lett. 62 2859 (1993)

[79] L.L. Smith, R.F. Davis, M.J. Kim, R. W. Carpenter and Y. Huang, J. Mater. Res. 11 2257 (1996)

[80] B.P. Luther, S.E. Mohney, T.N. Jackson, M.A. Khan, Q. Chen, and J. W. Yang, Appl. Phys. Lett. 70 57 (1997)

[81] L.L. Smith, M.D. Bremser, E.D. Carlson, T.W. Weeks, Jr. Y. Huang, M.J. Kim, R.W. Carpenter and R.F. Davis, Mat. Res. Soc. Symp. Proc. 395 861 (1996)

[82] S. Miller and R.H. Holloway, J. Electron. Mater. 25 1709 (1996)

[83] Y.-F. Wu, W.N. Jiang, B.P. Keller, S. Keller, D. Kapolneck, S.P. DenBaars, U.K. Mishra and B. Wilson, Solid-Sate Electron. 41 165 (1997)

[84] H. Cordes and Y.A. Chang, MRS Internet J. Nitride Semicond. Res. 2 2 (1997)

[85] M.E. Lin, Z. Ma, F.Y. Huang, Z.F. Fan, L.H. Allen and H. Morkoc, Appl. Phys. Lett. 61 1003 (1994)

[86] E. Kaminska, A. Piotrowska, M. Guziewicz, S. Kasjaniuk, A. Barcz, E. Dynowska, M.D. Bremser, O.H. Nam and R.F. Davis, Mat. Res. Soc. Symp. Proc. 449 1055 (1996)

[87] M.W. Cole, D.W. Eckart, W.Y. Han, R.L. Pfeffer, T. Monahan, F. Ren, C. Yuan, R.A. Stall, S.J. Pearton, Y. Li and Y. Lu, J. Appl. Phys. 80, 278 (1996)

[88] M.W. Cole, F. Ren and S.J. Pearton, J. Electrochem. Soc. 144 L275 (1997)

[89] S. E. Mohney and S.S. Lau, in GaN and Related Materials II, ed. S.J. Pearton (Gordon and Breach, NY 1997)

[90] Q.Z. Liu and S.S Lau, Solid-State Electron. 42 677 (1998)

[91] Z. Fan, S.N. Mohammad, W. Kim, Özgür Aktas, A.E. Botchkarev, and H. Morkoç, Appl. Phys. Lett. 68 1672 (1996)

[92] M. Murakumi, Y. Koide, T. Oku, H. Mori and C.J. Uchihori, Proc. Electrochem. Soc. 97-21 286(1997)

[93] S. Ruvimov, Z. Liliental-Weber, J. Washburn, K. J. Duxstad, E. E. Haller, Z.-F. Fan, S. N. Mohammad, W. Kim, A.E. Botchkarev, H. Morkoc, Appl. Phys. Lett. 69 2737 (1996)

[94] L. F. Lester, J. M. Brown, J. C. Ramer, L. Zhang, S. D. Hersee, and J. C. Zolper, Appl. Phys. Lett. 69 2737 (1996)

[95] A.T. Ping, Q. Chen, J.W. Yang, M.A. Khan and I. Adesida, J. Electron. Mater. 27 261 (1998)

[96] A. Vescan, R. Dietrich, A. Wieszt, H. Tobler, H. Leier, J.M. VanHove, P.P. Chow and A.M. Wowchak, J. Cryst. Growth 201/202 327 (1999)

[97] S.J. Lai, R. Li, Y.L. Chen, L. Wang, W.G. Wu, S.G. Thomas and K.L. Wang, Electron. Lett. (in Press)

[98] X.A. Cao, H. Cho, S.J. Pearton, G.T. Dang, A.P. Zhang, F. Ren, R.J. Shul, L. Zhang, R. Hickman and J.M. VanHove, Appl. Phys. Lett. 75 232 (1999)

[99] J.M. VanHove, G.J. Casimini, E. Nelson, A.M. Wowchak and P.P. Chow, J. Cryst. Growth 150 908 (1995)

[100] H. Akagi, IEEE Trans. Power Electron. 13, 345 (1998).

[101] G. T. Heydt and B. J. Skromme, Mater. Res. Soc. Symp. Proc. 483,3 (1998).

[102] E. R. Brown, Solid-State Electron. 43, 1918 (1998).

[103] J.B. Casady, A.K. Agarwal, L.B. Rowland, S. Seshadri, R.R. Siergiej, S.S. Mani, D.C. Sheridan, P.A. Sanger, C.D. Brandt, Mater. Res. Soc. Symp. Proc. 483 (1998) 27.

[104] R. Zehringer, A. Stack, T. Lang, Mater. Res. Soc. Symp. Proc. 483 (1998) 369. J. Mater. 50 (1998) 46.

[105] B.M. Green, K.K. Chu, E.M. Chumbes, J.A. Smart, J.R. Shealy, L.F. Eastman, IEEE Electron. Dev. Lett. 21 (2000) 268.

[106] J.-I. Chyi, C.-M. Lee, C.-C. Chuo, G.C. Chi, G.T. Dang, A.P. Zhang, F. Ren, X.A. Cao, S.J. Pearton, S.N.G. Chu and R.G. Wilson, MRS Internet J. Nitride Semicond. Res. 4(1999) 8.

[107] Z.Z. Bandic, D.M. Bridger, E.C. Piquette, T.C. McGill, R.P. Vaudo, V.M. Phanse and J.M. Redwing, Appl. Phys. Lett. 74 (1999) 1266.

[108] M. Trivedi and K. Shenai, J. Appl. Phys. 85 (1999) 6889.

[109] V.A. Dmitriev, K.G. Irvine, C.H. Carter, Jr., N.I. Kuznetsov and E.V. Kalinina, Appl. Phys. Lett. 68 (1996) 229.

[110] M.S. Shur, Solid-State Electron. 82 (1998) 2131.

[111] G.T. Heydt and B.J. Skromme, Mater. Res. Soc. Symp. Proc. 483 (1998) 3; R. Hickman, J.M. Van Hove, P.P. Chow, J.J. Klaassen, A.M. Wowchack, and K. Shenai, J. Appl. Phys. 85 (1999) 6889.

[112] C.I. Harris and A.O. Konstantinov, Phys. Scr., T 79 (1999) 27.

[113] K.G. Irvine, R. Singh, M.J. Paisley, J.W. Palmour, O. Kordina and C.H. Carter, Jr., Mater. Res. Soc. Symp. Proc. 512 (1998) 119.

[114] F. Dahlquist, C.-M. Zetterling, M. Ostling and K. Rottner, Mater. Sci. Forum 264-268 (1998) 1061.

[115] M. Adler, V. Temple, A. Ferro and E. Rustay, IEEE Trans. Electron Devices 24 (1977) 107.

[116] E. Stefanov, G. Charitat and L. Bailon, Solid-State Electron. 42 (1998) 2251.

[117] A.Y. Polyakov, N.B. Smirnov, A.V. Govorkov and J.M. Redwing, Soild-State Electron. 42 (1998) 831.

[118] H. Amano and I. Akasaki, in Properties, Processing and Applications of GaN and Related Semiconductors, EMIS Data Review No. 23, edited by J.H. Edgar, S. Strite, I. Akasaki, H. Amano and C. Welzel (IEE, London, 1999).

[119] N. Dyakonova, A. Dickens, M.S. Shur, R. Gaska and J.W. Yang, Appl. Phys. Lett. 72 (1998) 2562.

[120] V. Khemkar, P. Patel, T.P. Chow and R.J. Gutman, Solid-State Electron. 43 (1999) 1945.

[121] J.C. Zolper, Mater. Res. Symp. Proc. 622 (2000) T2.4.1.

BIOGRAPHICAL SKETCH

Anping Zhang was born in Shaanxi, China in 1970. He received a B.E. degree in chemical engineering from Tsinghua University in July 1993. After that he went to Graduate School of Chinese Academy of Sciences and University of Science and Technology of China, where he received an M.S. in chemical engineering in January 1996. In 1998 he was admitted to the University of Florida and joined Dr. Fan Ren's group in the same year. His research in UF is on III-V electronic and optoelectronic semiconductor devices design, fabrication, testing and simulation.